

NASA Contractor Report 3723

NASA
CR
3723
c.1

LOAN COPY
AFWL TECHNICAL
KIRTLAND AFB, NM

0062305



TECH LIBRARY KAFB, NM

Numerical Solutions of Navier-Stokes Equations for Compressible Turbulent Two/Three Dimensional Flows in the Terminal Shock Region of an Inlet/Diffuser

**N.-S. Liu, S. J. Shamroth,
and H. McDonald**

**CONTRACT NAS3-22747
AUGUST 1983**



25th Anniversary
1958-1983

NASA



0062305

NASA Contractor Report 3723

Numerical Solutions of Navier-Stokes Equations for Compressible Turbulent Two/Three Dimensional Flows in the Terminal Shock Region of an Inlet/Diffuser

**N.-S. Liu, S. J. Shamroth,
and H. McDonald**

***Scientific Research Associates, Inc.
Glastonbury, Connecticut***

**Prepared for
Lewis Research Center
under Contract NAS3-22747**



National Aeronautics
and Space Administration

**Scientific and Technical
Information Branch**

1983

TABLE OF CONTENTS

	Page
SUMMARY	1
INTRODUCTION	2
LIST OF SYMBOLS	5
ANALYSIS	8
Governing Equations	8
Dependent Variables and Coordinate Transformation	9
Turbulence Model	12
Boundary Conditions	15
Numerical Procedure	15
Artificial Dissipation	16
TEST CASES	18
COMPUTED RESULTS	21
Table I - Parameters For Test Cases	23
Steady 2-D Subsonic Diffuser Flow	24
Steady 2-D Transonic Diffuser Flow With a Normal Shock	24
Steady 2-D Supersonic Inlet Flow With Terminal Shock	25
Unsteady Shock Development in a 2-D Transonic Diffuser	26
Steady 3-D Transonic Diffuser Flow With a Normal Shock	28
CONCLUDING REMARKS	29
APPENDIX	30
Background	30
Spatial Differencing and Artificial Dissipation	31
Split LBI Algorithm	32
Linearization and Time Differencing	32
Special Treatment of Diffusive Terms	33
Consistent Splitting of the LBI Scheme	34
REFERENCES	36
FIGURES	38

TABLE OF CONTENTS (Continued)

	Page
USER'S MANUAL	58
CHART 1 Overall Program FLOW	60
CHART 2 Program Flow Chart for SUBROUTINE READA	61
CHART 3 Program Flow Chart for SUBROUTINE EXEC	62
Namelist Input Description	63
List of Major Fortran Variables	72
File Input/Output	77
Remarks on Storage Requirements and Run Time	77
PROCDEF MOD.	78
PROCDEF MODN	78
PROCDEF RUNMT.	78
Sample Input Cards and Printed Output.	79

Summary

The multi-dimensional ensemble-averaged compressible time-dependent Navier-Stokes equations in conjunction with mixing length turbulence model and shock capturing technique have been used to study the terminal shock type of flows in various flight regimes occurring in a diffuser/inlet model. The numerical scheme for solving the governing equations is based on a linearized block implicit approach and the following high Reynolds number calculations have been carried out: (1) 2-D, steady, subsonic; (2) 2-D, steady, transonic with normal shock, (3) 2-D, steady, supersonic with terminal shock, (4) 2-D, transient process of shock development and (5) 3-D, steady, transonic with normal shock. The numerical results obtained for the 2-D and 3-D transonic shocked flows have been compared with corresponding experimental data; the calculated wall static pressure distributions agree well with the measured data.

INTRODUCTION

Proper design of the inlet flow region upstream of the compressor face is an important component in the overall design of the aircraft gas turbine for subsonic, transonic and supersonic inlet configurations.

In principle many of the problems of subsonic aircraft inlets are also encountered with transonic and supersonic installations. However, particular complexity is found in practice with transonic and supersonic aircraft, since not only is there the enlarged flight regime to consider, but now the influence of inlet shock structure on flow stability and engine-inlet matching must be taken into account. The importance and complexity of the influence of this inlet shock structure requires detailed investigation, which at present is accomplished by extensive and expensive experimental testing. Recently, however, there have been encouraging developments in the potential use of analyses to reduce the required extensive experimental mapping. In the transonic and supersonic inlet, the flow field can be divided into three main components: a supersonic region in the upstream portion of the inlet which leads into the terminal shock region and finally a subsonic diffusion region downstream of the terminal shock. In regard to the supersonic region Buggeln, McDonald, Levy and Kreskovsky (Ref. 1) have developed a three-dimensional spatial forward marching viscous flow analysis which has been applied successfully to several supersonic inlet configurations (Refs. 1-4). Although this analysis has given very favorable results in the supersonic portion of the inlet, the assumptions required to allow a forward marching calculation are inappropriate in the region of the terminal shock. Downstream of the terminal shock region, the flow is entirely subsonic and in this region the subsonic spatial forward marching analysis of Levy, Briley and McDonald (Ref. 5) is available. However, a portion of the flow field still requiring attention is the terminal shock region where procedures which are based upon a spatial forward marching method are invalid. It is this terminal shock region which is the subject of the present effort.

The terminal shock region is a very difficult problem which impacts upon both the loss characteristics and stability characteristics of the inlet flow. In a practical mixed compression supersonic inlet, the requirement of shock structure stability determines to large extent the normal shock loss in the inlet, itself a major contribution to the overall inlet losses. In essence by allowing some supersonic expansion after the geometric throat i.e. supercritical operation,

with subsequent shock down to subsonic flow via a normal shock, stability margin is obtained at the cost of the normal shock loss. If the normal shock were to occur very near the geometric throat where the local Mach number was unity, the resulting normal shock loss would be minimal but the inlet would be susceptible to unstating. Having some supersonic reacceleration after the geometric throat places the normal shock downstream of the throat where a degree of stable upstream shock movement is possible without unstating the inlet. This upstream shock movement could be unavoidable in practice for instance as the result of changing engine operating conditions or the result of changes in the external flow. Thus, an inlet design in which a terminal shock of some finite strength occurs downstream of the throat is a common occurrence.

The flow in the region of the terminal shock is very complex. First of all it is transonic, secondly shockwave boundary layer interaction with possible accompanying separation occurs and thirdly the flow is very sensitive to area changes, and hence to the three-dimensionality of the geometry. As a result of these properties optimizing the location of the normal shock to maximize stability while minimizing losses is a very demanding, yet very important task for analysis. Further, although the flow downstream of the normal shock may be treated by viscous subsonic forward schemes, nevertheless it has the transonic region as initial conditions, and the forward marching calculation may prove sensitive to the inflow and hence require an accurate definition of the initial conditions. Thus, there exists powerful motivation to develop an analysis of the transonic region of the inlet, which would include three-dimensionality and viscous effects. The ability to compute time-dependent flows would also be valuable. With this feature the steady flow (should it exist) would be computed as the time asymptote of the integration from the initial time zero guess of the flow field. Following this, the steady transonic shock structure could be perturbed and the stability of the system determined. The transient perturbation could be introduced by varying the inlet or the exit condition, depending on the physical disturbance being simulated.

Insofar as the governing equations are concerned, the inherent mixed elliptic hyperbolic nature of steady transonic flow does not encourage the use of forward marching in space, except perhaps in some corrector sense once an approximate transonic solution has been obtained. For governing equations one could consider the transonic potential equation, however, in the current problem a knowledge of the shock losses is critical, and this

precludes a potential approach. Turning to the Euler equations, these would permit shock losses to occur; however, the interest in and flow sensitivity to the interaction with the wall boundary layers make a viscous correction mandatory. The prospect of performing a numerical solution of the Euler equations and coupling this in an iterative manner with a three-dimensional boundary layer scheme at transonic speeds is not attractive. Even if converged solutions could be obtained the resulting scheme would be unlikely to offer any significant savings in computational expense relative to solving the full Navier-Stokes equations, at least at transonic speeds where the interaction between the core flow and the boundary layer could be very sensitive and difficult to converge. In any event, the resulting procedure would still suffer difficulties with flow separation. The complex fluid mechanics involved in the transonic region of the inlet make the use of the three-dimensional compressible ensemble-averaged time-dependent Navier-Stokes equations attractive for this problem. Such an approach is described in the present report.

LIST OF SYMBOLS

Symbols

A^+	van Driest damping coefficient
C_p	specific heat at constant pressure
D	determinant of the Jacobian matrix
\mathbb{D}	dissipation function
d	distance to the nearest wall
d^+	dimensionless distance to the nearest wall
h	enthalpy, throat height
ℓ	mixing length
ℓ_∞	mixing length in the core flow region
p	static pressure
q	magnitude of the velocity
\vec{q}^T	turbulent heat flux vector
$\overline{\vec{q}}$	mean heat flux vector
R	universal gas constant
Re	Reynolds number
t	time
T	temperature
T°	stagnation temperature
\vec{u}	velocity vector

LIST OF SYMBOLS (continued)

Symbols

u	velocity component in x-direction
u_τ	friction velocity
v	velocity component in y-direction
w	velocity component in z-direction
w_e	w at the edge of the boundary layer
x, x_1	cartesian coordinate in transverse direction
y, x_2	cartesian coordinate in spanwise direction
y^1, y^2, y^3	computational coordinates
z, x_3	cartesian coordinate in streamwise direction

Greek Symbols

δ	boundary layer thickness
ε	turbulence energy dissipation rate
κ	von Karman constant
μ	dynamic viscosity
ν_{art}	artificial dissipation
ξ, η, ζ	computational coordinates
π	molecular stress tensor
π^T	turbulent stress tensor

LIST OF SYMBOLS (continued)

Greek Symbols

ρ	density
σ	artificial dissipation parameter
τ	time
τ_l	local shear stress
$\tau_{xx}, \tau_{xy}, \text{ etc.}$	component of stress tensor
Φ	meanflow dissipation rate

Subscripts

b	associated with the bottom wall
s	associated with the side wall
t	associated with the time or top wall
x	associated with the x-direction
y	associated with the y-direction
z	associated with the z-direction

Superscripts

T	associated with turbulent quantities, transpose of matrix
---	--

ANALYSIS

Governing Equations

The equations used in the present effort are the ensemble-averaged, time-dependent Navier-Stokes equations which can be written in vector form as

Continuity

$$\frac{\partial \rho}{\partial t} - \nabla \cdot \rho \vec{u} = 0 \quad (1)$$

Momentum

$$\frac{\partial \rho \vec{u}}{\partial t} + \nabla \cdot (\rho \vec{u} \vec{u}) = -\nabla p + \nabla \cdot (\bar{\bar{\pi}} + \pi^T) \quad (2)$$

Energy

$$\frac{\partial \rho h}{\partial t} + \nabla \cdot (\rho \vec{u} h) = -\nabla \cdot (\bar{\bar{q}} + \vec{q}^T) + \frac{\partial p}{\partial t} + \Phi + \rho \epsilon \quad (3)$$

where ρ is density, \vec{u} is velocity, p is pressure, $\bar{\bar{\pi}}$ is the molecular stress tensor, π^T is the turbulent stress tensor, h is enthalpy, $\bar{\bar{q}}$ is the mean heat flux vector, \vec{q}^T is the turbulent heat flux vector, Φ is the mean flow dissipation rate and ϵ is the turbulence energy dissipation rate. If the flow is assumed at a constant total temperature, the energy equation is replaced by

$$T^\circ = T + \frac{q^2}{2C_p} = \text{constant} \quad (4)$$

where T° is the stagnation temperature, q is the magnitude of the velocity and C_p is the specific heat at constant pressure. For the purpose of economy, both in terms of run time and computer storage, calculations presented in this report were run with the constant total temperature assumption. These equations, supplemented by an equation of state,

$$p = \rho R T \quad (5)$$

form the system governing the terminal shock region problem.

Dependent Variables and Coordinate Transformation

The governing equations, Eqs. (1) - (3), are written in general vector form and prior to their application to specific problems it is necessary to decide upon both a set of dependent variables and a proper coordinate transformation. Based upon previous investigations (e.g. Refs. 6 and 7) the specific scalar momentum equations to be solved are the x, y and z Cartesian momentum equations. The dependent variables chosen are the physical Cartesian velocities u, v, w and the density ρ .

The equations are then transformed to a general coordinate system in which the general coordinates, y^j are related to the Cartesian coordinates, x_1 , x_2 and x_3 by

$$y^j = y^j(x_1, x_2, x_3, t) \quad ; \quad j = 1, 2, 3. \quad (6)$$

$$\tau = t$$

As implied by Eq. (6), the general coordinate y^j may be a function of both the Cartesian coordinates and time. This coordinate time dependence will have an implication in so far as the choice of governing equation form is concerned.

The governing equations can be expressed in terms of the new independent variables y^j as

$$\begin{aligned} & \frac{\partial W}{\partial \tau} + \xi_t \frac{\partial W}{\partial \xi} + \xi_x \frac{\partial F}{\partial \xi} + \xi_y \frac{\partial G}{\partial \xi} + \xi_z \frac{\partial H}{\partial \xi} \\ & + \eta_t \frac{\partial W}{\partial \eta} + \eta_x \frac{\partial F}{\partial \eta} + \eta_y \frac{\partial G}{\partial \eta} + \eta_z \frac{\partial H}{\partial \eta} \\ & + \zeta_t \frac{\partial W}{\partial \zeta} + \zeta_x \frac{\partial F}{\partial \zeta} + \zeta_y \frac{\partial G}{\partial \zeta} + \zeta_z \frac{\partial H}{\partial \zeta} \\ & = \frac{1}{Re} \left[\xi_x \frac{\partial F_1}{\partial \xi} + \eta_x \frac{\partial F_1}{\partial \eta} + \zeta_x \frac{\partial F_1}{\partial \zeta} \right. \\ & \quad + \xi_y \frac{\partial G_1}{\partial \xi} + \eta_y \frac{\partial G_1}{\partial \eta} + \zeta_y \frac{\partial G_1}{\partial \zeta} \\ & \quad \left. + \xi_z \frac{\partial H_1}{\partial \xi} + \eta_z \frac{\partial H_1}{\partial \eta} + \zeta_z \frac{\partial H_1}{\partial \zeta} \right] \end{aligned} \quad (7)$$

through a straight forward application of chain rule differentiation. In Eq. (7)

$$\xi = y^1$$

$$\eta = y^2$$

$$\zeta = y^3$$

and

$$W = \begin{bmatrix} \rho \\ \rho u \\ \rho v \\ \rho w \end{bmatrix}, \quad F = \begin{bmatrix} \rho u \\ \rho u^2 + p \\ \rho uv \\ \rho uw \end{bmatrix}, \quad G = \begin{bmatrix} \rho v \\ \rho uv \\ \rho v^2 + p \\ \rho vw \end{bmatrix}$$

(8)

$$H = \begin{bmatrix} \rho w \\ \rho uw \\ \rho vw \\ \rho w^2 + p \end{bmatrix}, \quad F_1 = \begin{bmatrix} 0 \\ \tau_{xx} \\ \tau_{xy} \\ \tau_{xz} \end{bmatrix}, \quad G_1 = \begin{bmatrix} 0 \\ \tau_{xy} \\ \tau_{yy} \\ \tau_{yz} \end{bmatrix}, \quad H_1 = \begin{bmatrix} 0 \\ \tau_{xz} \\ \tau_{yz} \\ \tau_{zz} \end{bmatrix}$$

Since in general the computational coordinates may be a function of time with a time-dependent Jacobian, the equations are recast into the so-called 'strong conservation form' (Ref. 8).

$$\begin{aligned}
& \frac{\partial W/D}{\partial \tau} + \frac{\partial}{\partial \xi} \left[\frac{W\xi_t}{D} + \frac{F\xi_x}{D} + \frac{G\xi_y}{D} + \frac{H\xi_z}{D} \right] \\
& + \frac{\partial}{\partial \eta} \left[\frac{W\eta_t}{D} + \frac{F\eta_x}{D} + \frac{G\eta_y}{D} + \frac{H\eta_z}{D} \right] \\
& + \frac{\partial}{\partial \zeta} \left[\frac{W\zeta_t}{D} + \frac{F\zeta_x}{D} + \frac{G\zeta_y}{D} + \frac{H\zeta_z}{D} \right] \\
& = \frac{1}{Re} \left[\frac{\partial}{\partial \xi} \left(\frac{F_1 \xi_x}{D} + \frac{G_1 \xi_y}{D} + \frac{H_1 \xi_z}{D} \right) + \frac{\partial}{\partial \eta} \left(\frac{F_1 \eta_x}{D} + \frac{G_1 \eta_y}{D} + \frac{H_1 \eta_z}{D} \right) \right. \\
& \quad \left. + \frac{\partial}{\partial \zeta} \left(\frac{F_1 \zeta_x}{D} + \frac{G_1 \zeta_y}{D} + \frac{H_1 \zeta_z}{D} \right) \right] \tag{9}
\end{aligned}$$

where

$$D = \begin{vmatrix} \xi_x & \xi_y & \xi_z \\ \eta_x & \eta_y & \eta_z \\ \zeta_x & \zeta_y & \zeta_z \end{vmatrix}$$

Equation (9) represents the Navier-Stokes equation in strong conservation form and represents the set of equations solved in the present work.

Insofar as the coordinate system is concerned, the cases considered in the present effort used a simplified coordinate transformation in which;

$$\begin{aligned}\xi &= f_1(x, z) \\ \eta &= f_2(y) \\ \zeta &= f_3(z)\end{aligned}\tag{10}$$

i.e., a stretched and contour-fitted non-orthogonal grid was used. The specific grid transformation used in the streamwise direction is that of Oh (Ref. 9), which allows high resolution in user specified regions. In the cross-sectional plane hyperbolic tangent transformations were adopted. The regions of high resolution were taken to be those near solid walls (in the x and y directions) and those near the throat as well as region of sharp contraction of the contour in the z direction.

Turbulence Model

Since the flows of interest are in the turbulent regime, it is necessary to specify a turbulence model. The present results were obtained from the McDonald's model (Ref. 10) with Van Driest damping (Ref. 11),

$$l = l_{\infty} \tanh \left[\frac{\kappa d}{l_{\infty}} \right] \left[1 - \exp \left(- \frac{d^+}{A^+} \right) \right]\tag{11}$$

where κ is the von Karman constant, A^+ is the van Driest damping coefficient and d is the distance to the nearest solid wall.

$$l_{\infty} = 0.098 \quad , \quad A^+ = 26.0$$

and $\kappa = 0.40$ for two-dimensional calculations, while $\kappa = 0.41$ for three-dimensional calculations. The nondimensional distance d^+ is defined as

$$d^+ = d \left(\frac{\rho u_{\tau}}{\mu} \right)\tag{12}$$

and the friction velocity u_{τ} in the present analysis is taken as

$$u_{\tau} = \left(\frac{\tau_l}{\rho} \right)^{1/2}\tag{13}$$

where the local shear stress τ_l is obtained from

$$\tau_l = (2D:D)^{1/2} \quad (14)$$

where D is the dissipation function

$$D \equiv \frac{1}{2} [(\nabla \vec{U}) + (\nabla \vec{U})^T] \quad (15)$$

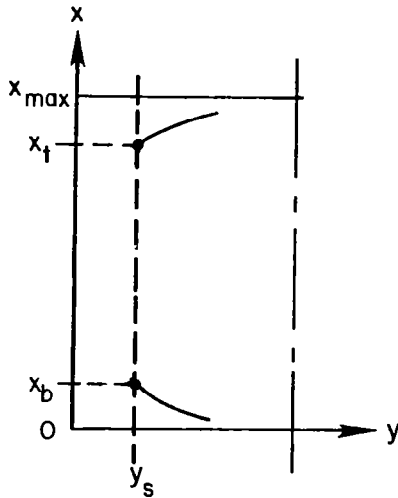
Note that for small d the tanh function in Eq. (11) reduces to kd while for large d it approaches ℓ_∞ .

In boundary layer analysis ℓ_∞ is usually taken as 0.09δ where δ is the boundary layer thickness taken at the location where $w/w_e = 0.99$. However, this definition of δ assumes the existence of an outer flow where the velocity w_e is independent of distance from the wall at a given streamwise station, i.e., it assumes w_e is only a function of the streamwise coordinate. Most Navier-Stokes calculations show no such definitive region to exist and, therefore, an alternate definition is required. In the present effort the boundary layer thickness in the two-dimensional region was set by first determining w_{\max} , the maximum streamwise velocity, at a given station and then setting δ via;

$$\delta = 2.0d_{(w/w_{\max}=k)} \quad (16)$$

i.e., δ was taken as twice the distance (measured away from the nearest wall) for which $w/w_{\max} = k$. The value of k used in the present effort was 0.90. The mixing length in the core region was set by linear interpolation between the top and bottom wall boundary layer edge values. The model described above was used in two-dimensional calculations as well as in the nominally two-dimensional region of three-dimensional calculation. This nominally two-dimensional region was defined as $y \geq y_s \approx \delta_s$, where δ_s was the side wall boundary layer thickness evaluated, according to Eq. (16), at the midpoint between the top and bottom corners, and was taken as a measure of the overall boundary layer thickness along the side wall. Once δ_s had been determined, y_s was then set as the nearest y -location of the grid points with y_s being slightly larger than δ_s . Henceforth, the mixing lengths at each point along $y = y_s$,

together with the locations of the top and bottom wall boundary layer edges, were obtained as described before. A schematic of the cross-sectional regions involved in the three-dimensional calculation is depicted in Fig. A, in which x_b and x_t are the edges of the bottom and top wall boundary layers at $y = y_s$. In the bottom wall corner region (i.e., $0 \leq y^* < y_s$ and $0 \leq x^* < x_b$), the mixing lengths were calculated according to Eq. (11) with a constant ℓ_∞ specified as the length scale at the point (x_b, y_s) . Similarly, the length scales of points in the top wall corner region (i.e., $0 \leq y^* < y_s$ and $x_t < x^* \leq x_{\max}$) were evaluated according to Eq. (11) with another constant ℓ_∞ specified as the mixing length at the point (x_t, y_s) . Finally, the length scales of points in the side wall boundary layer region (i.e., $0 \leq y^* < y_s$, $x_b \leq x^* \leq x_t$) were obtained by using Eq. (11) with ℓ_∞ specified as the respective mixing lengths at the points (x^*, y_s) .



- $y \geq y_s$: nominally 2-D region
- $0 \leq y^* < y_s$, $x_b \leq x^* \leq x_t$: side wall B. L. region
- $0 \leq y^* < y_s$, $0 \leq x^* < x_b$: bottom corner region
- $0 \leq y^* < y_s$, $x_t < x^* \leq x_{\max}$: top corner region

Figure A

Boundary Conditions

The authors' experience in solving Navier-Stokes equations has indicated the important role of boundary conditions in determining accurate solutions and rapid numerical convergence. The boundary conditions used in the present calculations with subsonic inflow and outflow follow the suggestion of Briley and McDonald [12] which specifies upstream total pressure and downstream static pressure conditions. Following this approach the stagnation pressure, transverse velocity and pressure derivative were set on the upstream boundary. In addition, a boundary layer thickness was specified and a dimensionless boundary layer profile set in that region. No-slip conditions in conjunction with zero pressure gradient were set at solid walls. The static pressure and velocity second derivatives were set at the downstream boundary. As mentioned above, this approach is valid for subsonic inflow. If the flow at the upstream boundary is supersonic, then, instead of the total core flow conditions, values of velocity components and density must be specified [27]. A more detailed description of the boundary conditions used for the present calculations will be given later in the section "Test Cases".

Numerical Procedure

The numerical procedure used to solve the governing equations is a consistently split linearized block implicit (LBI) scheme originally developed by Briley and McDonald [13]. A conceptually similar scheme has been developed for two-dimensional MHD problems by Lindemuth and Killeen [14]. More recently Beam and Warming (Ref. 25) have derived this and other related schemes by the method of approximate factorization. The procedure is discussed in detail in Refs. 13 and 15. The method can be briefly outlined as follows: the governing equations are replaced by an implicit time difference approximation, optionally a backward difference or Crank-Nicolson scheme. Terms involving nonlinearities at the implicit time level are linearized by Taylor expansion in time about the solution at the known time level, and spatial difference approximations are introduced. The result is a system of multidimensional coupled (but linear) difference equations for the dependent variables at the unknown or implicit time level. To solve these difference equations, the Douglas-Gunn [16] procedure for generating alternating-direction implicit

(ADI) schemes as perturbations of fundamental implicit difference schemes is introduced in its natural extension to systems of partial differential equations. This technique leads to systems of coupled linear difference equations having narrow block-banded matrix structures which can be solved efficiently by standard block-elimination methods.

The method centers around the use of a formal linearization technique adapted for the integration of initial-value problems. The linearization technique, which requires an implicit solution procedure, permits the solution of coupled nonlinear equations in one space dimension (to the requisite degree of accuracy) by a one-step noniterative scheme. Since no iteration is required to compute the solution for a single time step, and since only moderate effort is required for solution of the implicit difference equations, the method is computationally efficient; this efficiency is retained for multidimensional problems by using what might be termed block ADI techniques. The method is also economical in terms of computer storage, in its present form requiring only two time-levels of storage for each dependent variable. Furthermore, the block ADI technique reduces multidimensional problems to sequences of calculations which are one dimensional in the sense that easily-solved narrow block-banded matrices associated with one-dimensional rows of grid points are produced. A more detailed discussion of the solution procedure as discussed by Briley, Buggeln and McDonald [17] is given in the Appendix.

Artificial Dissipation

One major problem to be overcome in calculating high Reynolds number flows using the Navier-Stokes equations is the appearance of spatial oscillations associated with the so-called central difference problem. When spatial derivatives are represented by central differences, high Reynolds number flows can exhibit a saw tooth type oscillation unless some mechanism is added to the equations to suppress their appearance. This dissipation mechanism can be added implicitly to the equations via the spatial difference molecule (e.g. one-sided differencing) or explicitly through addition of a specific term. The present authors favor this latter approach for two reasons. First, if a specific artificial dissipation term is added to the equations, it is clear precisely what approximation is being made. Secondly, if a specific term is added to suppress oscillations, the amount of artificial dissipation added to the equations can be easily controlled in magnitude and location so as to add the minimum amount necessary to suppress spatial

oscillations. Studies can also be easily performed to evaluate the effect of the explicitly added dissipation on the solution.

Various methods of adding artificial dissipation were investigated in Ref. 18, and these were evaluated in the context of a one-dimensional model problem. The model problem used was one-dimensional flow with heat transfer. Flow was subsonic at the upstream boundary, accelerated via heat sources until a Mach number of unity was reached and then accelerated by heat sinks. The exit back pressure was raised to cause a shock to appear in the supersonic region. This basic one-dimensional problem contained many relevant features including strong accelerations and appearance of a normal shock wave and, therefore, it served as a good test case for various forms of artificial dissipation which could be used in the presence of shock waves.

The results of the Ref. 18 investigation led to the conclusion that for the model problem a second order artificial dissipation approach was the best of those considered. This approach adds a term of the form $\nu_{art} \frac{\partial^2 \phi}{\partial Z^2}$ or

$\frac{\partial}{\partial Z} \left\{ \nu_{art} \frac{\partial \phi}{\partial Z} \right\}$ to each governing equation where $\phi = \rho, u, v, w$ for the continuity, x-momentum, y-momentum and z-momentum equations respectively and ν_{art} is determined by $\frac{|U_Z| \Delta Z}{\nu + (\nu_{art})_Z} \leq \frac{1}{\sigma_Z}$

In the above equation ΔZ is the distance between grid points in a given coordinate direction, U_Z is the velocity in this direction, σ_Z is the artificial dissipation parameter for this direction and ν is the effective kinematic viscosity. The equation determines ν_{art} with ν_{art} taken as the smallest non-negative value which will satisfy the expression. It should be noted that in two space dimensions each equation contains two artificial dissipation terms, one in each coordinate direction. For example, the streamwise momentum equation expressed in two-dimensional Cartesian coordinates would contain the artificial dissipation terms

$$(\nu_{art})_x \frac{\partial^2 w}{\partial x^2} + (\nu_{art})_z \frac{\partial^2 w}{\partial z^2}$$

Obviously the desirable condition occurs when sufficient artificial dissipation is added to the equations to suppress spurious oscillations but the amount added does not perceptively change the physical solution. The results of Refs. 18 and 19 indicated that such conditions could be met when the dissipation parameter, σ , was varied between values of .10 and .025 and these results were confirmed for the terminal shock problem in the present effort.

Although the original artificial dissipation study was carried out with terms of the form $(v_{art})_Z \partial^2 \phi / \partial Z^2$, the form used in the present case was $\partial (v_{art} \partial \phi / \partial Z) / \partial Z$. However, recent studies for airfoil and cascade calculations indicate that for low values of σ little significant difference occurs as a result of using one form or the other.

Test Cases

Several test cases were run with the MINT computer code to evaluate the previously described computational procedures for inlet terminal shock flow problems. In general, works aimed at clarifying the fluid mechanical processes involved in the terminal shock region of channel flows are scarce and, in particular, the available data in many cases are not sufficiently complete to form the basis for detailed numerical comparisons. One experimental investigation which gives detailed measurements is that of Bogar, Sajben, Kroutil and Salmon (Refs. 20 and 21) which focuses upon flows in the terminal shock region of inlets/diffusers. More specifically, they investigated transonic flows in nominally two-dimensional, supercritically operated diffusers. These flows exhibit many significant features found in supersonic inlets of aircraft. A detailed description of the diffuser model and results describing both the time-mean and the oscillating flow properties were reported in Ref. 20, while laser Doppler velocimeter measurements were given in Ref. 21. Since these detailed data are considered as reliable and the trends observed are believed to be present in three-dimensional inlet flows as well, this particular data base was selected for designing the test cases for the present effort. The following five cases of different flows have been calculated: (1) two-dimensional subsonic diffuser flow, (2) two-dimensional transonic diffuser flow with a normal shock, (3) two-dimensional supersonic inlet flow with a terminal shock, (4) transient development of normal shock in a two-dimensional convergent-divergent channel and (5) three-dimensional transonic diffuser flow with a normal shock. In all of these calculations the flows are turbulent and, except for case (3), only the asymptotic steady-state solutions are of interest. Furthermore, the selected diffuser/inlet models are either geometrically similar or identical to each other.

A schematic of the inlet/diffuser geometry and the associated coordinate system is shown in Fig. 1. The diffuser/inlet model is a convergent-divergent channel with a flat bottom and a contoured top wall. In addition, the cross-section is rectangular everywhere. A detailed description of this model can be found in Ref. 20 and will not be repeated here. However, it should be noted that the computational domain extends from $3.75h$ upstream of the geometric throat to $8.65h$ downstream of the throat, where h is the throat height. For the three-dimensional calculation, the throat cross-sectional aspect ratio is 3.0 with the computational domain extending from one side wall to the center plane, and no-slip conditions are applied on all solid walls. This is somewhat different from the experimental conditions in which the throat cross-sectional aspect ratio is 4.0 and suction slots are used at several locations to establish the nominal two-dimensionality of the flow.

An important aspect of almost all numerical calculations is the generation of a suitable computational coordinate system. The present approach uses a contour fitted coordinate system in which both top and bottom as well as side channel walls (for the three-dimensional calculation) fall on coordinate lines. As mentioned earlier, high grid resolution near the walls is obtained by employing a hyperbolic tangent grid packing transformation; the streamwise resolution is obtained by clustering grid points near the location of sharp contraction of the contour as well as near the expected location of the shock. This grid is accomplished by using a versatile grid distribution generator which allows multiple regions of grid packing (Ref. 9). For the present calculations, 31 grid points are used in the transverse direction (x-direction) while 41 grid points are used in the streamwise direction (z-direction). In addition, for three-dimensional case, 16 grid points are used in the spanwise direction (y-direction). Results of all the five test cases were obtained with the same grid distributions.

For all of the test calculations, the Reynolds number based on the inlet core flow condition and the throat height is approximately 4.73×10^5 , the inlet core Mach number is approximately 0.46 for cases (1), (2), (4) and (5) while it is approximately 1.90 for case (3). Under the assumption that the flows are at constant total temperature, the equations solved are the continuity equation and momentum equations. The previously described mixing length model

and shock capturing technique are used to provide turbulent viscosity and to locate the shock. As for the boundary conditions, no-slip condition together with zero first derivative of the static pressure (with respect to the transverse computational coordinate) are imposed along the top and bottom walls. For three-dimensional case, no-slip condition together with zero first derivative of the static pressure (with respect to the spanwise computational coordinate) are applied along the side wall while the symmetry conditions are used for the center plane. At the exit where the flows are subsonic for all test cases, constant static pressure is specified and the second streamwise (computational coordinate) derivatives of all velocity components are set to be zero. For cases (1), (2), (4) and (5) the flows at the inlet are subsonic, the core flow total conditions together with wall boundary layer thicknesses and profile shapes of the streamwise velocity component are specified. In addition, the second streamwise (computational coordinate) derivatives of static pressure and velocity components in the cross-sectional plane are set to be zero. Experience indicates that it may be beneficial to freeze the cross-sectional velocity components after the initial impulsive transients had passed and this is done for case (5) to obtain the highly damped solution. As for the profile of the streamwise velocity component, the profile suggested by Musker (Ref. 22) supplemented by the Van Driest transformation (Ref. 23) to account for the effects of compressibility is adopted. In case (3), the flow at the inlet section is supersonic except in wall regions of the boundary layer, the velocity components, the density and the static enthalpy (temperature) are specified for the supersonic portion while the second streamwise (computational coordinate) derivatives of the velocity components and the pressure are set to be zero for the subsonic portion of the inflow section. Consequently, the density and temperature in the subsonic portion are calculated in accordance with the specified total enthalpy (temperature) and the equation of state. In this way, the disturbances occurring in the subsonic portions of the internal flow field are allowed to propagate through the upstream inflow section.

Since the governing equations are time-dependent, initial conditions are needed to start the calculation. In general, a relatively simple approximation to the flow field suffices as an initial condition, however, if a better estimate is easily available it should be used. The construction of the initial

conditions for each test case will be described in the following section. However, a general comment concerning the presence of the discontinuities in the initial conditions should be made here, since it is relevant to the terminal shock type of calculations. One of the most important reasons for the occurrence of surfaces of discontinuity in a gas is the possibility of discontinuities in the initial conditions. These conditions may in general be prescribed arbitrarily. It is known, however, that certain conditions must hold on stable surfaces of discontinuity in a gas; for instance, the discontinuities of pressure, density, etc. in a shock wave are related by the Rankine-Hugoniot relations. It is, therefore, clear that if these conditions are not satisfied in the initial discontinuity, it cannot continue to be a discontinuity at subsequent instants. Instead, it generally splits into several discontinuities (e.g. shock wave, tangential discontinuity and rarefaction wave); in the course of time, these discontinuities of different types move apart. Their propagation, reflection and subsequent interactions may cause undesirable transient impulsives with the possible consequences of prolonged computing time or even the instability of the calculation. Therefore, special attention should be paid to the construction of the initial condition for the terminal shock type of problems.

Computed Results

The previously described test cases cover various flow regimes occurring in a diffuser/inlet model. Depending on the specified upstream and downstream boundary conditions, the resultant internal flow field can be quite different in nature. In most of these cases, asymptotic steady-state solutions are of interest, however, physically meaningful transient solutions for the formation of shock waves have also been obtained. In addition, the effects of artificial dissipation on the numerical solutions have been studied and a three-dimensional calculation has been carried out. A vast amount of information is obtained from the computation of these test cases, and only selected, representative results are to be presented here. The relevant flow parameters describing these cases are given in Table I. These calculations were considered to reach an asymptotic steady-state when there was virtually no change in the wall static pressure

distributions over a (dimensionless) time interval of 2 to 6, where a dimensionless time of 12 is the time required for a particle moving at the inlet velocity to pass from inlet to exit, and the changes in other flow variables were of very minor significance. In addition, the maximum residual decreased by one to two orders of magnitude, depending upon the initial conditions and the flow problems.

TABLE I - Parameters for Test Cases

Case	Type	Re_h	Inlet Core Mach No.	Inlet Top Wall Boundary Layer Thickness δ/h	Inlet Bottom Wall Boundary Layer Thickness δ/h	Inlet Side Wall Boundary Layer Thickness δ/h
1	2-D, Steady Subsonic	4.73×10^5	0.46	0.12149	0.060745	/
2	2-D, Steady Transonic with Shock	4.73×10^5	0.46	0.12149	0.060745	/
3	2-D, Steady Supersonic with Terminal Shock	4.73×10^5	1.90	0.12149	0.060745	/
4	2-D, Transient Formation of a Normal Shock	4.73×10^5	0.46	0.12149	0.060745	/
5	3-D, Steady Transonic with Normal Shock	4.73×10^5	0.46	0.12149	0.060745	0.060745

Case (1): Steady 2-D Subsonic Diffuser Flow

The calculation was initiated with an initial condition which consisted of a one-dimensional inviscid flow corresponding to the specified diffuser contour with a simple boundary layer correction applied in the vicinity of no-slip surfaces. With this initial condition, it took about 60 time steps to reach an asymptotic steady state solution for $\sigma_x = \sigma_z = \sigma = 0.5$ (which corresponds to a cell Reynolds number of 2). At this stage, the artificial dissipation parameters were then lowered to $\sigma = 0.05$ (which corresponds to a cell Reynolds number 20), and it took about another 50 time steps to reach an asymptotic steady state wherein no observable changes occurred over a wide variation in time steps. The calculated top wall pressure distribution is depicted in Fig. 2, while the calculated bottom wall pressure distribution is shown in Fig. 3. For the purpose of reference, some relevant measured data for shocked flow, which is established by a lower exit pressure ($P_e = 0.933$ as compared to the present 0.96), are also given. It is obvious that the choice of the artificial dissipation parameters significantly affect the computed results. Previous experience at SRA with second order artificial dissipation calculations for transonic shock waves has indicated that accurate results and sharp shock representation can be obtained when σ is limited to 0.05. Although experimental data for this case is not available, the results shown in Figs. 2 and 3 are physically realistic. The wall pressures follow the data for a lower back pressure until slightly upstream of the throat as is expected. Since the calculation and the data are for cases with different back pressures, the results diverge as the throat is approached.

Case (2): Steady 2-D Transonic Diffuser Flow with a Normal Shock

The solutions obtained with exit pressure $P_e = 0.96$ and the artificial dissipation $\sigma = 0.5$ was used as the initial condition for this calculation. At first, the back pressure was dropped to 0.933 over a short period of time and then fixed for the subsequent computations. After approximately 40 time steps an asymptotic steady state solution for $P_e = 0.933$ and $\sigma = 0.5$ was obtained. Then the artificial dissipation parameter σ was dropped to 0.05 and after another 40 time steps, the final steady-state solution for $P_e = 0.933$ and $\sigma = 0.05$ was reached. The calculated top wall pressure distribution is given in Fig. 4 and the calculated bottom wall pressure distribution is shown in Fig. 5. The calculated results for $\sigma = 0.05$ agree very well with the corresponding experimentally measured data (case denoted by $M_{ou} = 1.235$ in

Ref. 20). Again, the artificial dissipation parameter plays an important role, the shock is captured with $\sigma = 0.05$ while the results are severely smeared with $\sigma = 0.5$. In fact, the $\sigma = 0.5$ calculation does not even contain a supersonic region (Fig. 6). Further investigation of the sensitivity of the calculated flow fields with respect to the choice of the artificial damping parameter σ has been carried out for $\sigma = 0.1$. The calculated wall static pressure distributions for this value of σ are essentially the same as those for $\sigma = 0.05$ and are not presented here. Therefore, it may be concluded that the present numerical results are insensitive to the choice of the parameter σ when σ is in the range from 0.1 to 0.05. It is noted that, based upon previous experience for shocked flow, if no artificial dissipation were used the calculation would be unstable. However, as indicated by the present calculations, if too much artificial dissipation is used the solution would be unrealistically contaminated by its presence.

Case (3): Steady 2-D Supersonic Inlet Flow with Terminal Shock

The construction of the initial condition for this case was essentially the same as that for Case (1) except that, by applying the Rankine-Hugoniot relations, an initial discontinuity of the pseudo two-dimensional flow field was generated in the vicinity and downstream of the geometrical throat. The pressure boundary condition at the exit was specified with its ratio to the pressure at the inflow section being 5.70; this value is consistent with the initially assumed shock wave. Such a back pressure was held fixed for subsequent calculations. The calculation required 70 time steps to reach an asymptotic steady-state solution for $\sigma = 0.5$, and then, after lowering the artificial dissipation parameter to 0.1, another additional 50 time steps was needed to reach the final asymptotic steady state solutions where no further observable changes in the solution occurred. In Fig. 7 a schematic flow field is depicted; the difference in the streamwise and normal scales used in this figure should be noted. An oblique shock is formed in the region of the compression corner of the top wall (ramp) while near the bottom wall (cowl) a Mach reflection occurs and the terminal shock stands at approximately one throat height downstream of the geometric throat. The existence of the Mach reflection is consistent with the prediction due to the inviscid theory by noting that the core flow Mach Number near the inflow section is about 1.90 and the deflection angle of the top wall is about 18° , under such conditions a regular reflection of the incident shock wave is not possible. Instead, a Mach reflection

must occur. At the compression corner there exists a separation region induced by the adverse pressure gradients near the wall. A relatively large shock-induced separation zone exists in the Mach reflection region. Further, there are terminal shock-induced separation regions along the top and bottom walls, although the one along the bottom wall is very thin. In Fig. 8 the corresponding dimensionless static pressure distribution along the top wall is presented and in Fig 9 the corresponding dimensionless static pressure distribution along the bottom wall is shown. No experimental data are available for comparison, nevertheless, these results are qualitatively in agreement with the known features of the supersonic inlet flow. The above calculations demonstrate the capability of the MINT code to compute turbulent flows in various flight regimes, as shown by the Mach Number contours depicted in Figs. 10a, b and c. In these figures, the main flow direction is from left to right. For Fig. 10a and Fig. 10b, the minimum contour value is 0.432 with constant increment of 0.032, while for Fig. 10c, the minimum contour value is 0.46 with constant increment of 0.06, the displayed domain extends from the inflow section to $3.4 h$ downstream of the throat where h is the throat height. Figure 10a shows the Mach Number contours of a subsonic diffuser flow, Fig. 10b illustrates that of a supercritically operated transonic diffuser flow with a normal shock region and Fig. 10c gives the Mach Number contours of a supersonic inlet in which the existence of the oblique shock waves, Mach leg and a terminal shock region is evident. The corresponding static pressure contours are given in Figs. 11a, b and c.

Case (4): Unsteady Shock Development in a 2-D Transonic Diffuser

An investigation of the formation of the normal shock by lowering the back pressure (P_e) from that of a subsonic diffuser flow to that of a supercritically operated transonic diffuser flow also has been performed. The calculation started with the steady-state solution of the subsonic flow ($P_e = 0.96$ and $\sigma = 0.05$) and over a very short period of time the back pressure was dropped to 0.933 which was then held as constant. Small artificial dissipation parameter ($\sigma = 0.05$) and (constant) small dimensionless time step ($\Delta t = 0.05$) were used. Figure 12 shows the transient development of the static pressure along the top wall and Fig 13 shows the transient development of the static pressure along the bottom wall. As it can be seen, the final asymptotic steady-state solutions agree very well with the corresponding experimentally measured data (case denoted by $M_{ou} = 1.235$ in Ref. 20). Although a dimensionless

time interval of 18 units was required for the flow to change from one steady-state (subsonic mode without shock) to another steady-state (transonic mode with a normal shock), the corresponding physical time interval is only about 0.53×10^{-2} second. Since its response to the changes of the back pressure are very rapid for this transient flow, very little information about the fluid mechanical process involved in the formation of shock has been provided by most of the relevant experiments for this problem. Some basic features of such a process are revealed by the present numerical investigation and will be presented here. The transient as well as spatial developments of the flow field are illustrated by Fig. 14, which is a history of Mach Number contours in a region which extends from two throat height upstream of the throat to 6 throat heights downstream of the throat. The minimum contour level is 0.432 with a constant increment of 0.032. The corresponding time history of static pressure contours are given in Fig. 15. In the early stages of the development, the disturbances originating at the outflow section propagate in the direction of the upstream; in particular, the propagating speed of the disturbances within the (contoured) top wall boundary layer is relatively large. Once these faster moving disturbances reach the throat region, disturbances transverse to the mean flow are generated, which then continue to propagate up-and downstream as they approach the (flat) bottom wall. In the later stages of shock development, disturbances propagating in upstream, downstream and transverse directions are undoubtedly present and they can interact with each other, but the most important disturbances responsible for the formation of the shock are the transverse waves originating at the boundary layer/core-flow interface, which are strongly influenced by the viscous-inviscid interactions.

Although the present calculation focuses upon the formation of the shock due to the small changes of the back pressure, the results obtained do strongly suggest that a one-dimensional inviscid approach is not appropriate for analyzing the response of the terminal shock in a supersonic inlet to the back pressure disturbances (i.e. the hammer shock problem). Such an indication is further supported by the results obtained from a relevant experimental work (Ref. 24) in which the shock motion induced by externally applied disturbances were investigated for a supercritically operated transonic diffuser.

Case (5): Steady 3-D Transonic Diffuser Flow with a Normal Shock

This calculation was initiated with an initial condition which consisted of a 2-D highly damped ($\sigma = 0.5$) solution with a simple boundary layer correction applied in the vicinity of the side wall ($y = 0$). With these initial conditions, it took about 80 time steps to reach an asymptotic steady-state solution for $\sigma_x = \sigma_y = \sigma_z = 0.5$. Then the calculation proceeded with reduced σ_z ($= 0.05$) for another 60 time steps. Finally, an additional 50 time steps were advanced with $\sigma_x = \sigma_y = \sigma_z = 0.05$ to reach an asymptotic steady state. The calculated top wall pressure distribution is given in Fig. 16 while the computed bottom wall pressure distribution is shown in Fig. 17. As would be expected for this flow, the 3-D results agree quite well with the 2-D numerical results of Case (2) and the nominally 2-D experimental data (Ref. 20), except that the 3-D shock is slightly weaker than, and its position is slightly upstream of the 2-D shock. The variation of the wall static pressure in the spanwise direction is small, as is shown in Fig. 18, which depicts the pressure contours at various spanwise locations. The displayed region extends from two throat heights upstream of the throat to 6 throat heights downstream of the throat. The minimum contour level is 0.502 with a constant increment of 0.02. Figure 19 presents the streamwise Mach Number distribution. Points A are inside the side wall boundary layer and Points B are on the center (symmetry) plane. Both Points A and B are located slightly below the midplane of each cross-section. The spanwise variation of the Mach Number contours is illustrated in Fig. 20, in which the displayed region is the same as that in Fig. 18, but the minimum contour level is 0.432 with a constant increment of 0.032. It is noted that, contrary to the static pressure distribution, the Mach Number distribution exhibits strong spanwise dependence.

As mentioned above, the strength of the three-dimensional shock is slightly weaker than its two-dimensional counterpart; such a three-dimensional effect on the shock strength is also reported in a recent work on the inviscid transonic flow in an axial compressor rotor (Ref. 28). Further, the position of the weaker 3-D shock is slightly upstream of the position of its corresponding stronger 2-D shock; this is consistent with the fact that the flows are in a supercritically operated inlet/diffuser.

Concluding Remarks

Due to the complexity of the fluid mechanics involved in the terminal shock region of the inlet, the three-dimensional ensemble-averaged compressible time-dependent Navier-Stokes equations in conjunction with suitable turbulence modeling and shock capturing technique have been used to study the terminal shock type of flow problems. The numerical scheme for solving the governing equations is based on a linearized block implicit approach which is embodied in a general computer code termed "MINT". The MINT code has been applied to calculate turbulent flows in various flight regimes occurring in a diffuser/inlet model. These high Reynolds number calculations are: (1) 2-D, steady, subsonic; (2) 2-D, steady, transonic with normal shock, (3) 2-D, steady, supersonic with terminal shock, (4) 2-D, transient process of shock development and (5) 3-D steady, transonic with normal shock. As an indication of the validity of these computations, the numerical results obtained for the 2-D/3-D transonic diffuser flows have been compared with corresponding experimental data, the calculated wall static pressure distributions agree quite well with the experimentally measured data. Also studied is the role of the artificial dissipation in the shock capturing technique, inappropriate choice of the artificial dissipation will severely smear the shock. These extensive and carefully designed calculations demonstrate the capabilities of the MINT code for predicting the complex flows commonly occurring in the engine inlets. Further investigations should concentrate on the problems concerning the response of the terminal shock to the externally applied disturbances and the effects of the turbulence modeling on the small scale flow properties. In this respect, the turbulence models for three-dimensional terminal shock flows are of particular concern.

APPENDIX - SOLUTION PROCEDURE [17]

Background

The solution procedure employs a consistently-split linearized block implicit (LBI) algorithm which has been discussed in detail in [13, 15].

There are two important elements of this method:

- (1) the use of a noniterative formal time linearization to produce a fully-coupled linear multidimensional scheme which is written in "block implicit" form; and
- (2) solution of this linearized coupled scheme using a consistent "splitting" (ADI scheme) patterned after the Douglas-Gunn [16] treatment of scalar ADI schemes.

The method is thus referred to as a split linearized block implicit (LBI) scheme. The method has several attributes:

- (1) the noniterative linearization is efficient;
- (2) the fully-coupled linearized algorithm eliminates instabilities and/or extremely slow convergence rates often attributed to methods which employ ad hoc decoupling and linearization assumptions to identify nonlinear coefficients which are then treated by lag and update techniques;
- (3) the splitting or ADI technique produces an efficient algorithm which is stable for large time steps and also provides a means for convergence acceleration for further efficiency in computing steady solutions;
- (4) intermediate steps of the splitting are consistent with the governing equations, and this means that the "physical" boundary conditions can be used for the intermediate solutions. Other splittings which are inconsistent can have severe difficulties in satisfying physical boundary conditions [15].
- (5) the convergence rate and overall efficiency of the algorithm are much less sensitive to mesh refinement and redistribution than algorithms based on explicit schemes or which employ ad hoc decoupling and linearization assumptions. This is important for accuracy and for computing turbulent flows with viscous sublayer resolution; and

- (6) the method is general and is specifically designed for the complex systems of equations which govern multiscale viscous flow in complicated geometries.

This same algorithm was later considered by Beam and Warming [25], but the ADI splitting was derived by approximate factorization instead of the Douglas-Gunn procedure. They refer to the algorithm as a "delta form" approximate factorization scheme. This scheme replaced an earlier non-delta form scheme [26], which has inconsistent intermediate steps.

Spatial Differencing and Artificial Dissipation

The spatial differencing procedures used are a straightforward adaption of those used in [13] and elsewhere. Three-point central difference formulas are used for spatial derivatives, including the first-derivative convection and pressure gradient terms. This has an advantage over one-sided formulas in flow calculations subject to "two-point" boundary conditions (virtually all viscous or subsonic flows), in that all boundary conditions enter the algorithm implicitly. In practical flow calculations, artificial dissipation is usually needed and is added to control high-frequency numerical oscillations which otherwise occur with the central-difference formula.

In the present investigation, artificial (anisotropic) dissipation terms of the form

$$\sum_j \frac{d_j}{h_j^2} \frac{\partial^2 u_k}{\partial x_j^2} \quad (1)$$

are added to the right-hand side of each (k-th) component of the momentum equation, where h_j is the metric coefficient and for each coordinate direction x_j , the dimensionless artificial diffusivity d_j is positive and is chosen as the larger of zero and the local quantity $\mu_e (\sigma \text{Re}_{\Delta x_j} - 1)/\text{Re}$. Here, μ_e is the effective dynamic viscosity and the local cell Reynolds number $\text{Re}_{\Delta x_j}$ for the j-th direction is defined by

$$\text{Re}_{\Delta x_j} = \text{Re} |\rho u_j| \Delta x_j / \mu_e \quad (2)$$

This treatment lowers the formal accuracy to $O(\Delta x)$, but the functional form is such that accuracy in representing physical shear stresses in thin shear layers with small normal velocity is not seriously degraded. This latter property follows from the anisotropic form of the dissipation and the combination of both small normal velocity and small grid spacing in thin shear layers.

Split LBI Algorithm

Linearization and Time Differencing

The system of governing equations to be solved consists of three/four equations: continuity and two/three components of momentum equation in three/four dependent variables: ρ, u, v, w . Using notation similar to that in [13], at a single grid point this system of equations can be written in the following form:

$$\partial H(\phi)/\partial t = D(\phi) + S(\phi) \quad (3)$$

where ϕ is the column-vector of dependent variables, H and S are column-vector algebraic functions of ϕ , and D is a column vector whose elements are the spatial differential operators which generate all spatial derivatives appearing in the governing equation associated with that element.

The solution procedure is based on the following two-level implicit time-difference approximations of (3):

$$(H^{n+1} - H^n)/\Delta t = \beta(D^{n+1} + S^{n+1}) + (1-\beta)(D^n + S^n) \quad (4)$$

where, for example, H^{n+1} denotes $H(\phi^{n+1})$ and $\Delta t = t^{n+1} - t^n$. The parameter β ($0.5 \leq \beta \leq 1$) permits a variable time-centering of the scheme, with a truncation error of order $[\Delta t^2, (\beta - 1/2) \Delta t]$.

A local time linearization (Taylor expansion about ϕ^n) of requisite formal accuracy is introduced, and this serves to define a linear differential operator L (cf. [13]) such that

$$D^{n+1} = D^n + L^n (\phi^{n+1} - \phi^n) + O(\Delta t^2) \quad (5)$$

Similarly,

$$H^{n+1} = H^n + (\partial H / \partial \phi)^n (\phi^{n+1} - \phi^n) + O(\Delta t^2) \quad (6)$$

$$S^{n+1} = S^n + (\partial S / \partial \phi)^n (\phi^{n+1} - \phi^n) + O(\Delta t^2) \quad (7)$$

Eqs. (5-7) are inserted into Eq. (4) to obtain the following system which is linear in ϕ^{n+1}

$$(A - \beta \Delta t L^n) (\phi^{n+1} - \phi^n) = \Delta t (D^n + S^n) \quad (8)$$

and which is termed a linearized block implicit (LBI) scheme. Here, A denotes a square matrix defined by

$$A \equiv (\partial H / \partial \phi)^n - \beta \Delta t (\partial S / \partial \phi)^n \quad (9)$$

Eq. (8) has $O(\Delta t)$ accuracy unless $H \equiv \phi$, in which case the accuracy is the same as Eq. (4).

Special Treatment of Diffusive Terms

The time differencing of diffusive terms is modified to accomodate cross-derivative terms and also turbulent viscosity and artificial dissipation coefficients which depend on the solution variables. Although formal linearization of the convection and pressure gradient terms and the resulting implicit coupling of variables is critical to the stability and rapid convergence of the algorithm, this does not appear to be important for the turbulent viscosity and artificial dissipation coefficients. Since the relationship between μ_e and d_j and the mean flow variables is not conveniently linearized, these diffusive coefficients are evaluated explicitly at t^n during each time step. Notationally, this is equivalent to neglecting terms proportional to $\partial \mu_e / \partial \phi$ or $\partial d_j / \partial \phi$ in L^n , which are formally present in the Taylor expansion (5), but retaining all terms proportional to μ_e or d_j in both L^n and D^n .

It has been found through extensive experience that this has little if any effect on the performance of the algorithm. This treatment also has the added benefit that the turbulence model equations can be decoupled from the system of mean flow equations by an appropriate matrix partitioning (cf. [15]) and solved separately in each step of the ADI solution procedure. This reduces the block size of the block tridiagonal systems which must be solved in each step and thus reduces the computational labor.

In addition, the viscous terms in the present formulation include a number of spatial cross-derivative terms. Although it is possible to treat cross-derivative terms implicitly within the ADI treatment which follows, it is not at all convenient to do so, and consequently, all cross-derivative terms are evaluated explicitly at t^n . For a scalar model equation representing combined convection and diffusion, it has been shown by Beam and Warming that the explicit treatment of cross-derivative terms does not degrade the unconditional stability of the present algorithm. To preserve notational simplicity, it is understood that all cross-derivative terms appearing in L^n are neglected but are retained in D^n . It is important to note that neglecting terms in L^n has no effect on steady solutions of Eq. (8), since $\phi^{n+1} - \phi^n \equiv 0$ and thus Eq. (8) reduces to the steady form of the equations: $D^n + S^n = 0$. Aside from stability considerations, the only effect of neglecting terms in L^n is to introduce an $O(\Delta t)$ truncation error.

Consistent Splitting of the LBI Scheme

To obtain an efficient algorithm, the linearized system (8) is split using ADI techniques. To obtain the split scheme, the multidimensional operator L is rewritten as the sum of three "one-dimensional" sub-operators L_i ($i = 1, 2, 3$) each of which contains all terms having derivatives with respect to the i -th coordinate. The split form of Eq. (8) can be derived either as in [13, 15] by following the procedure described by Douglas and Gunn [16] in their generalization and unification of scalar ADI schemes, or using approximate factorization. For the present system of equations, the split algorithm is given by

$$(A - \beta \Delta t L_1^n) (\phi^* - \phi^n) = \Delta t (D^n + S^n) \quad (10a)$$

$$(A - \beta \Delta t L_2^n) (\phi^{**} - \phi^n) = A (\phi^* - \phi^n) \quad (10b)$$

$$(A - \beta \Delta t L_3^n) (\phi^{n+1} - \phi^n) = A (\phi^{**} - \phi^n) \quad (10c)$$

where ϕ^* and ϕ^{**} are consistent intermediate solutions. If spatial derivatives appearing in L_i and D are replaced by three-point difference formulas, as indicated previously, then each step in Eqs. (10a-c) can be solved by a block-tridiagonal elimination.

Combining Eqs. (10a-c) gives

$$\begin{aligned} & (A - \beta \Delta t L_1^n) A^{-1} (A - \beta \Delta t L_2^n) A^{-1} (A - \beta \Delta t L_3^n) (\phi^{n+1} - \phi^n) \\ & = \Delta t (D^n + S^n) \end{aligned} \quad (11)$$

which approximates the unsplit scheme (8) to $O(\Delta t^2)$. Since the intermediate steps are also consistent approximations for Eq. (8), physical boundary conditions can be used for ϕ^* and ϕ^{**} [13, 15]. Finally, since the L_1 are homogeneous operators, it follows from Eqs. (10a-c) that steady solutions have the property that $\phi^{n+1} = \phi^* = \phi^{**} = \phi^n$ and satisfy

$$D^n + S^n = 0 \quad (12)$$

The steady solution thus depends only on the spatial difference approximations used for (12), and does not depend on the solution algorithm itself.

REFERENCES

1. Buggeln, R.C., McDonald, H., Levy, R. and Kreskovsky, J.P.: Development of a Three-Dimensional Supersonic Inlet Flow Analysis. NASA CR 3218, 1980.
2. Buggeln, R.C., McDonald, H., Kreskovsky, J.P. and Levy, R.: Computation of Three-Dimensional Supersonic Flow in Inlets. AIAA Paper 80-1094, 1980.
3. Anderson, B.H. and Towne, C.E.: Numerical Simulation of Supersonic Inlets Using a Three-Dimensional Viscous Flow Analysis. AIAA Paper 80-0384, 1980.
4. Buggeln, R.C., McDonald, H., Kim, Y.N.: Computation of Multidimensional Viscous Supersonic Flow. AIAA-83-0177.
5. Levy, R., Briley, W.R. and McDonald, H.: Viscous Primary/Secondary Flow Analysis for Use With Nonorthogonal Coordinate Systems. AIAA-83-0556.
6. Shamroth, S.J., Gibeling, H.J. and McDonald, H.: A Navier-Stokes Solution for Laminar and Turbulent Flow Through a Cascade of Airfoils. AIAA Paper No. 80-1426, 1980.
7. Gibeling, H.J., Shamroth, S.J. and Eiseman, P.R.: Analysis of Strong-Interaction Dynamic Stall for Laminar Flow on Airfoils. NASA CR-2969, April 1978.
8. Thomas, P.D. and Lombard, C.K.: Geometric Conservation Law and its Application to Flow Computations on Moving Grids, AIAA Journal, Vol. 17, No. 10, pp. 1030-1037, 1979.
9. Oh, Y.H.: An Analytic Transformation Technique for Generating Uniformly Spaced Computational Mesh, Final Report, NASA-Langley Research Grant NSG 1087, October, 1978.
10. McDonald, H. and Camarata, F.J.: An Extended Mixing Length Approach for Computing the Turbulent Boundary Layer Development, Proceedings Computation of Turbulent Boundary Layers - 1968 AFOSR-IFP Stanford Conference, Vol. 1, pp. 83-98, 1969.
11. Van Driest, E.R.: On Turbulent Flow Near a Wall. Journal of the Aeronautical Sciences, November 1956.
12. Briley, W.R. and McDonald, H.: Computation of Three-Dimensional Horseshoe Vortex Flow Using the Navier-Stokes Equations. Seventh International Conference on Numerical Methods in Fluid Dynamics, 1980.
13. Briley, W.R. and McDonald, H.: Solution of the Multidimensional Compressible Navier-Stokes Equations by a Generalized Implicit Method. Journal of Computational Physics, Vol. 24, pp. 372-397, 1977.

14. Lindemuth, I. and Killeen, J.: Alternating Direction Implicit Techniques for Two-Dimensional Magnetohydrodynamic Calculations. *Journal of Computational Physics*, Vol. 13, pp. 181, 1973.
15. Briley, W.R. and McDonald, H.: On the Structure and Use of Linearized Block Implicit Schemes. *Journal of Computational Physics*, Vol. 34, pp. 54-72, 1980.
16. Douglas, J. and Gunn, J.E.: A General Formulation of Alternating Direction Methods. *Numerische Math.*, Vol. 6, pp. 428-453, 1964.
17. Briley, W.R., Buggeln, R.C. and McDonald, H.: Computation of Laminar and Turbulent Flow in 90 Degree Square Duct and Pipe Bends Using the Navier-Stokes Equations. SRA Rpt. R82-920009-F, 1982.
18. Shamroth, S.J., McDonald, H. and Briley, W.R.: A Navier-Stokes Solution for Transonic Flow Through a Cascade. SRA Rpt. 81-920007-F, 1982.
19. Shamroth, S.J. and McDonald, H.: An Assessment of an Ensemble-Averaged Navier-Stokes Calculation Procedure for Cascade Flow Fields. SRA Rpt. 82-920011-F, 1982.
20. Bogar, T.J., Sajben, M. and Kroutil, J.C.: Characteristic Frequency and Length Scales in Transonic Diffuser Flow Oscillations. AIAA-81-1291.
21. Salmon, J.T., Bogar, T.J. and Sajben, M.: Laser Velocimeter Measurements in Unsteady, Separated, Transonic Diffuser Flows. AIAA-81-1197.
22. Musker, A.J.: Explicit Expression for the Smooth Wall Velocity Distribution in a Turbulent Boundary Layer. AIAA J. Vol. 17, No. 6, pp. 655-657, 1979.
23. Van Driest, E.R.: Turbulent Boundary Layer in Compressible Fluids. *Journal of the Aeronautical Sciences*, Vol. 18, pp. 145-160 and 216, 1951.
24. Sajben, M., Bogar, T.J. and Kroutil, J.C.: Forced Oscillation Experiments in Supercritical Diffuser Flows with Application to Ramjet Instabilities. AIAA-81-1487.
25. Beam, R.M. and Warming, R.F.: An Implicit Factored Scheme for the Compressible Navier-Stokes Equations. AIAA Journal, Vol. 16, pp. 393-402, 1978.
26. Beam, R.M. and Warming, R.F.: An Implicit Finite-Difference Algorithm for Hyperbolic Systems in Conservation-Law Form. *J.Comp. Physics*. Vol. 22, pp. 87-110, 1976.
27. McDonald, H. and Briley, W.R.: Some Observations on Numerical Solutions of the Three-Dimensional Navier-Stokes Equations. Symposium on Numerical and Physical Aspects of Aerodynamic Flows. January 1981.
28. Xu, J.-z., Jiang, Z.-r., Yang, J.-s., Zhang, Y. and Du, Z.-s.: An Aerothermodynamic Analysis of Transonic Compressor Rotors Containing Three-Dimensional Shocks. *J. of Engineering For Power*, Vol. 104, pp. 386-393, April 1982.

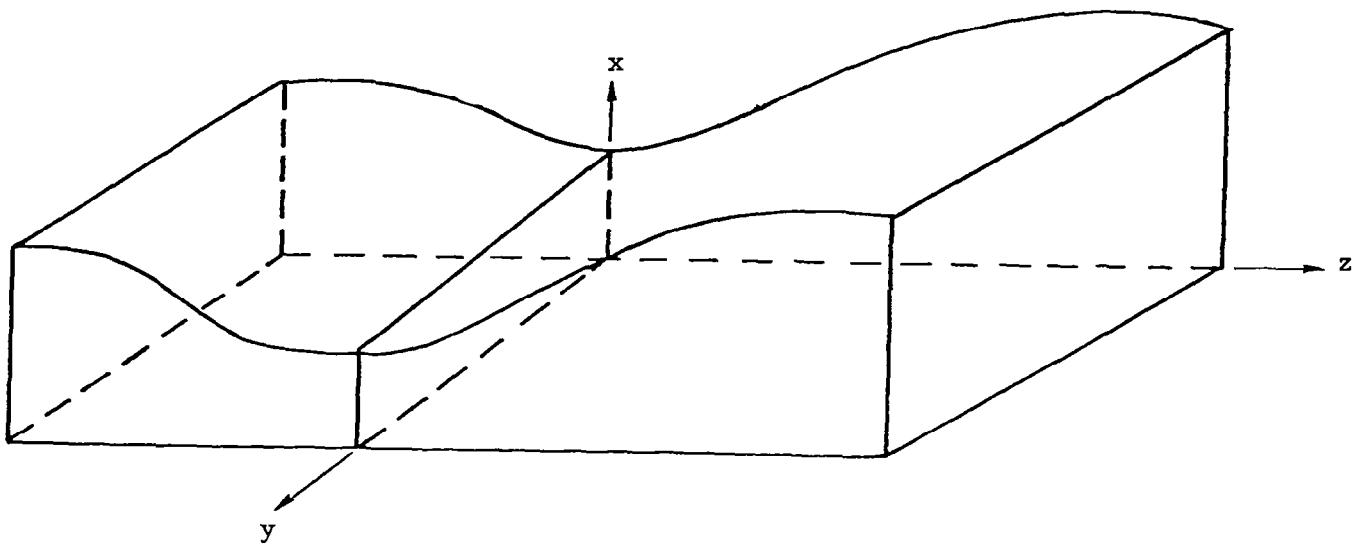


Fig. 1 - Schematic of the inlet/diffuser model.

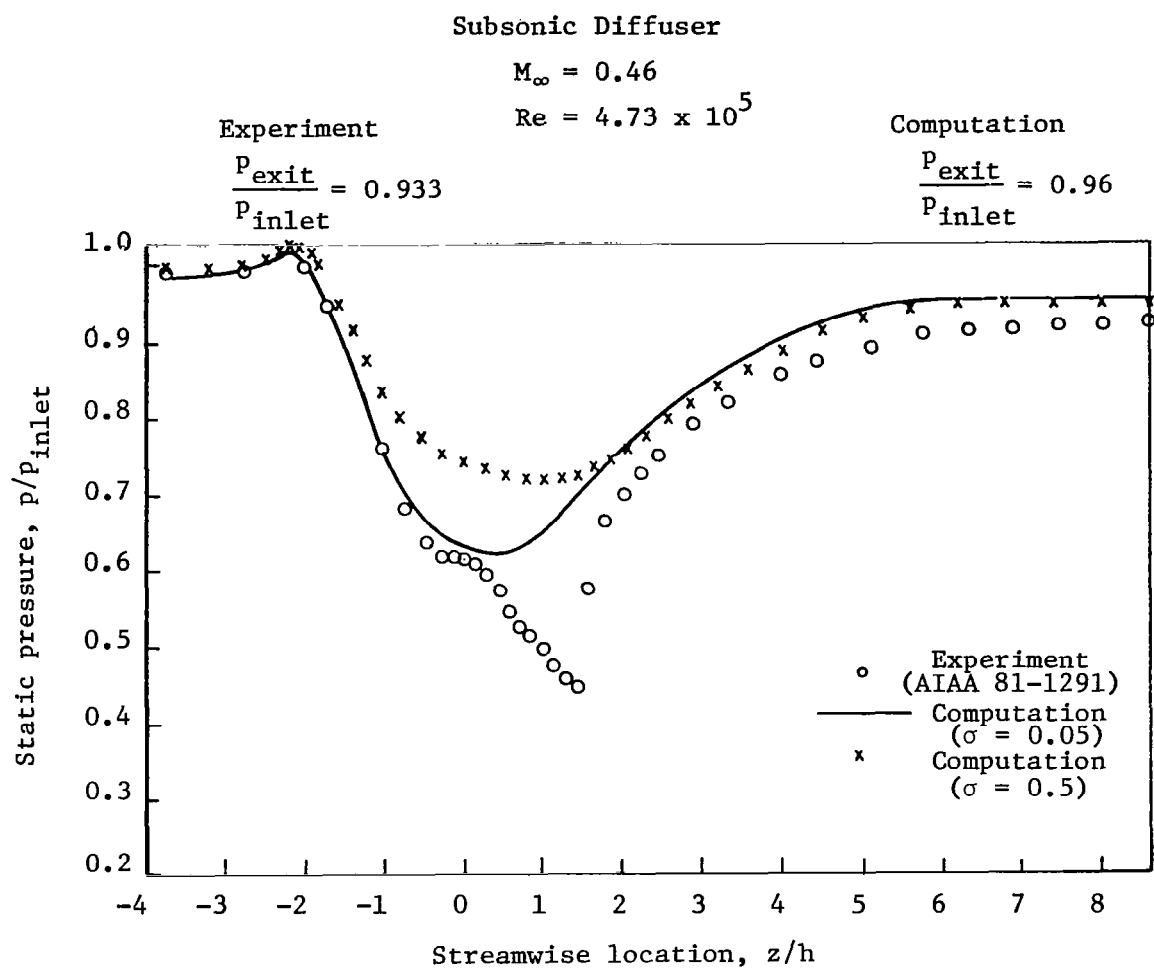


Fig. 2 - Top wall static pressure distribution

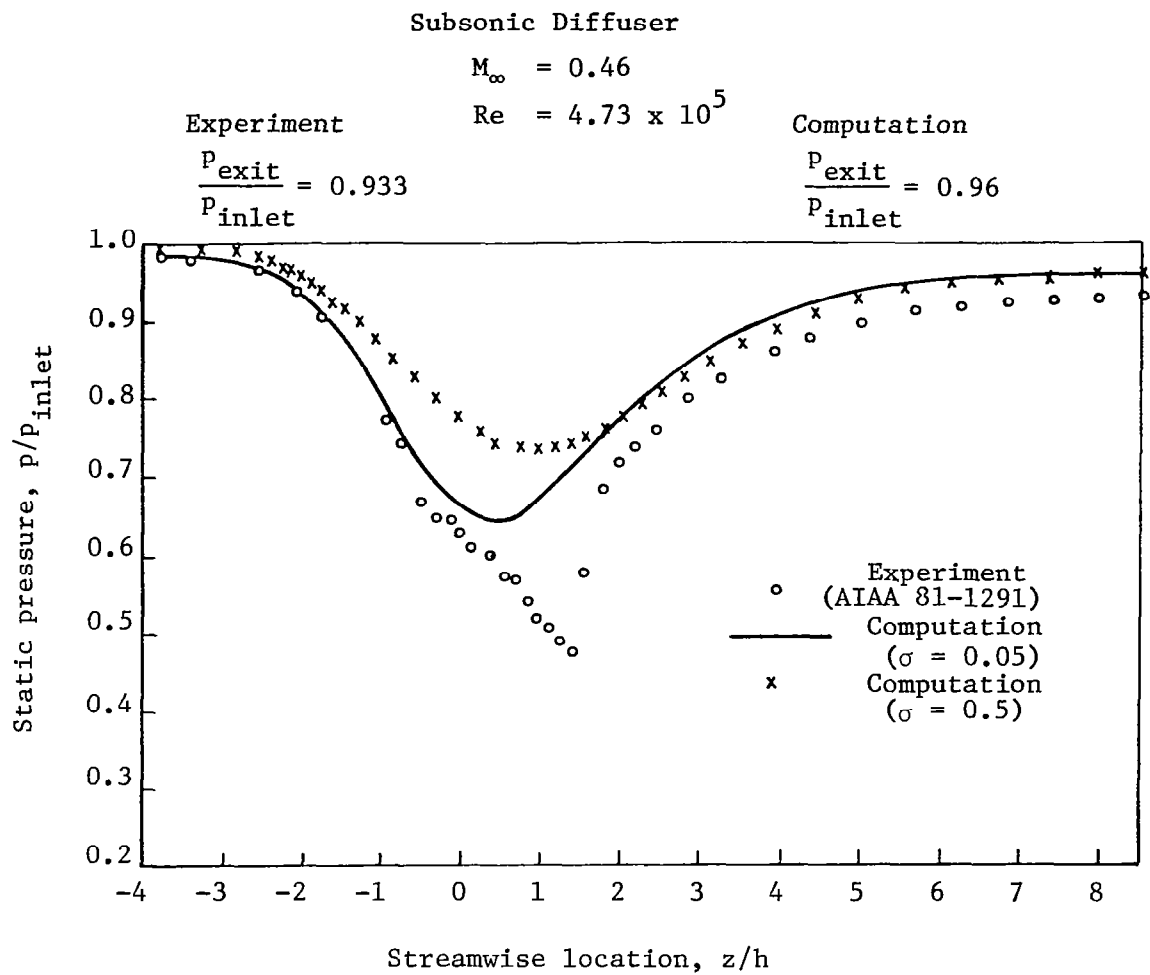


Fig. 3 - Bottom wall static pressure distribution

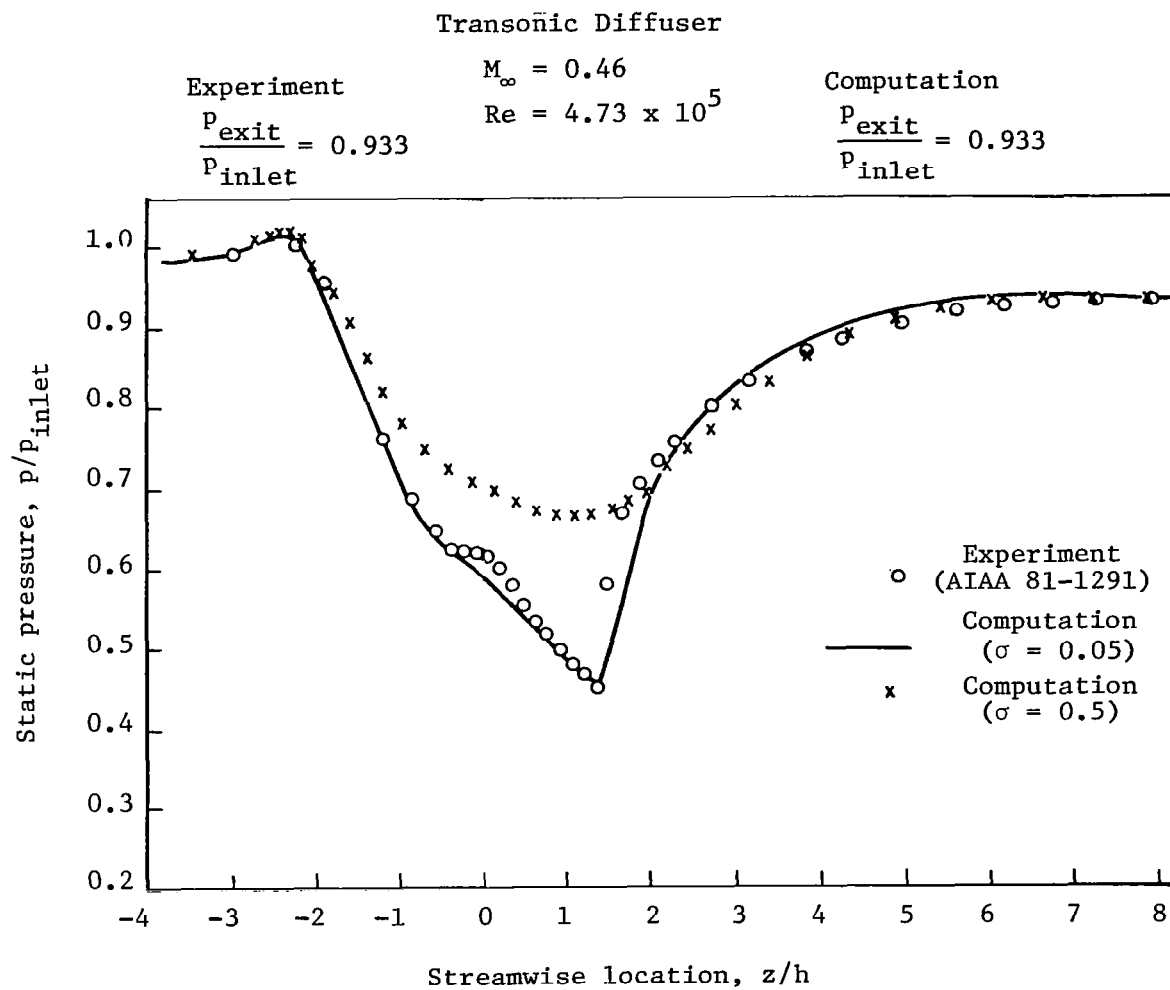


Fig. 4 - Top wall static pressure distribution.

Transonic Diffuser

$$M_{\infty} = 0.46$$

$$Re = 4.73 \times 10^5$$

Experiment
 $\frac{p_{exit}}{p_{inlet}} = 0.933$

Calculation
 $\frac{p_{exit}}{p_{inlet}} = 0.933$

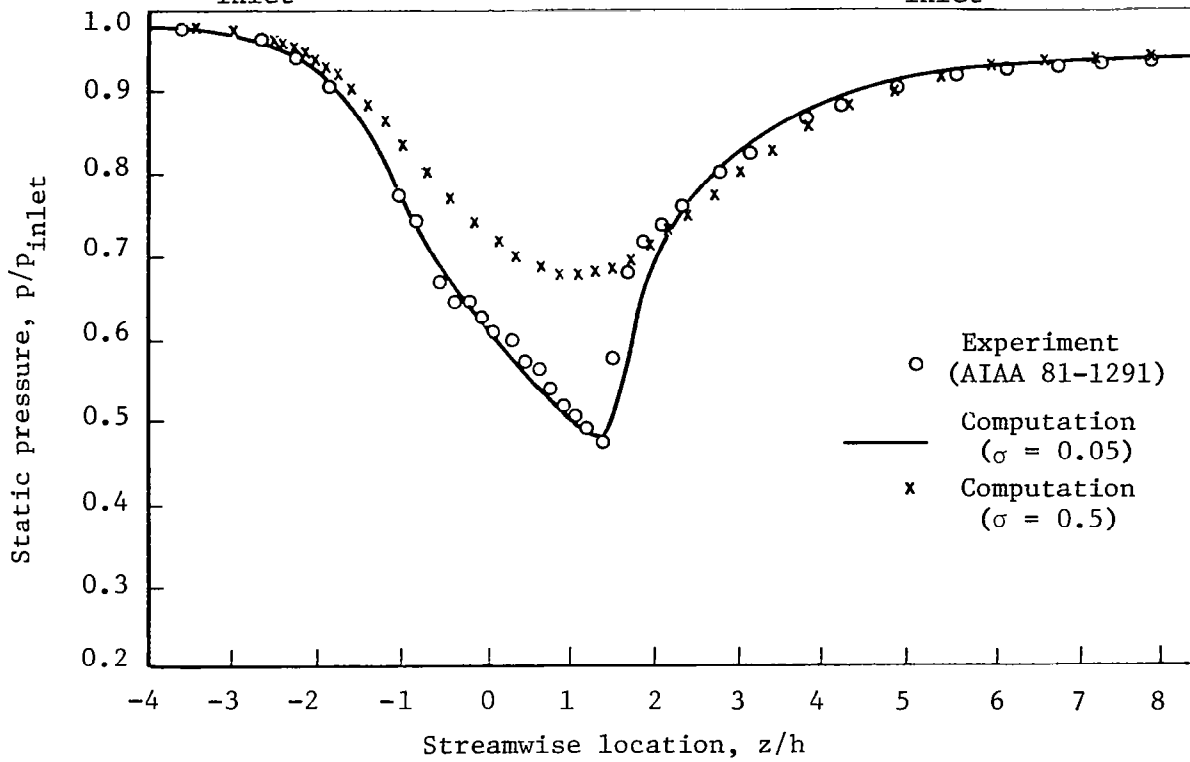


Fig. 5 - Bottom wall static pressure distribution.

Transonic Diffuser

$$M_{\infty} = 0.46$$

$$Re = 4.73 \times 10^5$$

Calculation

$$\frac{p_{exit}}{p_{inlet}} = 0.933$$

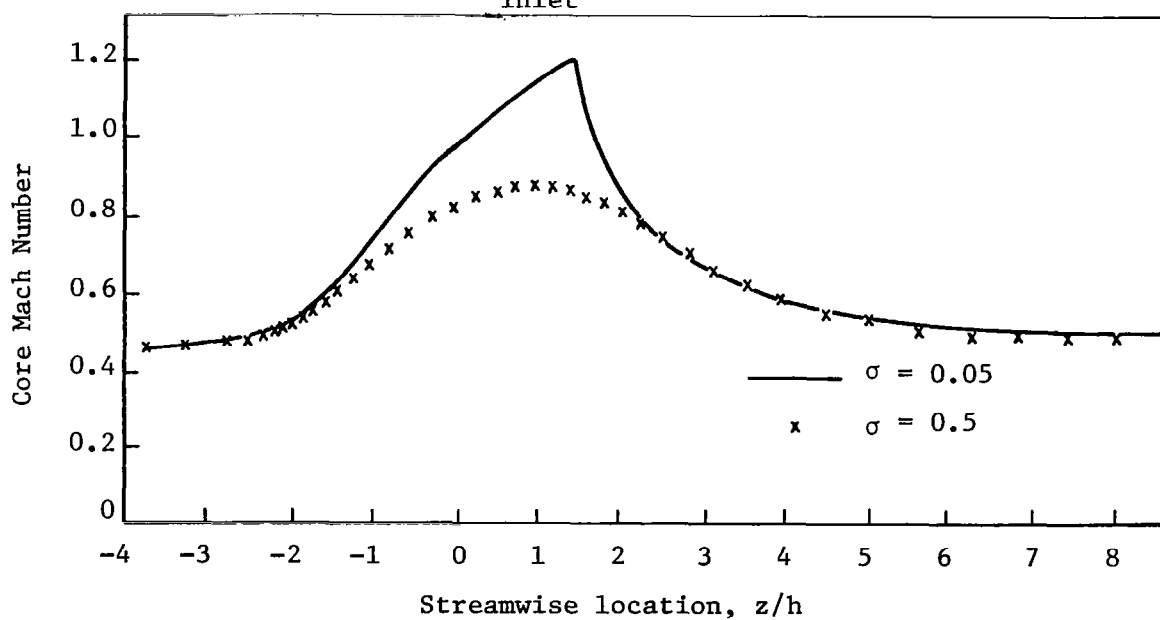


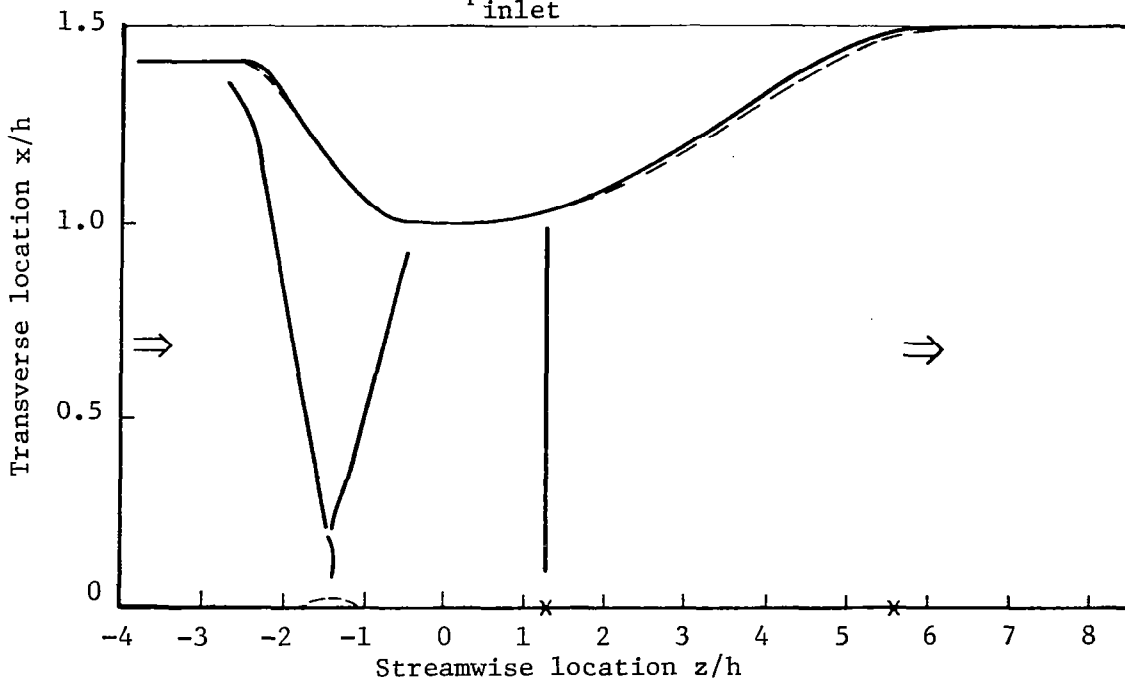
Fig. 6 - Core Mach number distribution and effects of artificial dissipation.

Supersonic Inlet

$$M_{\infty} = 1.90$$

$$Re = 4.73 \times 10^5$$

$$\frac{p_{\text{exit}}}{p_{\text{inlet}}} = 5.70$$



Note: The scale in transverse direction is 5 times larger than the scale in streamwise direction.

Fig. 7 - Schematic flow field.

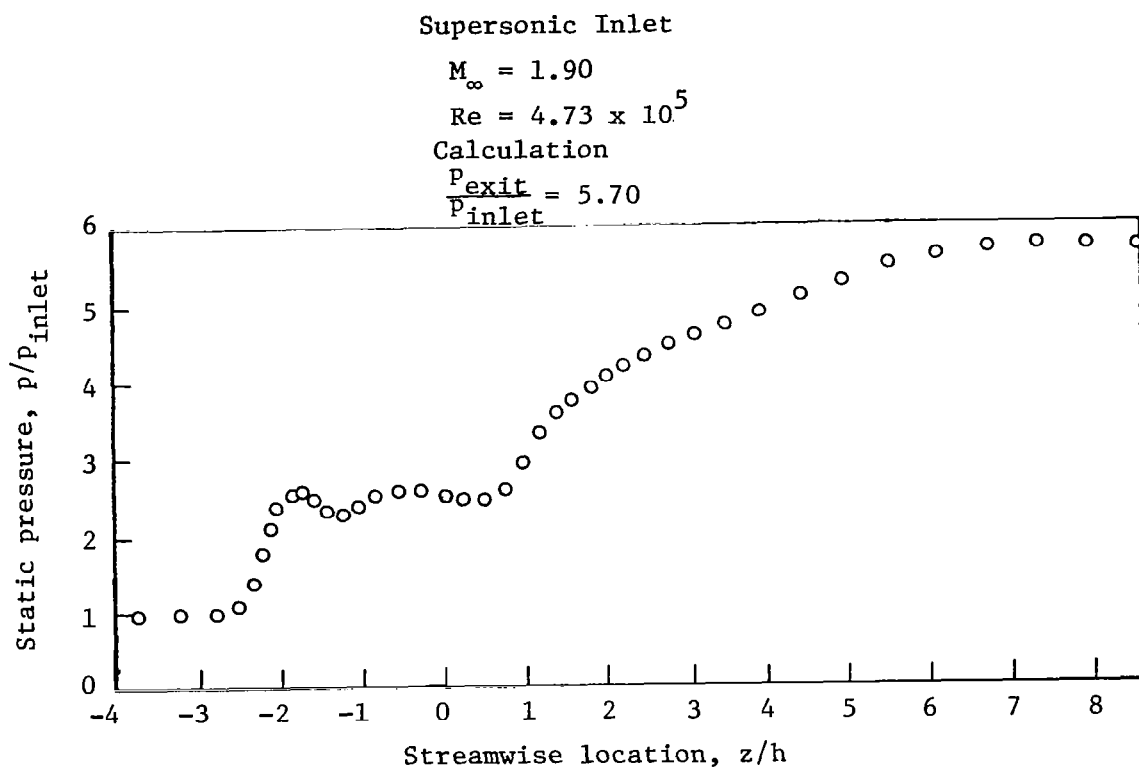


Fig. 8 - Top wall static pressure distribution.

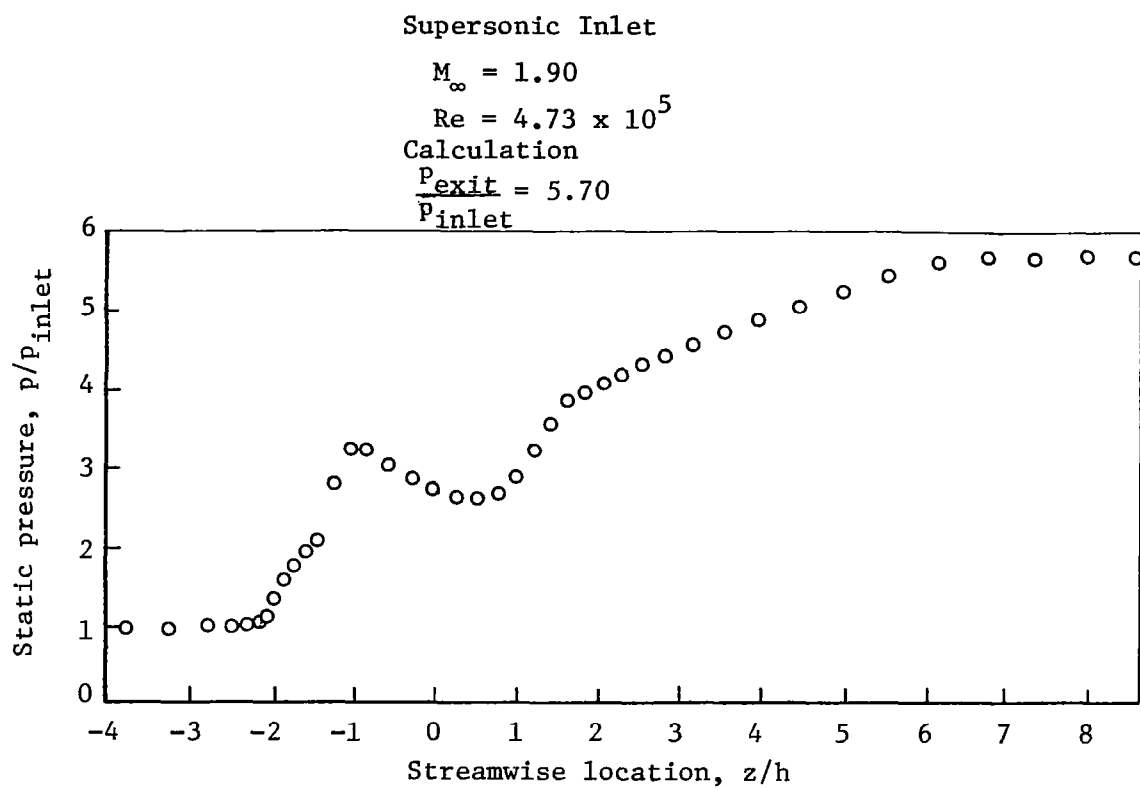
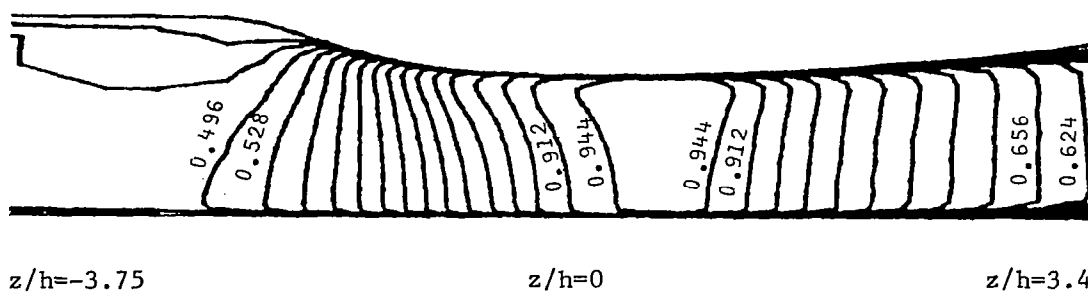
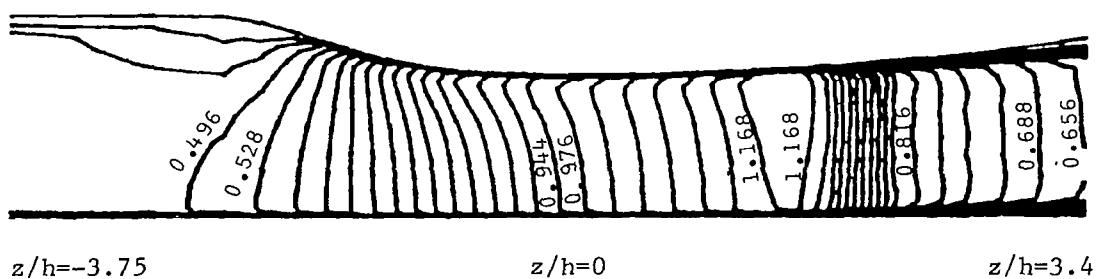


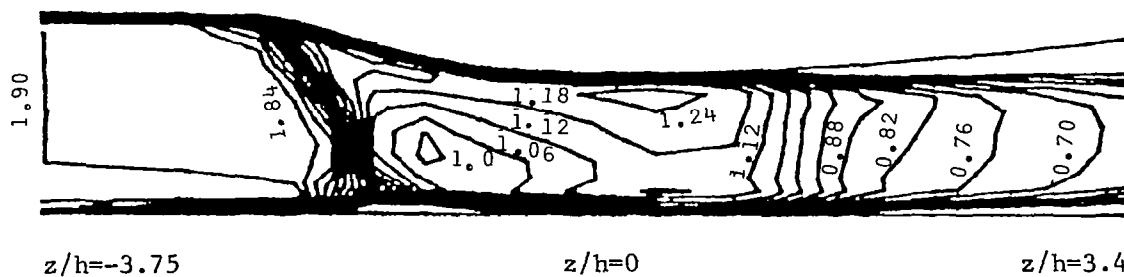
Fig. 9 - Bottom wall static pressure distribution.



(a) Subsonic diffuser

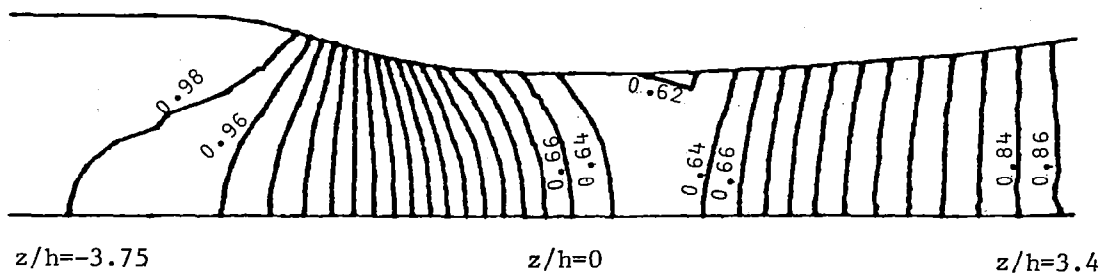


(b) Transonic diffuser

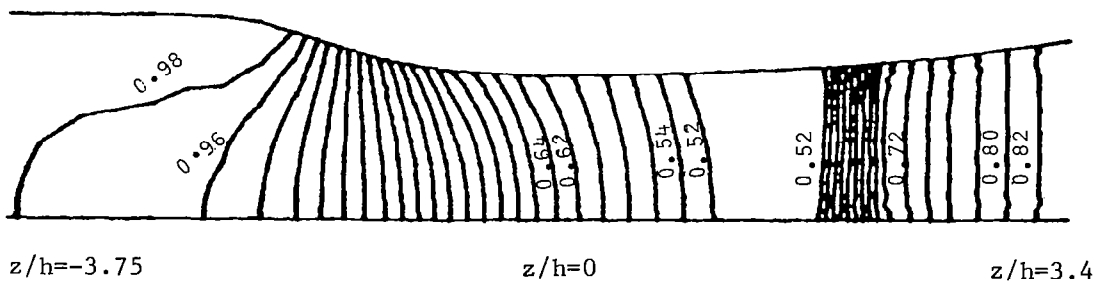


(c) Supersonic inlet

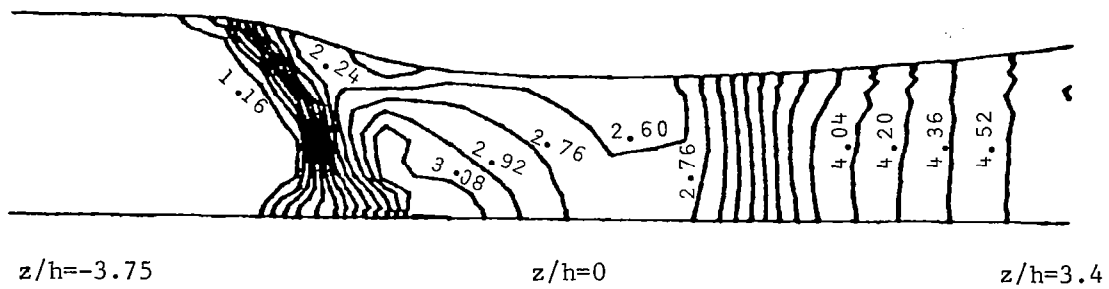
Fig. 10 - Mach number contours.



(a) Subsonic diffuser



(b) Transonic diffuser



(c) Supersonic inlet

Fig. 11 - Dimensionless static pressure contours.

Formation of the shock (transonic diffuser)

$$M_{\infty} = 0.46$$

$$Re = 4.73 \times 10^5$$

t=0:

$$\frac{p_{exit}}{p_{inlet}} = 0.96$$

t>0:

$$\frac{p_{exit}}{p_{inlet}} = 0.933$$

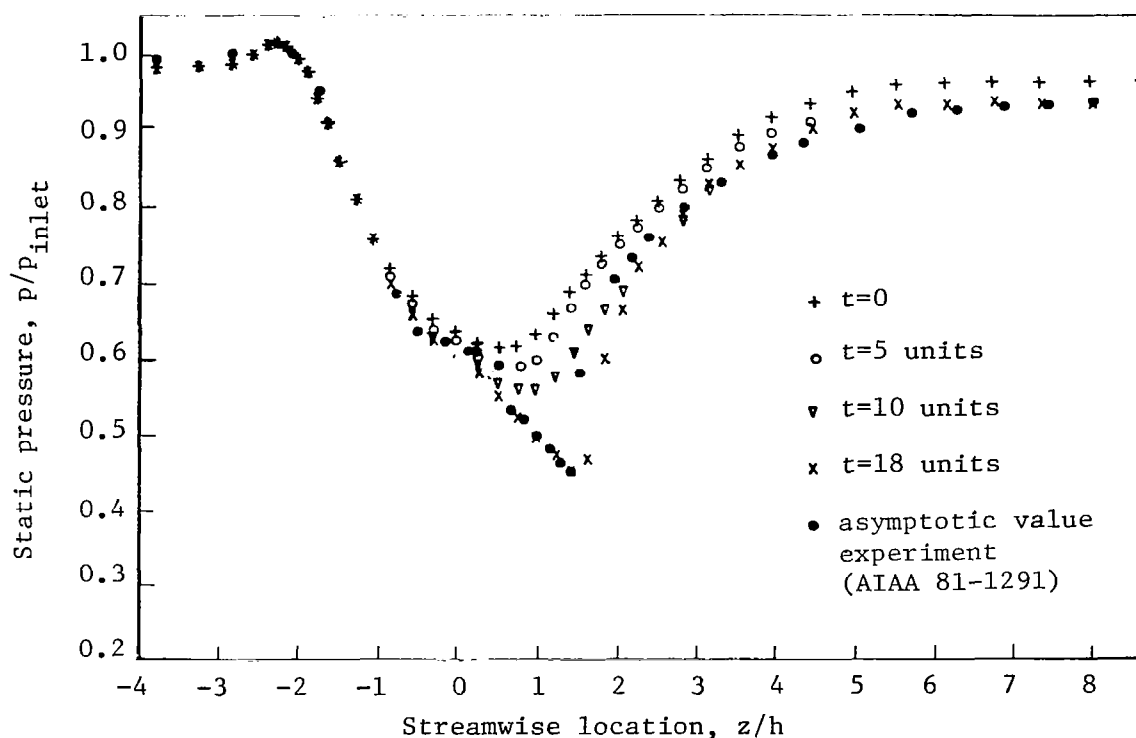


Fig. 12 - Time history of the top wall static pressure distribution. (1 time unit $\approx 0.3 \times 10^{-3}$ sec)

Formation of the shock (transonic diffuser)

$$M_{\infty} = 0.46$$

$$Re = 4.73 \times 10^5$$

t=0:

$$\frac{p_{exit}}{p_{inlet}} = 0.96$$

t>0:

$$\frac{p_{exit}}{p_{inlet}} = 0.933$$

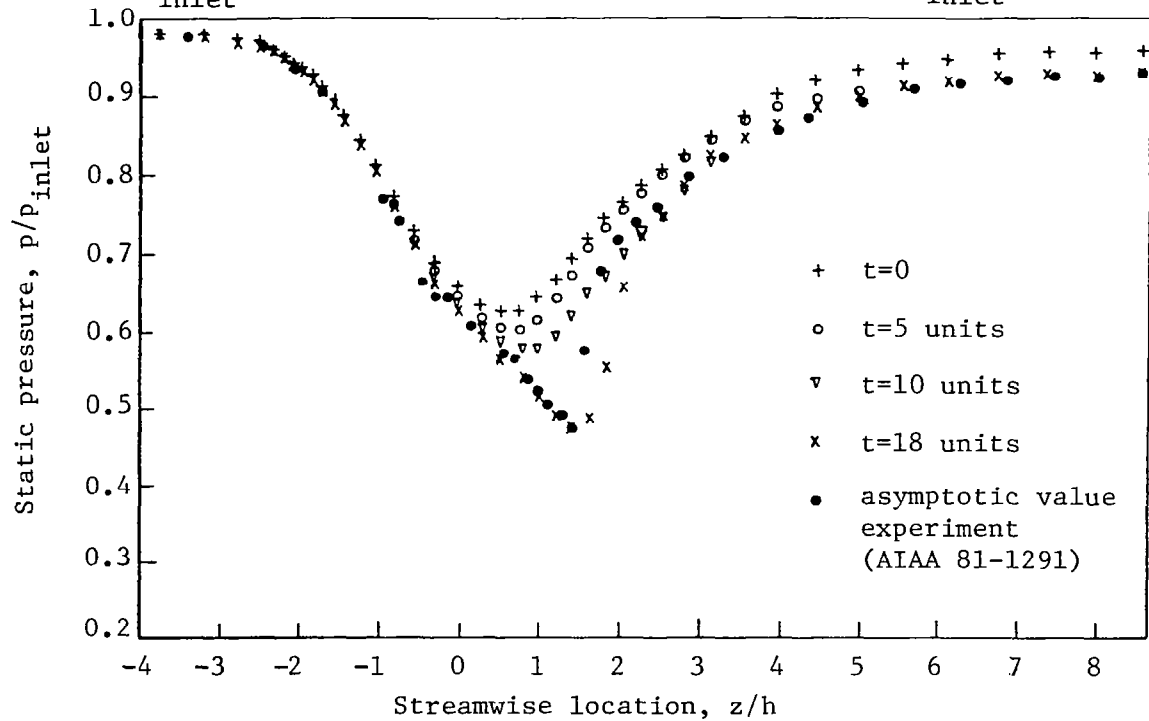
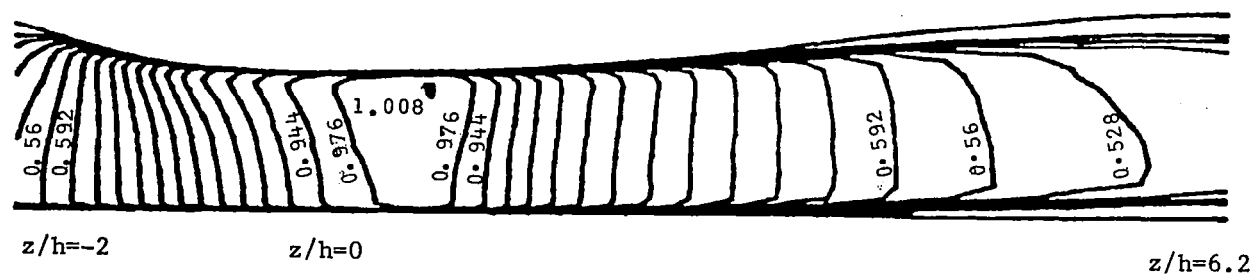
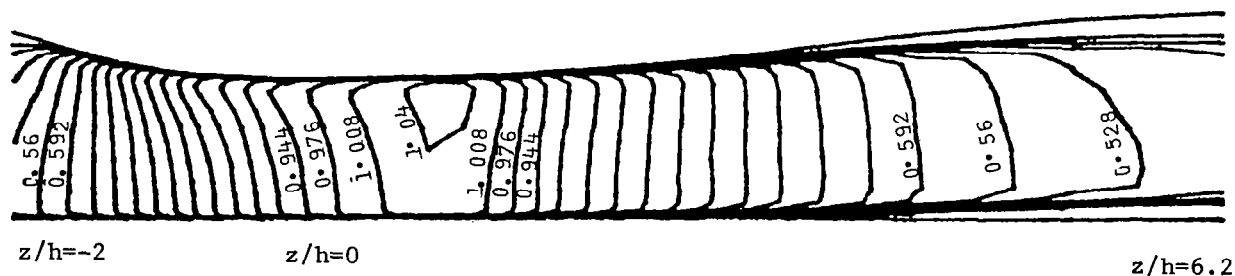


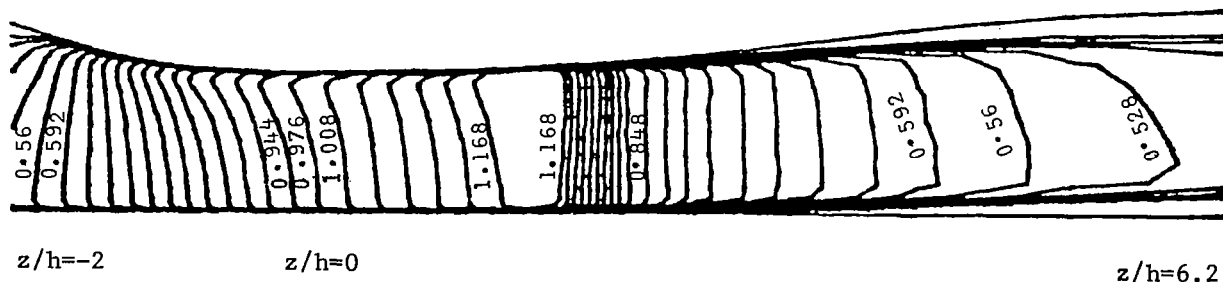
Fig. 13 - Time history of the bottom wall static pressure distribution. (1 time unit $\approx 0.3 \times 10^{-3}$ sec)



(a) $t = 5.0$ units

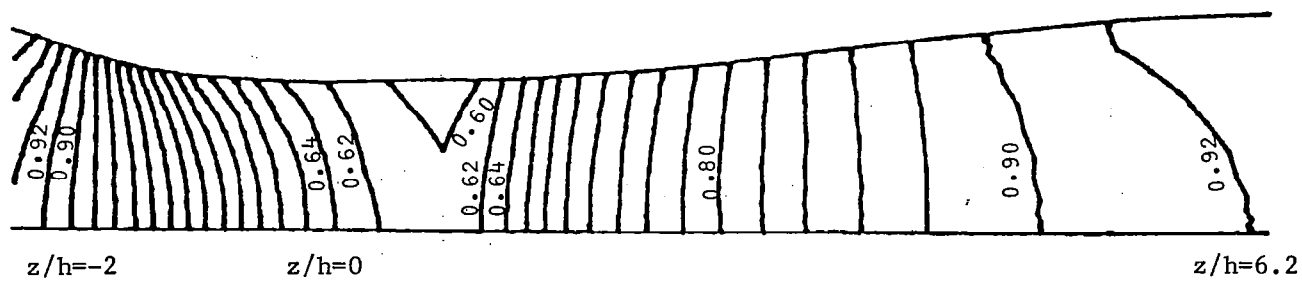


(b) $t = 10.0$ units

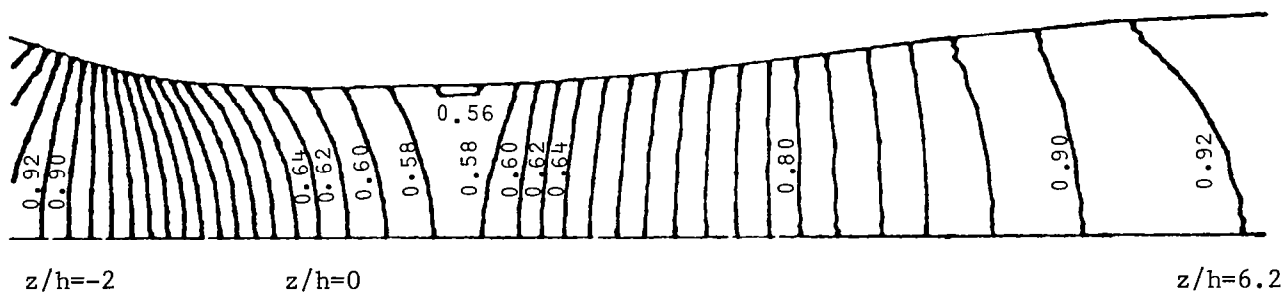


(c) $t = 18.0$ units

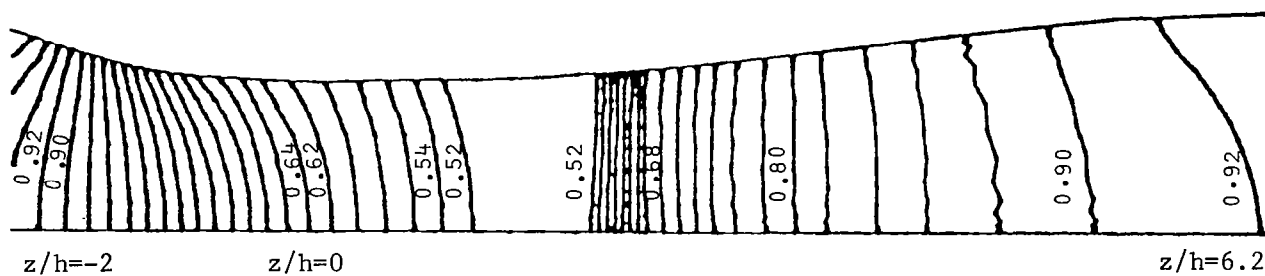
Fig. 14 - Time history of Mach number contours (transonic diffuser).



(a) $t = 5.0$ units



(b) $t = 10.0$ units



(c) $t = 18.0$ units

Fig. 15 - Time history of dimensionless static pressure contours
(transonic diffuser)

Transonic Diffuser (3-D)

$$M_{\infty} = 0.46$$

$$Re = 4.73 \times 10^5$$

Experiment

$$\frac{p_{exit}}{p_{inlet}} = 0.933$$

Calculation

$$\frac{p_{exit}}{p_{inlet}} = 0.933$$

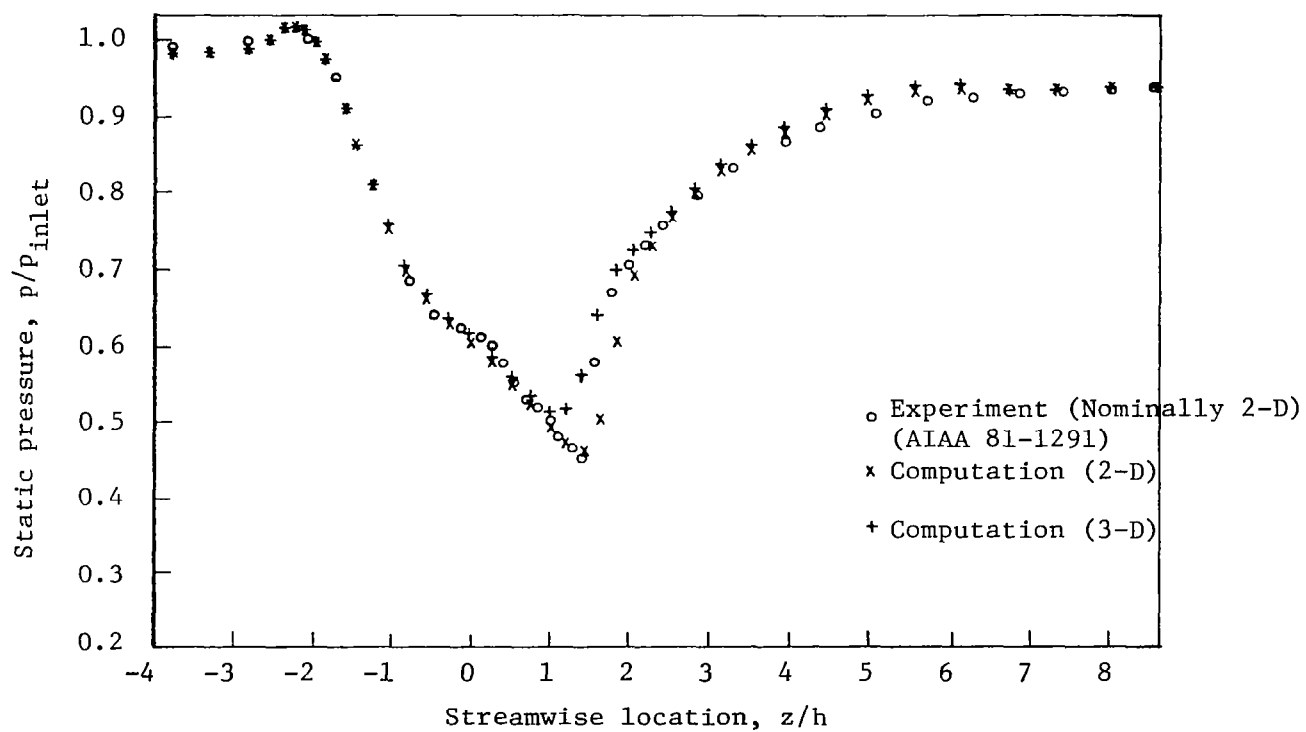


Fig. 16 - Top wall static pressure distribution

Transonic Diffuser (3-D)

$$M_{\infty} = 0.46$$

$$Re = 4.73 \times 10^5$$

Experiment

$$\frac{p_{exit}}{p_{inlet}} = 0.933$$

Calculation

$$\frac{p_{exit}}{p_{inlet}} = 0.933$$

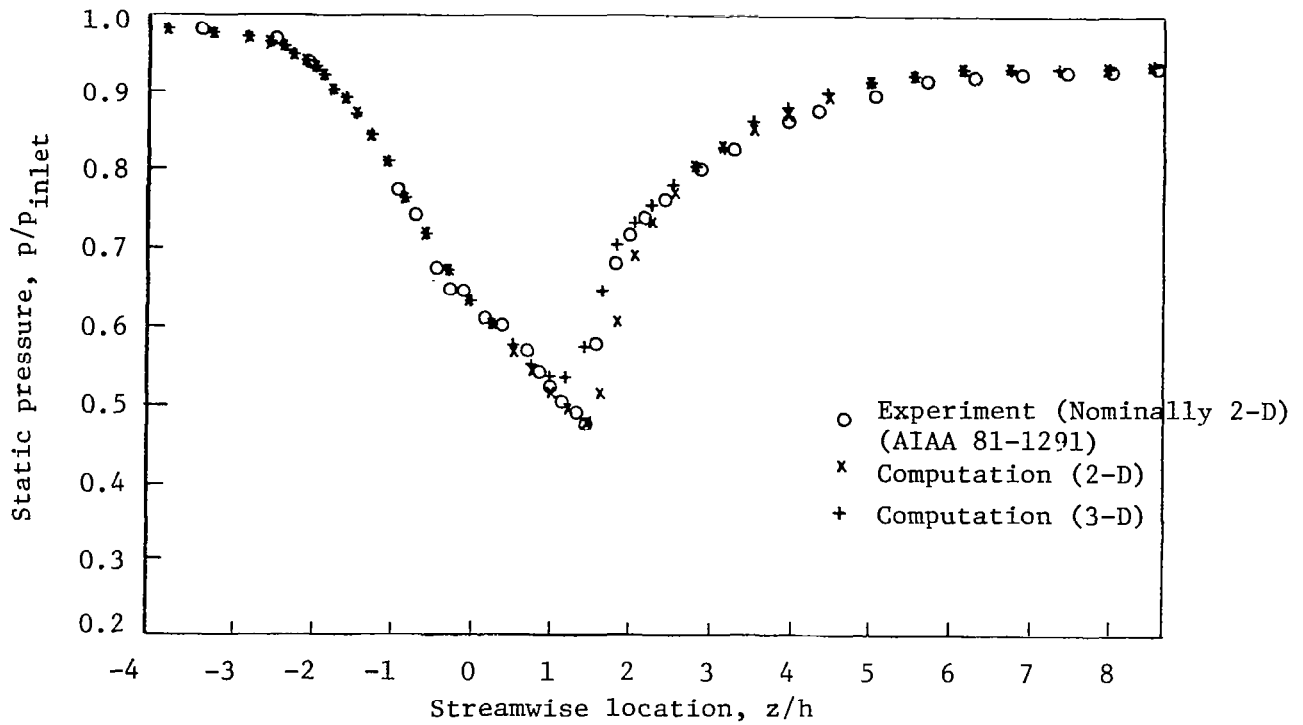
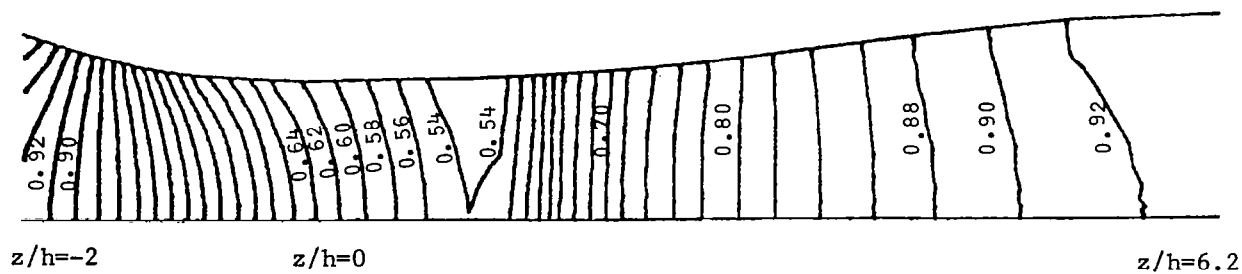
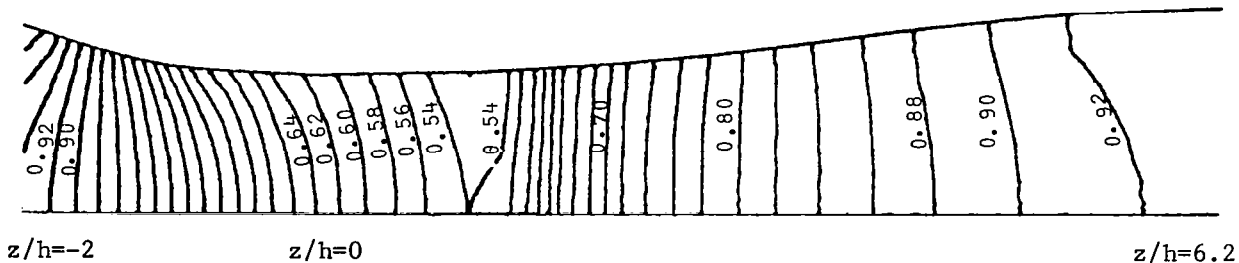


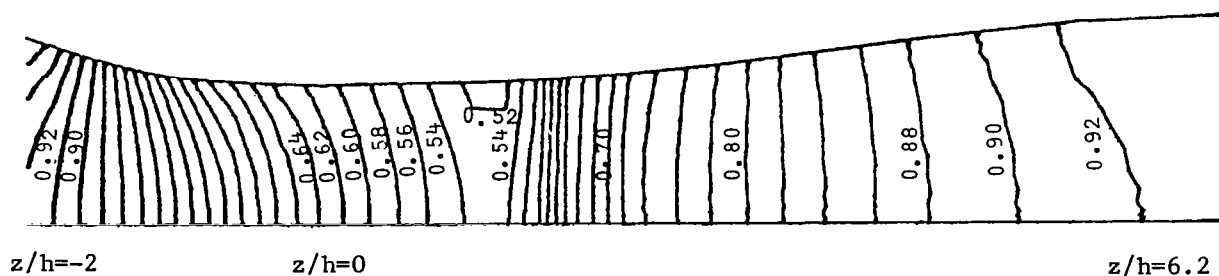
Fig. 17 - Bottom wall static pressure distribution



(a) $y/h = 0.216 \times 10^{-1}$



(b) $y/h = 0.732 \times 10^{-1}$



(c) $y/h = 1.50$

Fig. 18 - Dimensionless static pressure contours (3-D, transonic diffuser)

Transonic diffuser (3-D)

$$M_{\infty} = 0.46$$

$$Re = 4.73 \times 10^5$$

$$\frac{p_{exit}}{p_{inlet}} = 0.933$$

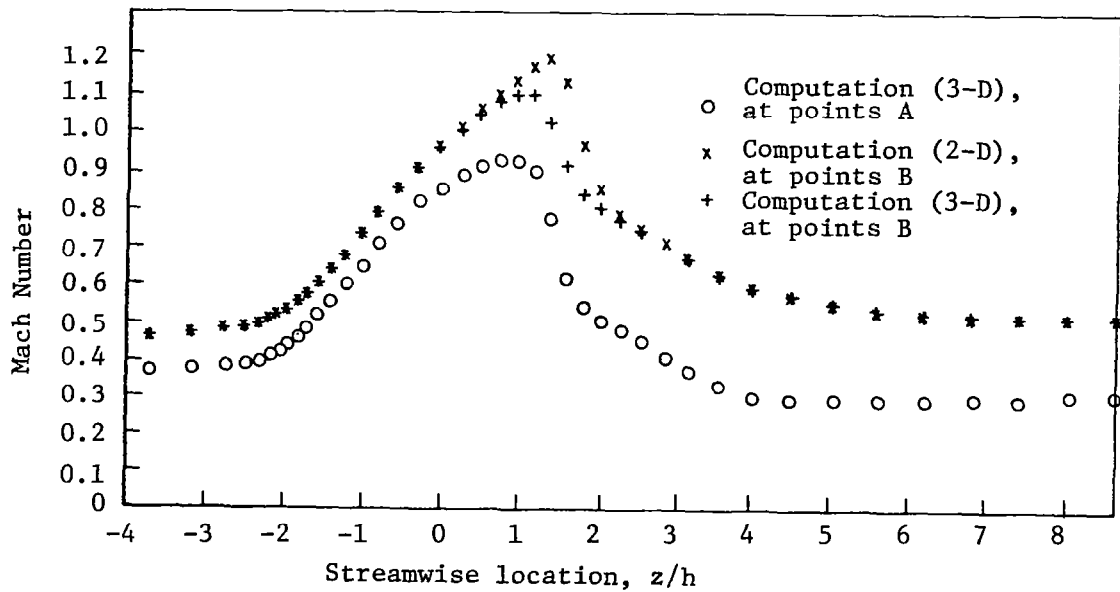
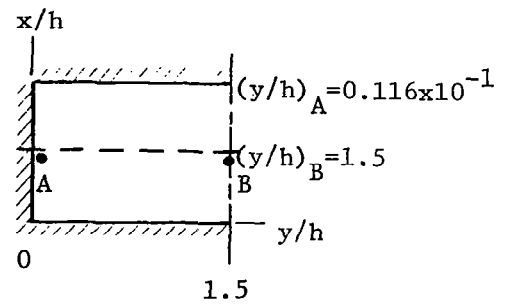
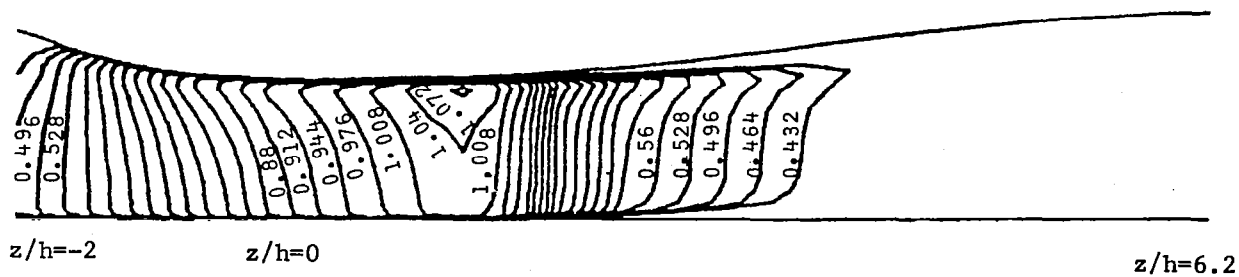
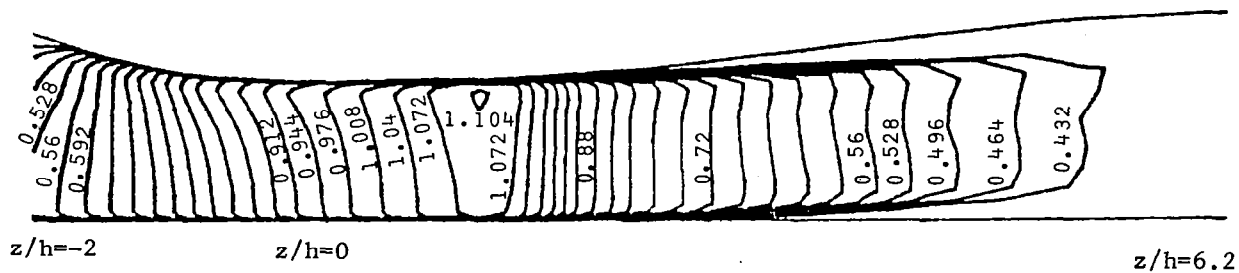


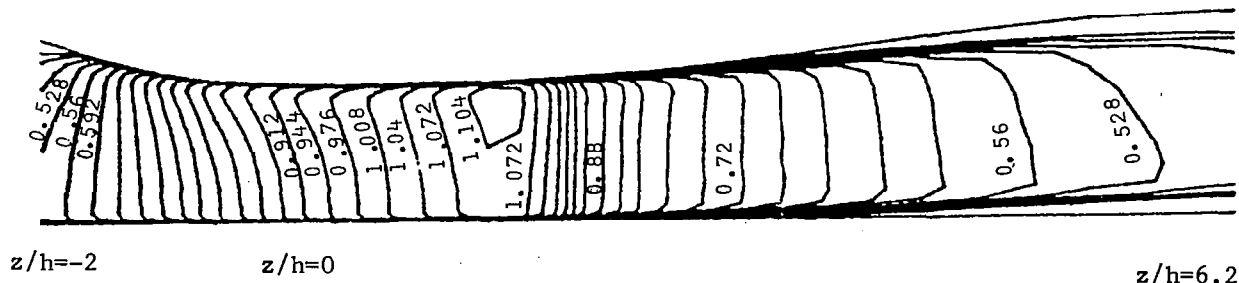
Fig. 19 - Streamwise Mach No. distribution



(a) $y/h = 0.216 \times 10^{-1}$



(b) $y/h = 0.732 \times 10^{-1}$



(c) $y/h = 1.50$

Fig. 20 - Mach Number contours (3-D, transonic diffuser)

User's Manual

The present manual is prepared for the INLTS.G01 CODE, which is the first version of the MINT INLET CODE. This particular version of the code is being stored on the Lewis IBM 370-3033 with TSS operating system and is written to solve the multi-dimensional ensemble-averaged time-dependent Navier-Stokes equations for turbulent, shocked flows in contoured, straight ducts with rectangular cross-sections. The coordinate system is nonorthogonal, contour-fitted and the equations are cast into the so-called strong conservation form. For the present time, the solution of the energy equation is replaced by the assumption that the total temperature is constant throughout the flowfield, although an energy equation can be activated. The effects of turbulence are represented by a mixing length model and the shock is captured by a second order artificial dissipation technique. The numerical procedure solves the time-dependent equations beginning with a specified initial condition and appropriate boundary conditions. Detailed descriptions of these various items can be found in the previous sections and will not be repeated here.

The INLTS.G01 CODE combines a BLOCK DATA program (BLKDAT) containing pertinent data statements, a main program (DAL) and a series of subroutines to perform the required calculations. Chart 1 shows the overall program flow, Chart 2 illustrates the input and initialization procedures, Chart 3 is a global description of the execution control. These program flow charts only provide a broad picture of the code. The interested user should consult the program listing about the details. Since the contour of the inlet varies from case to case according to user's interest, the user must set up the particular contour by slightly modifying the following subroutines: TIMGEO, INVICD and SPREAD.

In SUBROUTINE TIMGEO, the variables RBMAX and RBMIN must be specified by the user. RBMAX is the x-coordinate of the top wall at a given streamwise location and RBMIN is the x-coordinate of the bottom wall at the same streamwise location. In SUBROUTINE INVICD, the variable MZSHK must be given by the user. This variable indicates the initial location of the normal shock in the starting flow field, e.g., MZSHK = 10 means that at the 10th streamwise grid point a normal shock will be generated according to the Rankine-Hugoniot relation. Obviously, if the inflow is not supersonic and the

one-dimensional inviscid theory does not indicate an internal supersonic region, then MZSHK must be set to be an integer greater than the total number of streamwise grid points. In SUBROUTINE SPREAD, the variables PINVCD and HEIT must be specified by user. PINVCD is the dimensionless static pressure at the outflow section obtained by the one-dimensional inviscid theory under the condition that the dimensionless static pressure at the inflow section is 1. It should be noted that PINVCD may not be the actual static pressure used as boundary condition at the outflow section. HEIT is the height of the channel at the streamwise location denoted by KZ. Further, the variables MZSHK, PINVCD and HEIT are used only for setting up the starting flow field. The SUBROUTINE WRPLOT deals with the construction of plot files, since this also depends on the specific interest of the user, the coding of this subroutine must also be modified by the user to accommodate the user's interest. Nevertheless, since the structure of this subroutine is consistent with the NASA-Lewis inhouse plotting routines, the modifications should be quite straightforward.

The card input data is all in NAMELIST format: READ1, READ9, DATA1 and INFLW. The NAMELIST READ1 defines the restart option and input/output units. The NAMELIST READ9 specifies the grid parameters, reference quantities, time-step parameters, boundary conditions and print parameters. The NAMELIST DATA1 sets up the streamwise grid distribution, and the NAMELIST INFLW specifies the turbulent compressible boundary layer profiles at the inlet section. In the case of a restart run, the NAMELIST INFLW should not be supplied.

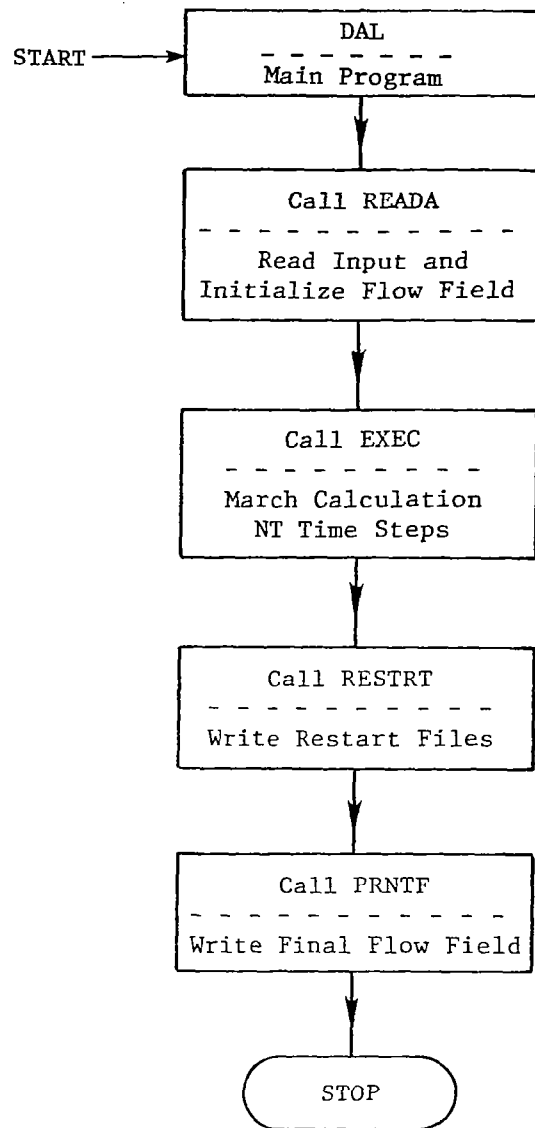


Chart 1. - Overall Program Flow, PROGRAM DAL

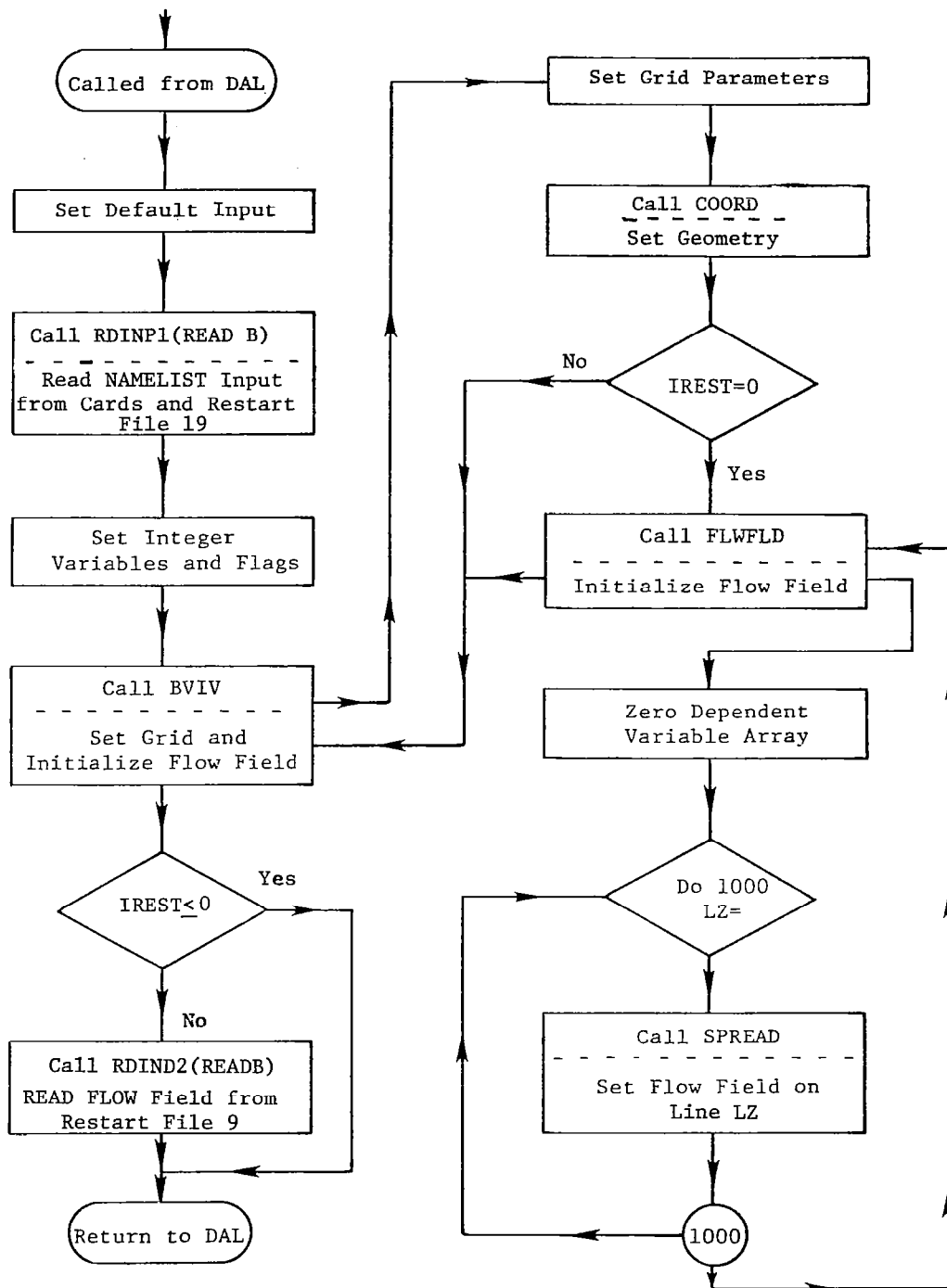


Chart 2. - Program flow chart for SUBROUTINE READA

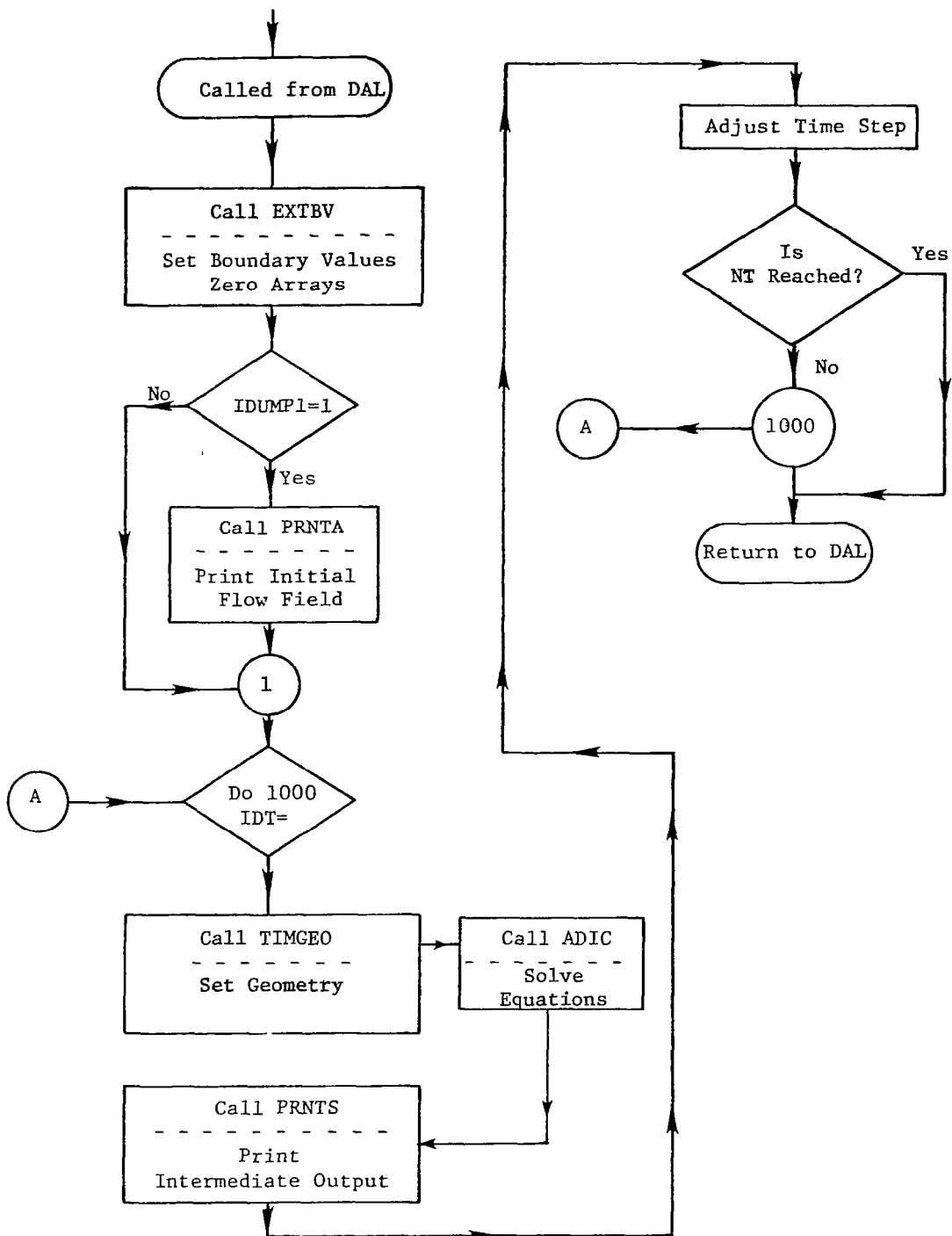


Chart 3. - Program flow chart for SUBROUTINE EXEC

NAMELIST INPUT Description

<u>Namelist or Variable Name</u>	<u>Description</u>
&READ1	
IREST = 0	A new calculation is being started.
IREST = 1	Case is being run from restart files.
IOTAPE =10	Output unit number for dependent variable array restart data.
INTAPE = 9	Input unit number for dependent variable array restart data.
IOTAP1 =20	Output unit number for namelist restart data.
INTAP1 =19	Input unit number for namelist restart data.
&READ9	
NUMDX	Number of interior grid points in the transverse direction (x or y^1 direction). Total number of points in this direction = NUMDX + 2. NUMDX \leq 29.
NUMDY	Number of interior grid points in the spanwise direction (y or y^2 direction). Total number of points in this direction = NUMDY + 2. NUMDY \leq 29.

Namelist or
Variable Name

Description

NUMDZ	Number of interior grid points in the streamwise direction (z or y ³ direction). Total number of points in this direction = NUMDZ + 2. NUMDZ ≤ 59.
XGMIN(1)	Dimensionless value of x-coordinate of the bottom wall at the inflow boundary.
XGMIN(2)	Dimensionless value of y-coordinate of the side wall.
XGMIN(3)	Dimensionless value of z-coordinate at the inflow boundary.
XGMAX(1)	Dimensionless value of x-coordinate of the top wall at the inflow boundary.
XGMAX(2)	Dimensionless value of y-coordinate of the (spanwise) symmetry plane.
XGMAX(3)	Dimensionless value of z-coordinate of the outflow boundary.
GRID(I), I = 1-6	<p>Define $\tau_1 \equiv \text{GRID}(2K-1)$ $\tau_2 \equiv \text{GRID}(2K)$ For each coordinate direction y^k ($K=1,2,3$). τ_1 and τ_2 are the grid stretching parameters for controlling grid spacing near the computational domain boundaries. In the present code this grid distribution technique is used for the x and y directions. The streamwise, z-direction, is constructed via variables in &DATA1. The limits on τ_1 and τ_2 are: $-1 < \tau_1 \leq 0$, $0 \leq \tau_2 < 1$. If $\tau_1 = \tau_2 = 0$, the grid spacing is uniform. If $\tau_1 = 0$, $\tau_2 > 0$, the grid points will be more dense near the XGMAX(K) boundary. If $\tau_1 < 0$, $\tau_2 = 0$, the grid points will be more dense near the XGMIN(K) boundary. The transformation is singular if $\tau_1 = -1$ or $\tau_2 = 1$.</p>

<u>Namelist or Variable Name</u>		<u>Description</u>
XCENTR(I), I=1-3.	= 0	Not used.
DAMPG(I), I=1-3.	= 0	Not used.
IGEOM	= 1	The height of the channel is not a function of streamwise coordinate.
	= 2	Contoured channel.
TWOD	= T	Logical variable for two-dimensional calculation.
	= F	Logical variable for three-dimensional calculation.
IGTYPE	= 1	Two-dimensional calculation. Used with TWOD = T
	= 2	Three-Dimensional calculation. Used with TWOD = F
LXSPLT		x grid point location for summary print.
LYSPLT		y grid point location for summary print. Default is 1.
REY		Reynolds number (calculated).
CLENG		Reference length, meters (throat height).
WREF		Reference velocity, m/sec (core-flow velocity at the inflow boundary).

<u>Namelist or Variable Name</u>	<u>Description</u>
DENSR	Reference density, kg/m ³ (core-flow density at the inflow boundary).
TREF	Reference temperature, °K (core-flow temperature at the inflow boundary).
PREF	Reference pressure, Pa (calculated).
VISCR	Reference dynamic viscosity, kg/m-sec (core-flow dynamic viscosity at the inflow boundary).
CMACH	Reference Mach Number (calculated)
LAMFLO = 0	Turbulent flow
≠ 0	Obsolete.
AVISC(IDIR,IEQ)	<p>Artificial dissipation parameter σ (See Eq. (1) of the Appendix). IEQ = 1-5, and IDIR=1-3. IEQ = 1 indicates the x-momentum equation. IEQ = 2 indicates the y-momentum equation. IEQ = 3 indicates the z-momentum equation. IEQ = 4 indicates the continuity equation. IEQ = 5 indicates the energy equation. IDIR=1 indicates the x second derivative term IDIR=2 indicates the y second derivative term IDIR=3 indicates the z second derivative term</p> <p>For example, AVISC(3, 1) is the value of σ used for the artificial dissipation term $\frac{\partial^2 U}{\partial Z^2}$ in the x-momentum equation.</p> <p>Note that even if the y-momentum equation is not solved, the corresponding AVISC must be supplied. Default values are 0.0. Recommended values are 0.50 initially followed by runs at 0.10.</p>

<u>Namelist or Variable Name</u>	<u>Description</u>
NT	Number of time steps to be run
DT	Initial nondimensional time step. If DT is omitted on a restart DT will be set to value at termination of last run.
DTMIN	Minimum nondimensional time step for this run
DTMAX	Maximum nondimensional time step for this run
IDTADJ = 0	Constant DT is used for this run
= 1	Time step adjusted. If maximum relative change in any flow variable is less than 0.04, DT is multiplied by 1.25. If maximum relative change in any flow variable is greater than 0.06, DT is divided by 1.25.
= 2	Time step is cycled between DTMIN and DTMAX using an acceleration parameter concept. A sequence of NTSTEP time steps is used under this option.
NTSTEP	Number of time steps used in cycling. Default value is 3.
ITEST	Steady state test is performed every ITEST time steps. Default value is 1.
SSEPS	Steady-state convergence criteria. Default is 0.001.
IPRINT	Complete flow field printouts are provided every IPRINT time steps.

<u>Namelist or Variable Name</u>	<u>Description</u>
LZPRNT(LZ)	Optional print control flag for three-dimensional calculations only.
= 0	No printout at streamwise station number LZ
= 1	Normal printout at Station LZ. Default is 1.
IVARPR(IV)	Optional print control flag for variable IV
= 0	Suppress printout of variable IV
= 1	Normal printout of variable IV
IV	IVARPR(IV)
1	transverse velocity, u
2	spanwise velocity, v
3	streamwise velocity, w
4	density, ρ
5	enthalpy, h
26	pressure, p
27	temperature, T
28	effective viscosity, ν_{eff}
33	mixing length, l
35	Mach number, M
36	total pressure, P_o
IDUMP1	
= 1	Print initial flow field for this run.
= 2	No initial printout.
IPLLOT	
= 0	No plot file (TAPE1) written.
> 0	Plot file written at time step increment IPLLOT.
NFPLOT	
= 0	NFPLOT must be set to zero.

<u>Namelist or Variable Name</u>		<u>Description</u>
IGPRT(1)	= 0	No x-coordinate printout.
	= 1	Print x-coordinate distribution.
IGPRT(2)	= 0	No y-coordinate printout.
	= 1	Print y-coordinate distribution. Default is 0.
IGPRT(3)	= 0	No z-coordinate printout.
	= 1	Print z-coordinate distribution.
ICASE	= 1	Inflow is not supersonic.
	= 2	Inflow is supersonic.
PRESS6		Dimensionless static pressure at the outflow section. Note that the reference condition is the inflow core condition.
&DATA1		
YFIRST	= XGMIN(3)	See &READ9.
YLAST	= XGMAX(3)	See &READ9.
NCLUST		Total number of the interior cluster points. A cluster point is the sequential number of the selected grid point which must coincide with particular predetermined value of the z-coordinate. Accordingly, pairs of (1, YFIRST) and (NUMDZ+2, YLAST) are also cluster points, but they are boundary cluster points.

<u>Namelist or Variable Name</u>	<u>Description</u>
CLPY(I), I=1-61	The z-coordinate of the cluster point. Note that both of boundary and internal cluster points must be specified.
CLPX(I), I=1-61	The sequential number of the grid point corresponding to CLPY(I).
ETAP(J), J=1-61	The sequential number of the grid point defined as pivot point. The grid spacing will have the fastest variation at a pivot point. For each of the interior cluster points there shall be a pair of pivot points: one ahead of the cluster point, the other one after the cluster point. However, only one pivot point shall be associated with each of the boundary cluster points.
ALPH(J), J=1-61	Width parameter specifying width (in terms of the number of grid points) in which 90 per cent of grid-size variation takes place around the pivot point ETAP(J).
> 0	decreasing grid-size.
< 0	increasing grid-size.
NEND = 0	No stretching at YFIRST and YLAST
= 1	Stretching at YFIRST only
= 2	Stretching at YLAST only
= 3	Stretching at YFIRST and YLAST
RHW always > 0.0	Approximate ratio of grid-size at CLPY(2) to the maximum grid-size in the interval CLPY(1) < Z < CLPY(2).
= 1.0	No stretching at YFIRST. Used with NEND = 0 or 2.

<u>Namelist or Variable Name</u>	<u>Description</u>
RATIO(K), K = 1-40. always > 0.0 = 1.0	Approximate ratio of grid-size at CLPY(K+1) to the maximum grid-size in the interval CLPY(K) <Z< CLPY(K+1) No grid-variation at CLPY(K+1).
BETA0 always > 0.0	Calculated. It indicates the first derivative of Z-coordinate with respect to the computational coordinate at YFIRST.
BET(L), L = 1-61. alwyas > 0.0	Calculated. It indicates the ratio between the grid sizes on both sides of the pivot point ETAP(L+1).
&INFLW	
CFLW	Coefficient of skin friction at the bottom wall of inflow boundary.
DELTAL	Dimensionless boundary layer thickness at the bottom wall of inflow boundary.
PRDL	Prandtl Numer used only for generating the bottom wall velocity profile.
CFUW	Coefficient of skin friction at the top wall of inflow boundary.
DELTAU	Dimensionless boundary layer thickness at the top wall of inflow boundary.
PRDU	Prandtl Number used only for generating the top wall velocity profile.
TINF = TREF	See &READ9

LIST OF MAJOR FORTRAN VARIABLES

FORTRAN SYMBOL	COMMON BLOCK	DESCRIPTION
AC(I,J,K)	BLK1	DEPENDENT VARIABLE ARRAY
ACG(J,J)	BLK1	GEOMETRY DATA ARRAY
AN(I,J)	BLKM	ARRAY STORING TIME TERM LINEARIZED COEFFICIENTS
APR(I,J)	PRNT	PRINT OUTPUT ARRAY
AVANDR	TURB	DAMPING CONSTANT
AVISC(I,J)	MISC2	ARTIFICIAL DISSIPATION PARAMETER
C(I,J,K)	BLKM	COUPLED MATRIX ARRAY STORAGE
CLENG	CREF	REFERENCE LENGTH
CMACH	MISC2	REFERENCE MACH NUMBER
D	VARNO	INDEX FOR DIVERGENCE
D1(I,J,K)	BLKM	ARRAY STORING FIRST SWEEP LINEARIZED COEFFICIENTS
D2(I,J,K)	BLKM	ARRAY STORING SECOND SWEEP LINEARIZED COEFFICIENTS
D3(I,J,K)	BLKM	ARRAY STORING THIRD SWEEP LINEARIZED COEFFICIENTS
DENSR	CREF	REFERENCE DENSITY
DFW(I,J,K)	ADI7	DIFFERENCE WEIGHT ARRAY
DIM1	NOND	INVERSE REYNOLDS NUMBER
DIM2	NOND	REFERENCE PRESSURE/REFERENCE DYNAMIC HEAD
DIM3	NOND	REFERENCE PRESSURE/(REFERENCE DENSITY * REFERENCE ENTHALPY)
DIM4	NOND	$1.0/(REY * P_r)$
DIM12	NOND	$2.0 * DIM1$
DS	VARNO	INDEX FOR DISSIPATION
DT	MISC2	TIME STEP

FORTRAN SYMBOL	COMMON BLOCK	DESCRIPTION
DTCON	MISC2	INVERSE STEP
DTMAX	MISC2	MAXIMUM ALLOWABLE TIME STEP
DTMIN	MISC2	MINIMUM ALLOWABLE TIME STEP
E(I,J,K)	BLKM	COUPLED MATRIX ARRAY STORAGE
GRID(I)	GTRAN	GRID DISTRIBUTION PARAMETER (SEE &READ9)
H	VARNO	INDEX FOR ENTHALPY
IL	MGAUS	LOWER LIMIT FOR MATRIX INVERSION
IADI	ADI1	ADI SWEEP NUMBER
IBC	ADI1	BOUNDARY CONDITION BOUNDARY PARAMETER
IDT	MISC2	TIME STEP INDEX
IDTADJ	MISC2	TIME STEP CONTROL PARAMETER (SEE &READ9)
IDUMP1	OUTA	PARAMETER CONTROLLING INITIAL STATION PRINT (SEE &READ9)
IEQ	ADI1	EQUATION NUMBER
IGPRT(I)	GEO1	GEOMETRY PRINT CONTROL (SEE &READ9)
IL	MGAUS	UPPER LIMIT FOR MATRIX INVERSION
IPRINT	MISC2	PRINT INTERVAL PARAMETER (SEE &READ9)
IRERUN	MISC2	RESTART WRITE CONTROL PARAMETER (SEE&READ1)
IREST	MISC2	RESTART READ CONTROL PARAMETER (SEE &READ1)
IVARPR(I)	MISC2	PRINT PARAMETER (SEE &READ9)
JADI	ADI1	ADI SWEEP PARAMETER
JEQBC(I,J,K)	ADI1	BOUNDARY CONDITION TYPE PARAMETER
JX	ADI2	DIRECTION-1 GRID POINT INDEX
KZ	ADI2	DIRECTION-3 GRID POINT INDEX

FORTTRAN SYMBOL	COMMON BLOCK	DESCRIPTION
LX	ADI2	DIRECTION-1 GRID POINT INDEX
LX1	ADI3	FIRST DIRECTION-1 INTERIOR POINT
LX2	ADI3	LAST DIRECTION-1 INTERIOR POINT
LY	ADI2	DIRECTION-2 GRID POINT INDEX
LY1	ADI3	FIRST DIRECTION-2 INTERIOR POINT
LY2	ADI3	LAST DIRECTION-2 INTERIOR POINT
LZ	ADI2	DIRECTION-3 GRID POINT INDEX
LZ1	ADI3	FIRST DIRECTION-3 INTERIOR POINT
LZ2	ADI3	LAST DIRECTION-3 INTERIOR POINT
LZPRNT	MISC2	THREE DIMENSIONAL PRINT CONTROL (SEE &READ9)
MEQS	ADI1	NUMBER OF EQUATIONS TO BE SOLVED
NT	MISC2	NUMBER OF TIME STEPS TO BE RUN
NUMDX	MISC2	NUMBER OF INTERIOR DIRECTION-1 POINTS
NUMDY	MISC2	NUMBER OF INTERIOR DIRECTION-2 POINTS
NUMDZ	MISC2	NUMBER OF INTERIOR DIRECTION-3 POINTS
NX1	ADI4	FIRST GRID POINT - DIRECTION 1
NX2	ADI4	LAST GRID POINT - DIRECTION 1
NY1	ADI4	FIRST GRID POINT - DIRECTION 2
NY2	ADI4	LAST GRID POINT - DIRECTION 2
NZ1	ADI4	FIRST GRID POINT - DIRECTION 3
NZ2	ADI4	LAST GRID POINT - DIRECTION 3

FORTRAN SYMBOL	COMMON BLOCK	DESCRIPTION
P	VARNO	INDEX FOR PRESSURE
PCNT1	MISC2	TIME STEP CONTROL PARAMETER
PCNT2	MISC2	TIME STEP CONTROL PARAMETER
PREF	CREF	REFERENCE PRESSURE
PRNDL	CREF	PRANDTL NUMBER
PTOT	BCCON	TOTAL PRESSURE
R	VARNO	INDEX FOR DENSITY
REY	CREF	REYNOLDS NUMBER
SN(I)	BLKM	ARRAY STORING SOURCE TERM LINEARIZED COEFFICIENT
SSTEST	MISC2	MAXIMUM CHANGE IN VARIABLE ACROSS TIME STEP
T	VARNO	INDEX FOR TEMPERATURE
TAUW	TURB	WALL SHEAR
TREF	CREF	REFERENCE TEMPERATURE
TTIME	MISC2	CUMULATIVE TIME
TTOT	BCCON	TOTAL TEMPERATURE
U	VARNO	INDEX FOR DIRECTION-1 VELOCITY
USTAR	TURB	DIMENSIONLESS VELOCITY
V	VARNO	INDEX FOR DIRECTION-2 VELOCITY
VISCL	TURB	LAMINAR REFERENCE VISCOSITY
VISCR	CREF	REFERENCE VISCOSITY
VS	VARNO	INDEX FOR VISCOSITY

FORTRAN SYMBOL	COMMON BLOCK	DESCRIPTION
W	VARNO	INDEX FOR DIRECTION-3 VELOCITY
WREF	CREF	REFERENCE VELOCITY
XGMAX(I)	GRID1	MAXIMUM COORDINATE VALUE (SEE &READ9)
XGMIN(I)	GRID1	MINIMUM COORDINATE VALUE (SEE &READ9)
YPLUS	TURB	DIMENSIONLESS DISTANCE FROM SURFACE

FILE INPUT/OUTPUT

To read restart files, the following commands must be given at the beginning of a run:

```
RMDS    A10, R9
RELEASE RMDS
RMDS    A20, R19
RELEASE RMDS
```

To write restart files, the following command must be given at the end of a run:

```
CATALOG SC10, U,, A10
MDS A10
CATALOG SC20, U,, A20
MDS A20
```

Where A10 and A20 are some given file names, SC10 and SC20 are scratch files defined in PROCDEF RUNMT.

Remarks on Storage Requirements and Run Time

When stored in data pool of the Lewis IBM 370, the files INLTS, INLTB and INLTCM (see page 83) occupy 171, 476 and 10 pages, respectively. The sizes of the restart files are problem dependent; as an example, for 2-D problems with 31 x 41 grid points, the file A10 requires 78 pages and the file A20 requires 2 pages. For 3-D problems with 31 x 41 x 16 grid points, the file A10 requires 640 pages, while the file A20 needs 3 pages. As for the run time, in terms of CPU sec per time-step per grid-point, approximately 0.013 sec is needed in a 2-D problem and 0.028 sec is required for a 3-D problem.

As a further indication of the storage requirements, information obtained from executing another version of the MINT Code on a CDC machine is also given here. With 3500 grid points, 225000 decimal words are needed; however, by using overlay and out-of-core-option, the storage requirement has been reduced to 90000 decimal words. Although this out-of-core-option is not included in the present INLTS.G01 version, the implementation of this option can be carried out in a straightforward manner.

Definition of PROCDEFS

```
PROCDEF MOD
PARAM $A
DDEF X,VI,SOURCE.$AN,RET=T
DEFAULT SYSINX=E
EDIT SOURCE.$AN
-REVISE 100, LAST
-EXCERPT M,$A,100, LAST

PROCDEF MODN
PARAM $A
-END
FIN $AN,LISTDS=N,SLIST=N,CRLIST=N
DEFAULT SYSINX=G
ERASE SOURCE.$AN

PROCDEF RUNMT
ERASE M
DDEF FT01F001,VS,SC01,RET=T
DDEF FT02F001,VS,SC02,RET=T
DDEF FT03F001,VS,SC03,RET=T
DDEF FT04F001,VS,SC04,RET=T
DDEF FT09F001,VS,R9,RET=T
DDEF FT10F001,VS,SC10,RET=T
DDEF FT11F001,VS,SC11,RET=T
DDEF FT12F001,VS,SC12,RET=T
DDEF FT13F001,VS,SC13,RET=T
DDEF FT14F001,VS,SC14,RET=T
DDEF FT15F001,VS,SC15,RET=T
DDEF FT16F001,VS,SC16,RET=T
DDEF FT17F001,VS,SC17,RET=T
DDEF FT19F001,VS,R19,RET=T
DDEF FT20F001,VS,SC20,RET=T
DDEF FT21F001,VS,SC21,RET=T
LOAD BLKDATN
LOAD DALN
DALN
```

Sample Input Cards and Printed Output

A sample case was run to illustrate the set up of input parameters and typical printouts of the INLTS.G01 code. The given input card deck is for a new calculation. In the case of restarted calculation, all parameters of &READ1 and &DATA1 must be specified, however, in &READ9, only NT, PRESS6 and ICASE must always be specified through input cards for restarted calculation, unless the user wants to change other parameters for other purposes. The Namelist &INFLW should be omitted for restarted calculation. Also note that, parameters associated with the grid point distribution should not be changed since the computational coordinate system is time-independent.

The code output first prints out a series of dimensionless parameters DIM1 - DIM10, DIM12 and DIM14, and the dimensionless total temperature, total pressure and total enthalpy. This is followed by the finite difference coefficients for first and second derivatives in both directions. In each direction three lines are written. The first and third lines give one-sided difference weights at the lower and upper boundaries; the second line of each set gives central differences used for the interior points. Six numbers are written on each line; the first set of three values represent the first derivative coefficients and the second set of three values represent the second derivative coefficients.

The next output item is the grid distribution data. They are quite self-explanatory. The first part indicates the results of streamwise coordinate transformation (see SUBROUTINES OHGRID, STCLST and FIXBY1). The second part gives the x-coordinates at each z location and the third part gives the z-coordinates of each streamwise grid point.

These geometry data are followed by the printout of NAMELIST INFLW and the results of the inflow boundary layer profiles calculation. These are printed out in the SUBROUTINE PROFIL, the user should consult this subroutine if detailed informations are desired. It is only noted here that the first part deals with the bottom wall boundary layer profile calculation and the second part deals with the top wall boundary layer profile calculation.

Following the boundary layer profiles printouts, the results of one-dimensional inviscid calculation are printed in the SUBROUTINE INVICD. The inviscid solutions are given at each streamwise grid point. The SUBROUTINES INVICD and SPREAD should be consulted about these results. The following item is the printouts of the NAMELISTS READ1, READ9 and DATA1. Note that values of some parameters may be changed by the internal operations.

The output of the namelist data is followed by estimations of the total mass and total energy within the computational domain, as well as the estimated mass flux at each streamwise section. This is then followed by the printouts of the flowfield variables at the starting time-step of this calculation. These printouts are quite self-explanatory and will not be described in detail here. At each time-step, a summary print is written, in which the maximum relative change over a time-step is given by SSTEEST along with the location. Also given are the maximum relative changes of each dependent variable. RESMAX is the maximum residual of the equations solved and indicates how well is the steady-state equation being satisfied. Finally, flow variables at (LXSPLT, LYSPLT) are written for each streamwise station. Note that PBOT, PTOP and DP represent static pressure at the bottom wall, top wall, and at the point indicated by LXSPLT. A typical set of output along with the corresponding given input will be presented in the following pages.

Note that the JOB CONTROL LANGUAGE (JCL) streams, as presented in pages 81 and 82, are for the IBM 370 and the command DDEF defines devices which must be assigned for any other type machine. Also note that all the level 1 errors appearing in pages 83 and 84 are due to the non-optimal arrangements of the common blocks involved in the subroutines and they do not adversely affect execution of the code.

```

      LOGON P      ,.,90
      ERASE R9
      ERASE R19
      ERASE MINT
      ERASE PROCM
      ERASE M
      RMDS INLTH,MINT
      RELEASE RMDS
      DDEF XXX,VP,DSNAME=MINT,OPTION=JOURNAL,DISP=OLD
      RMDS INLTS,M
      RELEASE RMDS
      RMDS INLTCM,PROCM
      RELEASE RMDS
      MOD SPREAD
      _REVISE 54300
          PINVCD=1.0
      _MODN SPREAD
      RUN*1
      &READ1
      IREST = 0,
      IOIAPF=10,
      INIAPF=9,
      IOIAP1=20,
      INIAP1=19,
      &END READ1
      &READ9
      NT=3,
      ICASE=1,
      PRESS6=0.993,
      NUMDX=18,NUMDZ=18,
      XGMIN=0.0+0.0+0.0,
      XGMAX=1.0+0.0+2.0,
      GR(1)=-0.9995 ,0.9995 ,4*0.0,
      XCENR(1) = 0.0, 0.0, 0.0,
      DAXPG=0.0+0.0+0.0,
      IGEOM = 1,
      TWON = 1,  IGIYPE=1,
      LXSPLT=10,
      CLENG =0.0441,
      WREF =149.17675,
      DENSR = 1.2692128,
      TREF = 247.623,
      VISCR = 1.76415880-05,
      LAMFLO=0,
      AVISC(1,1)=15*0.5,
      DT=0.005,DTMIN=0.001,DTMAX=0.10,
      IDIADJ = 1,
      ITEST = 1,
      IPRINT=10,
      IVARPR = 28*1,
      IVARPR(24) = 0,
      IVARPR(33) = 1,      IVARPR(35) = 1,
      IDUAP1= 1,
      IPLUT=0,
      IGPR1=1+0.1,
      &END READ9

```

```

&DATA1
NCLUST=0.
NEND=0.
BETA0=0.0.
ETAP=2.0.20.0.
ALPH=1.0.1.0.
YF1HST=0.0.
YLAST=2.0.
CLPA=1.0.20.0.
CLPY=0.0.2.0.
GAT[0]=1.0.
HEF=10.0.
HHD=1.0.
&END DATA1
&INFLW
CFLW=0.00106.
DELTA=0.12149.
PRDL=1.0.
CFUW=0.00106.
DELTAU=0.12149.
PRDU=1.0.
TINF=247.623.
&END INFLW
RELEASE FT
ERASE R4
ERASE R19
ERASE MINT
ERASE PHOCM
ERASE M
ERASE SC01
ERASE SC10
ERASE SC20
LUGOFF

```

P
ISS/370 RELEASE 3.0 PRPH2 PTF15
---> CLEAN UP LKDAT... <--- HSN=2755 PUCLID=LRCFM LOGON AT 15:07 ON 11/10/82.

ERASE HQ
DS12 CANCELLED: HQ UNKNOWN.
ERASE R19
DS12 CANCELLED: R19 UNKNOWN.
ERASE MINT
DS12 CANCELLED: MINT UNKNOWN.
ERASE PHUCH
DS12 CANCELLED: PHUCH UNKNOWN.
ERASE M
DS12 CANCELLED: M UNKNOWN.
4M05 INLT MINT
CZAR2527 SUCCESSFUL (TEMP) RESTORE INLT AS (MINT)
RELEASE 4M05
JDEF xxx,VP,USNAME=MINT,OPTION=JULI8,DISP=DLU
4M05 INLT M
CZAR2527 SUCCESSFUL (TEMP) RESTORE INLT AS (M)
RELEASE 4M05
4M05 INLT CM,PHUCH
CZAR2527 SUCCESSFUL (TEMP) RESTORE INLT CM AS (PHUCH)
RELEASE 4M05
M00 SPFAH
REVISE 54300
7054100 PINVCD=1.0
M00N 4PRFAH

15PRH00N 11/10/82 15:10:52
15PRH00N 11/10/82 15:10:52
CFAD017 MINOR ERRORS

PAGE 002
PAGE 003

4M05
CZC0L005 PROCEEDING: MODULE HLKDATN PRODUCED WITH LEVEL 1 ERRORS
CZC0L005 PROCEEDING: MODULE DALN PRODUCED WITH LEVEL 1 ERRORS
CZC0L005 PROCEEDING: MODULE EXECN PRODUCED WITH LEVEL 1 ERRORS
CZC0L005 PROCEEDING: MODULE ADICN PRODUCED WITH LEVEL 1 ERRORS
CZC0L005 PROCEEDING: MODULE ADICXN PRODUCED WITH LEVEL 1 ERRORS
CZC0L005 PROCEEDING: MODULE ADICPIN PRODUCED WITH LEVEL 1 ERRORS
CZC0L005 PROCEEDING: MODULE DOPN PRODUCED WITH LEVEL 1 ERRORS
CZC0L005 PROCEEDING: MODULE GENEQ2N PRODUCED WITH LEVEL 1 ERRORS
CZC0L005 PROCEEDING: MODULE DIFFN PRODUCED WITH LEVEL 1 ERRORS
CZC0L005 PROCEEDING: MODULE EOSN PRODUCED WITH LEVEL 1 ERRORS
CZC0L005 PROCEEDING: MODULE HCCHFMN PRODUCED WITH LEVEL 1 ERRORS
CZC0L005 PROCEEDING: MODULE GASPX PRODUCED WITH LEVEL 1 ERRORS
CZC0L005 PROCEEDING: MODULE MINMAXN PRODUCED WITH LEVEL 1 ERRORS
CZC0L005 PROCEEDING: MODULE EATENTN PRODUCED WITH LEVEL 1 ERRORS
CZC0L005 PROCEEDING: MODULE DELUN PRODUCED WITH LEVEL 1 ERRORS
CZC0L005 PROCEEDING: MODULE SURCHN PRODUCED WITH LEVEL 1 ERRORS
CZC0L005 PROCEEDING: MODULE MADEQNN PRODUCED WITH LEVEL 1 ERRORS
CZC0L005 PROCEEDING: MODULE CURVTN PRODUCED WITH LEVEL 1 ERRORS
CZC0L005 PROCEEDING: MODULE CURVCTN PRODUCED WITH LEVEL 1 ERRORS
CZC0L005 PROCEEDING: MODULE ARTVISN PRODUCED WITH LEVEL 1 ERRORS
CZC0L005 PROCEEDING: MODULE GENEQ3N PRODUCED WITH LEVEL 1 ERRORS
CZC0L005 PROCEEDING: MODULE GENHCN PRODUCED WITH LEVEL 1 ERRORS
CZC0L005 PROCEEDING: MODULE HCN PRODUCED WITH LEVEL 1 ERRORS
CZC0L003 UNDEFINED REF ALFA IN MODULE HCN * ADDRESS FFFFF000 ASSIGNED
CZC0L005 PROCEEDING: MODULE HCPMN PRODUCED WITH LEVEL 1 ERRORS
CZC0L005 PROCEEDING: MODULE ATIMEN PRODUCED WITH LEVEL 1 ERRORS
CZC0L005 PROCEEDING: MODULE SOURCEN PRODUCED WITH LEVEL 1 ERRORS
CZC0L005 PROCEEDING: MODULE TCMU1 PRODUCED WITH LEVEL 1 ERRORS
CZC0L005 PROCEEDING: MODULE MATCHAN PRODUCED WITH LEVEL 1 ERRORS
CZC0L005 PROCEEDING: MODULE RM0XN PRODUCED WITH LEVEL 1 ERRORS
CZC0L005 PROCEEDING: MODULE SUBAUXN PRODUCED WITH LEVEL 1 ERRORS
CZC0L005 PROCEEDING: MODULE FPORTN PRODUCED WITH LEVEL 1 ERRORS
CZC0L003 UNDEFINED REF IPOR1 IN MODULE FPORTN * ADDRESS FFFFF000 ASSIGNED
CZC0L003 UNDEFINED REF IPOR2 IN MODULE FPORTN * ADDRESS FFFFF000 ASSIGNED
CZC0L003 UNDEFINED REF LCPOMT IN MODULE FPORTN * ADDRESS FFFFF000 ASSIGNED
CZC0L005 PROCEEDING: MODULE USTARN PRODUCED WITH LEVEL 1 ERRORS
CZC0L005 PROCEEDING: MODULE WALLEF PRODUCED WITH LEVEL 1 ERRORS
CZC0L005 PROCEEDING: MODULE MGAUSEN PRODUCED WITH LEVEL 1 ERRORS
CZC0L005 PROCEEDING: MODULE QUIJCN PRODUCED WITH LEVEL 1 ERRORS
CZC0L005 PROCEEDING: MODULE MGERRN PRODUCED WITH LEVEL 1 ERRORS
CZC0L005 PROCEEDING: MODULE WMDATRN PRODUCED WITH LEVEL 1 ERRORS
CZC0L005 PROCEEDING: MODULE WMDISKX PRODUCED WITH LEVEL 1 ERRORS
CZC0L005 PROCEEDING: MODULE MATPRTN PRODUCED WITH LEVEL 1 ERRORS
CZC0L005 PROCEEDING: MODULE MATPRAN PRODUCED WITH LEVEL 1 ERRORS
CZC0L005 PROCEEDING: MODULE MGAUSPN PRODUCED WITH LEVEL 1 ERRORS
CZC0L005 PROCEEDING: MODULE MSORTN PRODUCED WITH LEVEL 1 ERRORS
CZC0L005 PROCEEDING: MODULE MMLTH PRODUCED WITH LEVEL 1 ERRORS
CZC0L005 PROCEEDING: MODULE FINVRSN PRODUCED WITH LEVEL 1 ERRORS
CZC0L005 PROCEEDING: MODULE MINVRSN PRODUCED WITH LEVEL 1 ERRORS

```

CZCUL005 PROCEEDING: MODULE ADIUNIN PRODUCED WITH LEVEL 1 ERRORS
CZCUL005 PROCEEDING: MODULE GENUHCH PRODUCED WITH LEVEL 1 ERRORS
1 CZCUL005 PROCEEDING: MODULE GAUSSN PRODUCED WITH LEVEL 1 ERRORS
CZCUL005 PROCEEDING: MODULE JUBULEN PRODUCED WITH LEVEL 1 ERRORS
CZCUL005 PROCEEDING: MODULE PHINTIN PRODUCED WITH LEVEL 1 ERRORS
CZCUL005 PROCEEDING: MODULE WSLAHN PRODUCED WITH LEVEL 1 ERRORS
CZCUL005 PROCEEDING: MODULE AUCYN PRODUCED WITH LEVEL 1 ERRORS
CZCUL005 PROCEEDING: MODULE AUCP2N PRODUCED WITH LEVEL 1 ERRORS
CZCUL005 PROCEEDING: MODULE ADIUN2N PRODUCED WITH LEVEL 1 ERRORS
CZCUL005 PROCEEDING: MODULE AUCZIN PRODUCED WITH LEVEL 1 ERRORS
CZCUL005 PROCEEDING: MODULE AUCZON PRODUCED WITH LEVEL 1 ERRORS
CZCUL005 PROCEEDING: MODULE ROTATEN PRODUCED WITH LEVEL 1 ERRORS
CZCUL005 PROCEEDING: MODULE EXTBNV PRODUCED WITH LEVEL 1 ERRORS
CZCUL005 PROCEEDING: MODULE DIVN PRODUCED WITH LEVEL 1 ERRORS
CZCUL005 PROCEEDING: MODULE DISFCNN PRODUCED WITH LEVEL 1 ERRORS
CZCUL005 PROCEEDING: MODULE TMEN PRODUCED WITH LEVEL 1 ERRORS
CZCUL005 PROCEEDING: MODULE LOADACN PRODUCED WITH LEVEL 1 ERRORS
CZCUL005 PROCEEDING: MODULE MAXPN PRODUCED WITH LEVEL 1 ERRORS
CZCUL005 PROCEEDING: MODULE SETBNV PRODUCED WITH LEVEL 1 ERRORS
CZCUL005 PROCEEDING: MODULE LINCORIN PRODUCED WITH LEVEL 1 ERRORS
CZCUL005 PROCEEDING: MODULE TEMPNN PRODUCED WITH LEVEL 1 ERRORS
CZCUL005 PROCEEDING: MODULE MFNOXN PRODUCED WITH LEVEL 1 ERRORS
CZCUL005 PROCEEDING: MODULE MAXDEHN PRODUCED WITH LEVEL 1 ERRORS
CZCUL005 PROCEEDING: MODULE TEMPSN PRODUCED WITH LEVEL 1 ERRORS
CZCUL005 PROCEEDING: MODULE TERMSN PRODUCED WITH LEVEL 1 ERRORS
CZCUL005 PROCEEDING: MODULE PROJCTN PRODUCED WITH LEVEL 1 ERRORS
CZCUL005 PROCEEDING: MODULE VISCOSN PRODUCED WITH LEVEL 1 ERRORS
CZCUL005 PROCEEDING: MODULE MIXLENN PRODUCED WITH LEVEL 1 ERRORS
CZCUL005 PROCEEDING: MODULE CRJETN PRODUCED WITH LEVEL 1 ERRORS
CZCUL005 PROCEEDING: MODULE MIXL3DN PRODUCED WITH LEVEL 1 ERRORS
CZCUL005 PROCEEDING: MODULE SETJKN PRODUCED WITH LEVEL 1 ERRORS
CZCUL005 PROCEEDING: MODULE SETHVN PRODUCED WITH LEVEL 1 ERRORS
CZCUL005 PROCEEDING: MODULE VITALN PRODUCED WITH LEVEL 1 ERRORS
CZCUL005 PROCEEDING: MODULE WALLYSN PRODUCED WITH LEVEL 1 ERRORS
CZCUL005 PROCEEDING: MODULE SSTSTN PRODUCED WITH LEVEL 1 ERRORS
CZCUL005 PROCEEDING: MODULE HTFLUXN PRODUCED WITH LEVEL 1 ERRORS
CZCUL005 PROCEEDING: MODULE EXITPRN PRODUCED WITH LEVEL 1 ERRORS
CZCUL005 PROCEEDING: MODULE PHNTAN PRODUCED WITH LEVEL 1 ERRORS
CZCUL005 PROCEEDING: MODULE RESULTN PRODUCED WITH LEVEL 1 ERRORS
CZCUL005 PROCEEDING: MODULE TPLOTN PRODUCED WITH LEVEL 1 ERRORS
CZCUL005 PROCEEDING: MODULE TIMGEON PRODUCED WITH LEVEL 1 ERRORS
CZCUL005 PROCEEDING: MODULE EVALIN PRODUCED WITH LEVEL 1 ERRORS
CZCUL005 PROCEEDING: MODULE MNFTN PRODUCED WITH LEVEL 1 ERRORS
CZCUL005 PROCEEDING: MODULE PHGEON PRODUCED WITH LEVEL 1 ERRORS
CZCUL005 PROCEEDING: MODULE WRPLTN PRODUCED WITH LEVEL 1 ERRORS
CZCUL005 PROCEEDING: MODULE HEADAN PRODUCED WITH LEVEL 1 ERRORS
CZCUL005 PROCEEDING: MODULE BVIVN PRODUCED WITH LEVEL 1 ERRORS
CZCUL005 PROCEEDING: MODULE FLW3DN PRODUCED WITH LEVEL 1 ERRORS
CZCUL005 PROCEEDING: MODULE PROFILN PRODUCED WITH LEVEL 1 ERRORS
CZCUL005 PROCEEDING: MODULE CUORUN PRODUCED WITH LEVEL 1 ERRORS
CZCUL005 PROCEEDING: MODULE INTGEON PRODUCED WITH LEVEL 1 ERRORS
CZCUL005 PROCEEDING: MODULE FLWFLUN PRODUCED WITH LEVEL 1 ERRORS
CZCUL005 PROCEEDING: MODULE SPREADN PRODUCED WITH LEVEL 1 ERRORS
CZCUL003 UNDEFINED REF IPOR1 IN MODULE SPREADN . ADDRESS FFFFF000 ASSIGNED
CZCUL003 UNDEFINED REF IPOR2 IN MODULE SPREADN . ADDRESS FFFFF000 ASSIGNED
CZCUL005 PROCEEDING: MODULE INTDATN PRODUCED WITH LEVEL 1 ERRORS
1 CZCUL003 UNDEFINED REF LCPOR1 IN MODULE SPREADN . ADDRESS FFFFF000 ASSIGNED
CZCUL005 PROCEEDING: MODULE CURNEHN PRODUCED WITH LEVEL 1 ERRORS
CZCUL005 PROCEEDING: MODULE LOCEAN PRODUCED WITH LEVEL 1 ERRORS
CZCUL005 PROCEEDING: MODULE HEADAN PRODUCED WITH LEVEL 1 ERRORS
CZCUL005 PROCEEDING: MODULE ROLISTN PRODUCED WITH LEVEL 1 ERRORS
CZCUL005 PROCEEDING: MODULE NORMDN PRODUCED WITH LEVEL 1 ERRORS
CZCUL005 PROCEEDING: MODULE OPENMSN PRODUCED WITH LEVEL 1 ERRORS
CZCUL005 PROCEEDING: MODULE INTERPN PRODUCED WITH LEVEL 1 ERRORS
CZCUL005 PROCEEDING: MODULE HEZUNEN PRODUCED WITH LEVEL 1 ERRORS
CZCUL005 PROCEEDING: MODULE CHUATN PRODUCED WITH LEVEL 1 ERRORS
CZCUL005 PROCEEDING: MODULE HESTRTN PRODUCED WITH LEVEL 1 ERRORS

```

***** MINT INLET CODE *****

INITIAL INPUT STREAM

ORESTART OUTPUT UNIT TP20 POSITIONED AT RESTART DUMP NO. 0 0 PARTITIONS SKIPPED.

ORESTART OUTPUT UNIT TP10 POSITIONED AT RESTART DUMP NO. 0 0 PARTITIONS SKIPPED.

DIM1-DIM10,DIM12,DIM14
 2.1128E-06 3.7099E 00 2.8567E-01 2.8943E-06 7.7001E-02 1.6269E-07 2.2286E-07 2.8943E-06 1.0000E 00 7.0915E-06 4.2256E-06 0.000
 OT, P, H-TOTAL = 1.03850E 00 1.14139E 00 1.03850E 00

ODIRECTION-1 DIFFERENCE OPERATORS

```

1 -1.50000000E 00 2.00000000E 00-5.00000000E-01 1.00000000E 00-2.00000000E 00 1.00000000E 00
2 -5.00000000E-01 0.00000000 5.00000000E-01 1.00000000E 00-2.00000000E 00 1.00000000E 00
3 5.00000000E-01-2.00000000E 00 1.50000000E 00 1.00000000E 00-2.00000000E 00 1.00000000E 00

```

ODIRECTION-3 DIFFERENCE OPERATORS

```

1 -1.50000000E 00 2.00000000E 00-5.00000000E-01 1.00000000E 00-2.00000000E 00 1.00000000E 00
2 -5.00000000E-01 0.00000000 5.00000000E-01 1.00000000E 00-2.00000000E 00 1.00000000E 00
3 5.00000000E-01-2.00000000E 00 1.50000000E 00 1.00000000E 00-2.00000000E 00 1.00000000E 00

```

OFIRST AND LAST TRANSFORMED AND PHYSICAL COORDS
 0 TRANSFORMED COORDINATE RANGE- XFIRST= 1.0000000000 XLAST= 20.0000000000
 0 PHYSICAL COORDINATE RANGE- XFIRST= 0.0000000000 XLAST= 2.0000000000

0 NO. OF GRID POINTS= 20
 NO. OF PIVOTS = 0
 BASE SLOPE = 0.0000000000

I	X	Y	RATIO
1	20.000000	2.000000	1.000000
1	ETA	ALPHA	
1	2.000000	1.000000	
2	20.000000	1.000000	

BETA0= 0.105263158

0	I	ETA	ALPHA	BETA
0	1	2.000000000	1.000000000	0.000000000
0	1	X	Y	Z
1	1	1.000000000	0.000000000	0.000000000
2	2	2.000000000	0.105263158	0.105263158
3	3	3.000000000	0.210526316	0.210526316
4	4	4.000000000	0.315789474	0.315789474
5	5	5.000000000	0.421052632	0.421052632
6	6	6.000000000	0.526315789	0.526315789
7	7	7.000000000	0.631578947	0.631578947
8	8	8.000000000	0.736842105	0.736842105
9	9	9.000000000	0.842105263	0.842105263
10	10	10.000000000	0.947368421	0.947368421
11	11	11.000000000	1.052631579	1.052631579
12	12	12.000000000	1.157894737	1.157894737
13	13	13.000000000	1.263157895	1.263157895
14	14	14.000000000	1.368421053	1.368421053
15	15	15.000000000	1.473684211	1.473684211
16	16	16.000000000	1.578947368	1.578947368
17	17	17.000000000	1.684210526	1.684210526
18	18	18.000000000	1.789473684	1.789473684
19	19	19.000000000	1.894736842	1.894736842
20	20	20.000000000	2.000000000	2.000000000

1
 0 GEOMETRY DATA AT TSTEP NO. 0 GTIME = 0.00000000

0***** X1-COORD-FIX *****

01Z=	1	2	3	4	5	6	7	8	9	10
Z=	0.0000000	0.105263E	0.00.210526E	0.00.315789E	0.00.421053E	0.00.526316E	0.00.631579E	0.00.736842E	0.00.842105E	0.00.947368E
20	0.10000E 01	0.10000E 01	0.10000E 01	0.10000E 01	0.10000E 01	0.10000E 01	0.10000E 01	0.10000E 01	0.10000E 01	0.10000E 01
19	0.99965E 00	0.99965E 00	0.99965E 00	0.99965E 00	0.99965E 00	0.99965E 00	0.99965E 00	0.99965E 00	0.99965E 00	0.99965E 00
18	0.99882E 00	0.99882E 00	0.99882E 00	0.99882E 00	0.99882E 00	0.99882E 00	0.99882E 00	0.99882E 00	0.99882E 00	0.99882E 00
17	0.99683E 00	0.99683E 00	0.99683E 00	0.99683E 00	0.99683E 00	0.99683E 00	0.99683E 00	0.99683E 00	0.99683E 00	0.99683E 00
16	0.99210E 00	0.99210E 00	0.99210E 00	0.99210E 00	0.99210E 00	0.99210E 00	0.99210E 00	0.99210E 00	0.99210E 00	0.99210E 00
15	0.98095E 00	0.98095E 00	0.98095E 00	0.98095E 00	0.98095E 00	0.98095E 00	0.98095E 00	0.98095E 00	0.98095E 00	0.98095E 00
14	0.95525E 00	0.95525E 00	0.95525E 00	0.95525E 00	0.95525E 00	0.95525E 00	0.95525E 00	0.95525E 00	0.95525E 00	0.95525E 00
13	0.89387E 00	0.89387E 00	0.89387E 00	0.89387E 00	0.89387E 00	0.89387E 00	0.89387E 00	0.89387E 00	0.89387E 00	0.89387E 00
12	0.78758E 00	0.78758E 00	0.78758E 00	0.78758E 00	0.78758E 00	0.78758E 00	0.78758E 00	0.78758E 00	0.78758E 00	0.78758E 00
11	0.60748E 00	0.60748E 00	0.60748E 00	0.60748E 00	0.60748E 00	0.60748E 00	0.60748E 00	0.60748E 00	0.60748E 00	0.60748E 00
10	0.39252E 00	0.39252E 00	0.39252E 00	0.39252E 00	0.39252E 00	0.39252E 00	0.39252E 00	0.39252E 00	0.39252E 00	0.39252E 00
9	0.21242E 00	0.21242E 00	0.21242E 00	0.21242E 00	0.21242E 00	0.21242E 00	0.21242E 00	0.21242E 00	0.21242E 00	0.21242E 00
8	0.10113E 00	0.10113E 00	0.10113E 00	0.10113E 00	0.10113E 00	0.10113E 00	0.10113E 00	0.10113E 00	0.10113E 00	0.10113E 00
7	0.44748E-01	0.44748E-01	0.44748E-01	0.44748E-01	0.44748E-01	0.44748E-01	0.44748E-01	0.44748E-01	0.44748E-01	0.44748E-01
6	0.19050E-01	0.19050E-01	0.19050E-01	0.19050E-01	0.19050E-01	0.19050E-01	0.19050E-01	0.19050E-01	0.19050E-01	0.19050E-01
5	0.79030E-02	0.79030E-02	0.79030E-02	0.79030E-02	0.79030E-02	0.79030E-02	0.79030E-02	0.79030E-02	0.79030E-02	0.79030E-02
4	0.31715E-02	0.31715E-02	0.31715E-02	0.31715E-02	0.31715E-02	0.31715E-02	0.31715E-02	0.31715E-02	0.31715E-02	0.31715E-02
3	0.11819E-02	0.11819E-02	0.11819E-02	0.11819E-02	0.11819E-02	0.11819E-02	0.11819E-02	0.11819E-02	0.11819E-02	0.11819E-02
2	0.34851E-03	0.34851E-03	0.34851E-03	0.34851E-03	0.34851E-03	0.34851E-03	0.34851E-03	0.34851E-03	0.34851E-03	0.34851E-03
1	-0.10857E-15	-0.10857E-15	-0.10857E-15	-0.10857E-15	-0.10857E-15	-0.10857E-15	-0.10857E-15	-0.10857E-15	-0.10857E-15	-0.10857E-15

01Z= 11 12 13 14 15 16 17 18 19 20
 Z= 0.105263E 010.115789E 010.126316E 010.136842E 010.147368E 010.157895E 010.168421E 010.178947E 010.189474E 010.200000E 01


```

&END
1
1 0.000000 0.000000 0.103851E 01 0.962918E 00
2 0.348505E-03 0.452883E 01 0.442439E 01 0.129883E 00 0.129897E 00 0.129883E 00 0.103786E 01 0.963521E 00 0.299720E-03
3 0.118190E-02 0.153588E 02 0.105461E 02 0.309441E 00 0.309624E 00 0.309441E 00 0.103482E 01 0.966349E 00 0.343079E-02
4 0.317153E-02 0.412141E 02 0.139703E 02 0.409731E 00 0.410157E 00 0.409731E 00 0.103204E 01 0.968950E 00 0.244238E-01
5 0.790299E-02 0.102699E 03 0.164365E 02 0.481869E 00 0.482563E 00 0.481869E 00 0.102957E 01 0.971281E 00 0.147512E 00
6 0.190504E-01 0.247561E 03 0.192304E 02 0.563477E 00 0.564589E 00 0.563477E 00 0.102628E 01 0.974390E 00 0.800417E 00
7 0.447482E-01 0.581504E 03 0.241939E 02 0.708100E 00 0.710313E 00 0.708100E 00 0.101920E 01 0.931161E 00 0.369478E 01
8 0.101126E 00 0.131414E 04 0.332628E 02 0.970824E 00 0.976570E 00 0.970824E 00 0.100221E 01 0.997791E 00 0.107855E 02
9 0.212419E 00 0.276039E 04 0.356323E 02 0.103908E 01 0.104614E 01 0.100000E 01 0.100000E 01 0.100000E 01 0.113521E 02
10 0.392518E 00 0.510077E 04 0.371247E 02 0.108197E 01 0.108995E 01 0.100000E 01 0.100000E 01 0.100000E 01 0.113521E 02
CFC,CF,UTAU = 0.182327E-02 0.166000E-02 0.293592E-01
YPLUSD,UPLUSD,PIXDK = 0.157876E 04 0.342750E 02 0.232718E 01
1
1 0.000000 0.000000 0.103851E 01 0.962918E 00
2 0.348505E-03 0.452883E 01 0.442439E 01 0.129883E 00 0.129897E 00 0.129883E 00 0.103786E 01 0.963521E 00 0.299720E-03
3 0.118190E-02 0.153588E 02 0.105461E 02 0.309441E 00 0.309624E 00 0.309441E 00 0.103482E 01 0.966349E 00 0.343079E-02
4 0.317153E-02 0.412141E 02 0.139703E 02 0.409731E 00 0.410157E 00 0.409731E 00 0.103204E 01 0.968950E 00 0.244238E-01
5 0.790299E-02 0.102699E 03 0.164365E 02 0.481869E 00 0.482563E 00 0.481869E 00 0.102957E 01 0.971281E 00 0.147512E 00
6 0.190504E-01 0.247561E 03 0.192304E 02 0.563477E 00 0.564589E 00 0.563477E 00 0.102628E 01 0.974390E 00 0.800417E 00
7 0.447482E-01 0.581504E 03 0.241939E 02 0.708100E 00 0.710313E 00 0.708100E 00 0.101920E 01 0.931161E 00 0.369478E 01
8 0.101126E 00 0.131414E 04 0.332628E 02 0.970824E 00 0.976570E 00 0.970824E 00 0.100221E 01 0.997791E 00 0.107855E 02
9 0.212419E 00 0.276039E 04 0.356323E 02 0.103908E 01 0.104614E 01 0.100000E 01 0.100000E 01 0.100000E 01 0.113521E 02
10 0.392518E 00 0.510077E 04 0.371247E 02 0.108197E 01 0.108995E 01 0.100000E 01 0.100000E 01 0.100000E 01 0.113521E 02
CFC,CF,UTAU = 0.182327E-02 0.166000E-02 0.293592E-01
YPLUSD,UPLUSD,PIXDK = 0.157876E 04 0.342750E 02 0.232718E 01
MZ,XMAX,AMCH,TDUM,PDUM,RDUM,WDUM
1 0.100000E 01 0.438805E 00 0.100000E 01 0.100000E 01 0.100000E 01 0.100000E 01 0.100000E 01
2 0.100000E 01 0.438805E 00 0.100000E 01 0.100000E 01 0.100000E 01 0.100000E 01 0.100000E 01
3 0.100000E 01 0.438805E 00 0.100000E 01 0.100000E 01 0.100000E 01 0.100000E 01 0.100000E 01
4 0.100000E 01 0.438805E 00 0.100000E 01 0.100000E 01 0.100000E 01 0.100000E 01 0.100000E 01
5 0.100000E 01 0.438805E 00 0.100000E 01 0.100000E 01 0.100000E 01 0.100000E 01 0.100000E 01
6 0.100000E 01 0.438805E 00 0.100000E 01 0.100000E 01 0.100000E 01 0.100000E 01 0.100000E 01
7 0.100000E 01 0.438805E 00 0.100000E 01 0.100000E 01 0.100000E 01 0.100000E 01 0.100000E 01
8 0.100000E 01 0.438805E 00 0.100000E 01 0.100000E 01 0.100000E 01 0.100000E 01 0.100000E 01
9 0.100000E 01 0.438805E 00 0.100000E 01 0.100000E 01 0.100000E 01 0.100000E 01 0.100000E 01
10 0.100000E 01 0.438805E 00 0.100000E 01 0.100000E 01 0.100000E 01 0.100000E 01 0.100000E 01
11 0.100000E 01 0.438805E 00 0.100000E 01 0.100000E 01 0.100000E 01 0.100000E 01 0.100000E 01
12 0.100000E 01 0.438805E 00 0.100000E 01 0.100000E 01 0.100000E 01 0.100000E 01 0.100000E 01
13 0.100000E 01 0.438805E 00 0.100000E 01 0.100000E 01 0.100000E 01 0.100000E 01 0.100000E 01
14 0.100000E 01 0.438805E 00 0.100000E 01 0.100000E 01 0.100000E 01 0.100000E 01 0.100000E 01
15 0.100000E 01 0.438805E 00 0.100000E 01 0.100000E 01 0.100000E 01 0.100000E 01 0.100000E 01
16 0.100000E 01 0.438805E 00 0.100000E 01 0.100000E 01 0.100000E 01 0.100000E 01 0.100000E 01
17 0.100000E 01 0.438805E 00 0.100000E 01 0.100000E 01 0.100000E 01 0.100000E 01 0.100000E 01
18 0.100000E 01 0.438805E 00 0.100000E 01 0.100000E 01 0.100000E 01 0.100000E 01 0.100000E 01
19 0.100000E 01 0.438805E 00 0.100000E 01 0.100000E 01 0.100000E 01 0.100000E 01 0.100000E 01
20 0.100000E 01 0.438805E 00 0.100000E 01 0.100000E 01 0.100000E 01 0.100000E 01 0.100000E 01

```

```

*****
*****

```

```

1
&READ1
IREST= -1
IOTAPE= 10
INTAPE= 9
IOTAP1= 20
INTAP1= 19
&END
&READ9
NUMDX= 18
NUMDY= 0
NUMDZ= 18
XGRIN= 3*0.0
XGMAX= 1.0, 0.0, 2.0
GRID= -0.99950, 0.99950, 0.0, 0.0, 0.0, 0.0
XCENR= 3*0.0
DAMPG= 3*0.0
IGEOM= 1
TWOD= T
IGTYPE= 1
LXSPLT= 10
LYSPLT= 1
REY= 473299.99367414
CLENG= 0.44100-01
WREF= 149.176750
DENS= 1.26921280
TREF= 287.6230

```

MASS FLUX AT IDT = 0

LZ	FLUX * 10 ¹⁰	MASS FLUX
1	0.93722E 00	
2	0.93687E 00	
3	0.93653E 00	
4	0.93618E 00	
5	0.93584E 00	
6	0.93549E 00	
7	0.93515E 00	
8	0.93480E 00	
9	0.93446E 00	
10	0.93411E 00	
11	0.93377E 00	
12	0.93342E 00	
13	0.93308E 00	
14	0.93273E 00	
15	0.93239E 00	
16	0.93204E 00	
17	0.93169E 00	
18	0.93135E 00	
19	0.93100E 00	
20	0.93066E 00	

```

***** STARTING FLOW FIELD *****
RESULTS AT TSTEP NO.    0    TIME =    0.000000

```

0***** U-VL

[illegible]

01Z=	11	12	13	14	15	16	17	18	19	20
Z=	0.105263E	010.115789E	010.126316E	010.136842E	010.147368E	010.157895E	010.168421E	010.178947E	010.189474E	010.200090E
20	0.00000	0.00000	0.00000	0.00000	0.00000	0.00000	0.00000	0.00000	0.00000	0.00000
19	0.00000	0.00000	0.00000	0.00000	0.00000	0.00000	0.00000	0.00000	0.00000	0.00000
18	0.00000	0.00000	0.00000	0.00000	0.00000	0.00000	0.00000	0.00000	0.00000	0.00000
17	0.00000	0.00000	0.00000	0.00000	0.00000	0.00000	0.00000	0.00000	0.00000	0.00000
16	0.00000	0.00000	0.00000	0.00000	0.00000	0.00000	0.00000	0.00000	0.00000	0.00000
15	0.00000	0.00000	0.00000	0.00000	0.00000	0.00000	0.00000	0.00000	0.00000	0.00000
14	0.00000	0.00000	0.00000	0.00000	0.00000	0.00000	0.00000	0.00000	0.00000	0.00000
13	0.00000	0.00000	0.00000	0.00000	0.00000	0.00000	0.00000	0.00000	0.00000	0.00000
12	0.00000	0.00000	0.00000	0.00000	0.00000	0.00000	0.00000	0.00000	0.00000	0.00000
11	0.00000	0.00000	0.00000	0.00000	0.00000	0.00000	0.00000	0.00000	0.00000	0.00000
10	0.00000	0.00000	0.00000	0.00000	0.00000	0.00000	0.00000	0.00000	0.00000	0.00000
9	0.00000	0.00000	0.00000	0.00000	0.00000	0.00000	0.00000	0.00000	0.00000	0.00000
8	0.00000	0.00000	0.00000	0.00000	0.00000	0.00000	0.00000	0.00000	0.00000	0.00000
7	0.00000	0.00000	0.00000	0.00000	0.00000	0.00000	0.00000	0.00000	0.00000	0.00000
6	0.00000	0.00000	0.00000	0.00000	0.00000	0.00000	0.00000	0.00000	0.00000	0.00000
5	0.00000	0.00000	0.00000	0.00000	0.00000	0.00000	0.00000	0.00000	0.00000	0.00000
4	0.00000	0.00000	0.00000	0.00000	0.00000	0.00000	0.00000	0.00000	0.00000	0.00000
3	0.00000	0.00000	0.00000	0.00000	0.00000	0.00000	0.00000	0.00000	0.00000	0.00000
2	0.00000	0.00000	0.00000	0.00000	0.00000	0.00000	0.00000	0.00000	0.00000	0.00000
1	0.00000	0.00000	0.00000	0.00000	0.00000	0.00000	0.00000	0.00000	0.00000	0.00000
RESULTS AT TSTEP NO.	0	TIME =	0.000000							

[illegible][illegible]

```

10 0.10000E 01 0.10000E 01 0.10000E 01 0.10000E 01 0.10000E 01 0.10000E 01 0.10000E 01 0.10000E 01 0.10000E 01 0.10000E 01 0.10000E 01
9 0.10000E 01 0.10000E 01 0.10000E 01 0.10000E 01 0.10000E 01 0.10000E 01 0.10000E 01 0.10000E 01 0.10000E 01 0.10000E 01 0.10000E 01 0.10000E 01
8 0.97082E 00 0.97082E 00 0.97082E 00 0.97082E 00 0.97082E 00 0.97082E 00 0.97082E 00 0.97082E 00 0.97082E 00 0.97082E 00 0.97082E 00 0.97082E 00
7 0.70810E 00 0.70810E 00 0.70810E 00 0.70810E 00 0.70810E 00 0.70810E 00 0.70810E 00 0.70810E 00 0.70810E 00 0.70810E 00 0.70810E 00 0.70810E 00 0.70810E 00
6 0.56348E 00 0.56348E 00 0.56348E 00 0.56348E 00 0.56348E 00 0.56348E 00 0.56348E 00 0.56348E 00 0.56348E 00 0.56348E 00 0.56348E 00 0.56348E 00 0.56348E 00
5 0.48187E 00 0.48187E 00 0.48187E 00 0.48187E 00 0.48187E 00 0.48187E 00 0.48187E 00 0.48187E 00 0.48187E 00 0.48187E 00 0.48187E 00 0.48187E 00 0.48187E 00
4 0.40973E 00 0.40973E 00 0.40973E 00 0.40973E 00 0.40973E 00 0.40973E 00 0.40973E 00 0.40973E 00 0.40973E 00 0.40973E 00 0.40973E 00 0.40973E 00 0.40973E 00
3 0.30944E 00 0.30944E 00 0.30944E 00 0.30944E 00 0.30944E 00 0.30944E 00 0.30944E 00 0.30944E 00 0.30944E 00 0.30944E 00 0.30944E 00 0.30944E 00 0.30944E 00
2 0.12988E 00 0.12988E 00 0.12988E 00 0.12988E 00 0.12988E 00 0.12988E 00 0.12988E 00 0.12988E 00 0.12988E 00 0.12988E 00 0.12988E 00 0.12988E 00
1 0.00000 0.00000 0.00000 0.00000 0.00000 0.00000 0.00000 0.00000 0.00000 0.00000 0.00000 0.00000 0.00000 0.00000 0.00000
RESULTS AT TSTEP NO. 0 TIME = 0.000000

```

***** DENS *****

```

OLZ= 1 2 3 4 5 6 7 8 9 10
Z= 0.0000000.105263E 000.210526E 000.315789E 000.421053E 000.526316E 000.631579E 000.736842E 000.842105E 000.947368E 00
20 0.96293E 00 0.96257E 00 0.96222E 00 0.96186E 00 0.96151E 00 0.96115E 00 0.96080E 00 0.96044E 00 0.96009E 00 0.95973E 00
19 0.96353E 00 0.96317E 00 0.96282E 00 0.96246E 00 0.96211E 00 0.96175E 00 0.96140E 00 0.96104E 00 0.96069E 00 0.96033E 00
18 0.96636E 00 0.96600E 00 0.96565E 00 0.96529E 00 0.96493E 00 0.96458E 00 0.96422E 00 0.96386E 00 0.96351E 00 0.96315E 00
17 0.96896E 00 0.96860E 00 0.96824E 00 0.96789E 00 0.96753E 00 0.96717E 00 0.96682E 00 0.96646E 00 0.96610E 00 0.96574E 00
16 0.97129E 00 0.97093E 00 0.97057E 00 0.97021E 00 0.96986E 00 0.96950E 00 0.96914E 00 0.96878E 00 0.96843E 00 0.96807E 00
15 0.97440E 00 0.97404E 00 0.97368E 00 0.97332E 00 0.97296E 00 0.97260E 00 0.97224E 00 0.97188E 00 0.97152E 00 0.97117E 00
14 0.98117E 00 0.98080E 00 0.98044E 00 0.98008E 00 0.97972E 00 0.97936E 00 0.97900E 00 0.97863E 00 0.97827E 00 0.97791E 00
13 0.99779E 00 0.99742E 00 0.99706E 00 0.99669E 00 0.99632E 00 0.99595E 00 0.99559E 00 0.99522E 00 0.99485E 00 0.99448E 00
12 0.10000E 01 0.99963E 00 0.99926E 00 0.99889E 00 0.99853E 00 0.99816E 00 0.99779E 00 0.99742E 00 0.99705E 00 0.99668E 00
11 0.10000E 01 0.99963E 00 0.99926E 00 0.99889E 00 0.99853E 00 0.99816E 00 0.99779E 00 0.99742E 00 0.99705E 00 0.99668E 00
10 0.10000E 01 0.99963E 00 0.99926E 00 0.99889E 00 0.99853E 00 0.99816E 00 0.99779E 00 0.99742E 00 0.99705E 00 0.99668E 00
9 0.10000E 01 0.99963E 00 0.99926E 00 0.99889E 00 0.99853E 00 0.99816E 00 0.99779E 00 0.99742E 00 0.99705E 00 0.99668E 00
8 0.99779E 00 0.99742E 00 0.99706E 00 0.99669E 00 0.99632E 00 0.99595E 00 0.99559E 00 0.99522E 00 0.99485E 00 0.99448E 00
7 0.98117E 00 0.98080E 00 0.98044E 00 0.98008E 00 0.97972E 00 0.97936E 00 0.97900E 00 0.97863E 00 0.97827E 00 0.97791E 00
6 0.97440E 00 0.97404E 00 0.97368E 00 0.97332E 00 0.97296E 00 0.97260E 00 0.97224E 00 0.97188E 00 0.97152E 00 0.97117E 00
5 0.97129E 00 0.97093E 00 0.97057E 00 0.97021E 00 0.96986E 00 0.96950E 00 0.96914E 00 0.96878E 00 0.96843E 00 0.96807E 00
4 0.96896E 00 0.96860E 00 0.96824E 00 0.96789E 00 0.96753E 00 0.96717E 00 0.96682E 00 0.96646E 00 0.96610E 00 0.96574E 00
3 0.96636E 00 0.96600E 00 0.96565E 00 0.96529E 00 0.96493E 00 0.96458E 00 0.96422E 00 0.96386E 00 0.96351E 00 0.96315E 00
2 0.96353E 00 0.96317E 00 0.96282E 00 0.96246E 00 0.96211E 00 0.96175E 00 0.96140E 00 0.96104E 00 0.96069E 00 0.96033E 00
1 0.96293E 00 0.96257E 00 0.96222E 00 0.96186E 00 0.96151E 00 0.96115E 00 0.96080E 00 0.96044E 00 0.96009E 00 0.95973E 00

```

```

OLZ= 11 12 13 14 15 16 17 18 19 20
Z= 0.105263E 010.115789E 010.126316E 010.136842E 010.147368E 010.157895E 010.168421E 010.178947E 010.189474E 010.200000E 01
20 0.95938E 00 0.95902E 00 0.95867E 00 0.95831E 00 0.95796E 00 0.95761E 00 0.95725E 00 0.95690E 00 0.95654E 00 0.95619E 00
19 0.95998E 00 0.95962E 00 0.95927E 00 0.95891E 00 0.95856E 00 0.95820E 00 0.95785E 00 0.95749E 00 0.95714E 00 0.95678E 00
18 0.96280E 00 0.96244E 00 0.96208E 00 0.96173E 00 0.96137E 00 0.96102E 00 0.96066E 00 0.96030E 00 0.95995E 00 0.95959E 00
17 0.96539E 00 0.96503E 00 0.96467E 00 0.96432E 00 0.96396E 00 0.96360E 00 0.96325E 00 0.96289E 00 0.96253E 00 0.96217E 00
16 0.96771E 00 0.96735E 00 0.96699E 00 0.96664E 00 0.96628E 00 0.96592E 00 0.96556E 00 0.96520E 00 0.96485E 00 0.96449E 00
15 0.97081E 00 0.97045E 00 0.97009E 00 0.96973E 00 0.96937E 00 0.96901E 00 0.96865E 00 0.96829E 00 0.96793E 00 0.96758E 00
14 0.97755E 00 0.97719E 00 0.97683E 00 0.97647E 00 0.97610E 00 0.97574E 00 0.97538E 00 0.97502E 00 0.97466E 00 0.97430E 00
13 0.99412E 00 0.99375E 00 0.99338E 00 0.99301E 00 0.99264E 00 0.99228E 00 0.99191E 00 0.99154E 00 0.99117E 00 0.99081E 00
12 0.99632E 00 0.99595E 00 0.99558E 00 0.99521E 00 0.99484E 00 0.99447E 00 0.99411E 00 0.99374E 00 0.99337E 00 0.99300E 00
11 0.99632E 00 0.99595E 00 0.99558E 00 0.99521E 00 0.99484E 00 0.99447E 00 0.99411E 00 0.99374E 00 0.99337E 00 0.99300E 00
10 0.99632E 00 0.99595E 00 0.99558E 00 0.99521E 00 0.99484E 00 0.99447E 00 0.99411E 00 0.99374E 00 0.99337E 00 0.99300E 00
9 0.99632E 00 0.99595E 00 0.99558E 00 0.99521E 00 0.99484E 00 0.99447E 00 0.99411E 00 0.99374E 00 0.99337E 00 0.99300E 00
8 0.99412E 00 0.99375E 00 0.99338E 00 0.99301E 00 0.99264E 00 0.99228E 00 0.99191E 00 0.99154E 00 0.99117E 00 0.99081E 00
7 0.97755E 00 0.97719E 00 0.97683E 00 0.97647E 00 0.97610E 00 0.97574E 00 0.97538E 00 0.97502E 00 0.97466E 00 0.97430E 00
6 0.97081E 00 0.97045E 00 0.97009E 00 0.96973E 00 0.96937E 00 0.96901E 00 0.96865E 00 0.96829E 00 0.96793E 00 0.96758E 00
5 0.96771E 00 0.96735E 00 0.96699E 00 0.96664E 00 0.96628E 00 0.96592E 00 0.96556E 00 0.96520E 00 0.96485E 00 0.96449E 00
4 0.96539E 00 0.96503E 00 0.96467E 00 0.96432E 00 0.96396E 00 0.96360E 00 0.96325E 00 0.96289E 00 0.96253E 00 0.96217E 00
3 0.96280E 00 0.96244E 00 0.96208E 00 0.96173E 00 0.96137E 00 0.96102E 00 0.96066E 00 0.96030E 00 0.95995E 00 0.95959E 00
2 0.95998E 00 0.95962E 00 0.95927E 00 0.95891E 00 0.95856E 00 0.95820E 00 0.95785E 00 0.95749E 00 0.95714E 00 0.95678E 00
1 0.95938E 00 0.95902E 00 0.95867E 00 0.95831E 00 0.95796E 00 0.95761E 00 0.95725E 00 0.95690E 00 0.95654E 00 0.95619E 00
RESULTS AT TSTEP NO. 0 TIME = 0.000000

```

***** PRES *****

```

OLZ= 1 2 3 4 5 6 7 8 9 10
Z= 0.0000000.105263E 000.210526E 000.315789E 000.421053E 000.526316E 000.631579E 000.736842E 000.842105E 000.947368E 00
20 0.10000E 01 0.99963E 00 0.99926E 00 0.99889E 00 0.99853E 00 0.99816E 00 0.99779E 00 0.99742E 00 0.99705E 00 0.99668E 00
19 0.10000E 01 0.99963E 00 0.99926E 00 0.99889E 00 0.99853E 00 0.99816E 00 0.99779E 00 0.99742E 00 0.99705E 00 0.99668E 00
18 0.10000E 01 0.99963E 00 0.99926E 00 0.99889E 00 0.99853E 00 0.99816E 00 0.99779E 00 0.99742E 00 0.99705E 00 0.99668E 00
17 0.10000E 01 0.99963E 00 0.99926E 00 0.99889E 00 0.99853E 00 0.99816E 00 0.99779E 00 0.99742E 00 0.99705E 00 0.99668E 00
16 0.10000E 01 0.99963E 00 0.99926E 00 0.99889E 00 0.99853E 00 0.99816E 00 0.99779E 00 0.99742E 00 0.99705E 00 0.99668E 00
15 0.10000E 01 0.99963E 00 0.99926E 00 0.99889E 00 0.99853E 00 0.99816E 00 0.99779E 00 0.99742E 00 0.99705E 00 0.99668E 00
14 0.10000E 01 0.99963E 00 0.99926E 00 0.99889E 00 0.99853E 00 0.99816E 00 0.99779E 00 0.99742E 00 0.99705E 00 0.99668E 00
13 0.10000E 01 0.99963E 00 0.99926E 00 0.99889E 00 0.99853E 00 0.99816E 00 0.99779E 00 0.99742E 00 0.99705E 00 0.99668E 00
12 0.10000E 01 0.99963E 00 0.99926E 00 0.99889E 00 0.99853E 00 0.99816E 00 0.99779E 00 0.99742E 00 0.99705E 00 0.99668E 00
11 0.10000E 01 0.99963E 00 0.99926E 00 0.99889E 00 0.99853E 00 0.99816E 00 0.99779E 00 0.99742E 00 0.99705E 00 0.99668E 00
10 0.10000E 01 0.99963E 00 0.99926E 00 0.99889E 00 0.99853E 00 0.99816E 00 0.99779E 00 0.99742E 00 0.99705E 00 0.99668E 00
9 0.10000E 01 0.99963E 00 0.99926E 00 0.99889E 00 0.99853E 00 0.99816E 00 0.99779E 00 0.99742E 00 0.99705E 00 0.99668E 00

```


[illegible]


```

D** TIME STEP NO. 1 CPTIME= 0.00 MIN. TPHYS= 0.50000E-02 DT= 0.50000E-02 VISC STAB= 0.122E-06 IDTADJ= 1
** STEST= 0.7961E-02 AT LX= 19 LY= 1 LZ= 20 RATIO= 7.961 MAX. CHANGE -- (IEQ)=
** (1)= -0.1641E-04 (3)= -0.7961E-02 (4)= 0.4877E-03 (
D** REAVG= 0.112E 01 RESMAX= 0.231E 01 LX= 11 LY= 1 LZ= 19
IEQ= 1 RESAVG= 0.143E-03 RESEQ= -0.409E-03 LX= 7LY= 1 LZ= 3 IEQ= 3 RESAVG= 0.112E 01 RESEQ= 0.231E 01 LX= 11 LY= 1 LZ= 19
IEQ= 4 RESAVG= 0.209E 00 RESEQ= 0.490E 00 LX= 11LY= 1 LZ= 19 IEQ=
CONV = AMP(L,M,H),RMS CONV . CONV+DIFF, AMP(L,M,H),RMS DIFF
MAX -0.10000E 26 -0.10000E 26 -0.10000E 26 -0.10000E 26 -0.10000E 26 -0.10000E 26 -0.10000E 26 -0.10000E 26
MIN 0.10000E 26 0.10000E 26 0.10000E 26 0.10000E 26 0.10000E 26 0.10000E 26 0.10000E 26 0.10000E 26
DTISAV, JCBN= 0.20000E 03 0.14858E-03
AN VAR(N) DVAR(N+1) A/DT*DVAR L1*DVAR L2*DVAR L3*DVAR DVAR(*) A/DT*DVAR* L1*(DV-DV*)
EQ 1 VAR 1 0.96565E 00 0.00000 0.16050E-04 0.30996E-02-0.61176E-04 0.00000 0.89177E-09
EQ 1 VAR 3 0.00000 0.30944E 00-0.12851E-02 0.00000 0.98861E-01 0.00000 0.00000
EQ 1 VAR 4 0.00000 0.96565E 00-0.17707E-04 0.00000 0.91884E-01 0.00000 0.00000
EQ= 1 A,L1,L2,L3,RES,SPLIT= 0.30996E-02 0.69157E-02 0.00000 0.89177E-09-0.89677E-06 0.38152E-02
EQ 3 VAR 1 0.00000 0.16050E-04 0.00000-0.21880E-02 0.00000 0.00000
EQ 3 VAR 3 0.96565E 00 0.30944E 00-0.12851E-02-0.24818E 00-0.12999E-01 0.00000 0.83808E-04
EQ 3 VAR 4 0.30944E 00 0.96565E 00-0.17707E-04-0.10958E-02 0.00000 0.00000 0.56482E-03
EQ= 3 A,L1,L2,L3,RES,SPLIT= -0.24928E 00-0.15187E-01 0.00000 0.64863E-03-0.23471E 00 0.28081E-04
EQ 4 VAR 1 0.00000 0.16050E-04 0.00000-0.47840E-02 0.00000 0.00000
EQ 4 VAR 3 0.00000 0.30944E 00-0.12851E-02 0.00000 0.00000 0.10980E-03
EQ 4 VAR 4 0.10000E 01 0.96565E 00-0.17707E-04-0.35414E-02 0.00000 0.00000 0.86212E-04
EQ= 4 A,L1,L2,L3,RES,SPLIT= -0.35414E-02-0.47840E-02 0.00000 0.19601E-03 0.10466E-02-0.57593E-08
LZ Z U-VEL V-VEL W-VEL DENSITY ENTHALPY PBOT PTOP DP
1 0.00000000 0.73010E-08 0.00000 0.99997E 00 0.10000E 01 0.10385E 01 0.10005E 01 0.10005E 01 0.10000E 01
2 0.10526316E 00 0.73006E-08 0.00000 0.10001E 01 0.99965E 00 0.10385E 01 0.99988E 00 0.99988E 00 0.99964E 00
3 0.21052632E 00 0.73002E-08 0.00000 0.10001E 01 0.99928E 00 0.10385E 01 0.99928E 00 0.99928E 00 0.99928E 00
4 0.31578947E 00 0.72998E-08 0.00000 0.10001E 01 0.99891E 00 0.10385E 01 0.99891E 00 0.99891E 00 0.99891E 00
5 0.42105263E 00 0.72994E-08 0.00000 0.10001E 01 0.99854E 00 0.10385E 01 0.99854E 00 0.99854E 00 0.99854E 00
6 0.52631579E 00 0.72990E-08 0.00000 0.10001E 01 0.99818E 00 0.10385E 01 0.99817E 00 0.99817E 00 0.99817E 00
7 0.63157895E 00 0.72986E-08 0.00000 0.10001E 01 0.99781E 00 0.10385E 01 0.99780E 00 0.99780E 00 0.99780E 00
8 0.73684211E 00 0.72982E-08 0.00000 0.10001E 01 0.99744E 00 0.10385E 01 0.99743E 00 0.99743E 00 0.99743E 00
9 0.84210526E 00 0.72978E-08 0.00000 0.10001E 01 0.99707E 00 0.10385E 01 0.99706E 00 0.99706E 00 0.99707E 00
10 0.94736842E 00 0.72974E-08 0.00000 0.10001E 01 0.99670E 00 0.10385E 01 0.99669E 00 0.99669E 00 0.99670E 00
11 0.10526316E 01 0.72970E-08 0.00000 0.10001E 01 0.99633E 00 0.10385E 01 0.99633E 00 0.99633E 00 0.99633E 00
12 0.11578947E 01 0.72965E-08 0.00000 0.10001E 01 0.99596E 00 0.10385E 01 0.99596E 00 0.99596E 00 0.99596E 00
13 0.12631579E 01 0.72961E-08 0.00000 0.10001E 01 0.99560E 00 0.10385E 01 0.99559E 00 0.99559E 00 0.99559E 00
14 0.13684211E 01 0.72957E-08 0.00000 0.10001E 01 0.99523E 00 0.10385E 01 0.99522E 00 0.99522E 00 0.99522E 00
15 0.14736842E 01 0.72953E-08 0.00000 0.10001E 01 0.99486E 00 0.10385E 01 0.99485E 00 0.99485E 00 0.99485E 00
16 0.15789474E 01 0.72949E-08 0.00000 0.10001E 01 0.99449E 00 0.10385E 01 0.99448E 00 0.99448E 00 0.99449E 00
17 0.16842105E 01 0.72945E-08 0.00000 0.10001E 01 0.99412E 00 0.10385E 01 0.99412E 00 0.99412E 00 0.99412E 00
18 0.17894737E 01 0.72941E-08 0.00000 0.10001E 01 0.99375E 00 0.10385E 01 0.99375E 00 0.99375E 00 0.99375E 00
19 0.18947368E 01 0.72937E-08 0.00000 0.10001E 01 0.99339E 00 0.10385E 01 0.99338E 00 0.99338E 00 0.99338E 00
20 0.20000000E 01 0.72933E-08 0.00000 0.10001E 01 0.99301E 00 0.10385E 01 0.99300E 00 0.99300E 00 0.99300E 00
0 START -- TOTAL MASS = 0.1985675364E 01 TOTAL ENERGY = 0.1561919368E 01
CURRENT -- TOTAL MASS = 0.1985745486E 01 TOTAL ENERGY = 0.1561995107E 01
PERCENT DIFFERENCE -- IN MASS = 0.00353 IN ENERGY = 0.00485

```

```

D** TIME STEP NO. 2 CPTIME= 0.00 MIN. TPHYS= 0.11250E-01 DT= 0.62500E-02 VISC STAB= 0.152E-06 IDTADJ= 1
** STEST= 0.8492E-02 AT LX= 19 LY= 1 LZ= 20 RATIO= 8.492 MAX. CHANGE -- (IEQ)=
** (1)= -0.1488E-03 (3)= -0.8492E-02 (4)= 0.2076E-03 (
D** REAVG= 0.115E 01 RESMAX= 0.234E 01 LX= 10 LY= 1 LZ= 19
IEQ= 1 RESAVG= 0.338E-01 RESEQ= -0.276E 00 LX= 19LY= 1 LZ= 2 IEQ= 3 RESAVG= 0.115E 01 RESEQ= 0.234E 01 LX= 10 LY= 1 LZ= 19
IEQ= 4 RESAVG= 0.214E 00 RESEQ= 0.490E 00 LX= 11LY= 1 LZ= 8 IEQ=
CONV = AMP(L,M,H),RMS CONV . CONV+DIFF, AMP(L,M,H),RMS DIFF
MAX -0.10000E 26 -0.10000E 26 -0.10000E 26 -0.10000E 26 -0.10000E 26 -0.10000E 26 -0.10000E 26 -0.10000E 26
MIN 0.10000E 26 0.10000E 26 0.10000E 26 0.10000E 26 0.10000E 26 0.10000E 26 0.10000E 26 0.10000E 26
DTISAV, JCBN= 0.16000E 03 0.14858E-03
AN VAR(N) DVAR(N+1) A/DT*DVAR L1*DVAR L2*DVAR L3*DVAR DVAR(*) A/DT*DVAR* L1*(DV-DV*)
EQ 1 VAR 1 0.96563E 00 0.16050E-04 0.26463E-05 0.40886E-03-0.10728E-03 0.00000 0.20670E-03
EQ 1 VAR 3 0.00000 0.30816E 00-0.16803E-02 0.00000 0.98377E-01 0.00000 0.27092E-08
EQ 1 VAR 4 0.16050E-04 0.96563E 00-0.41388E-04-0.10628E-06-0.10103E 00 0.00000 0.10908E-08
EQ= 1 A,L1,L2,L3,RES,SPLIT= 0.40875E-03-0.27628E-02 0.00000 0.20670E-03 0.69159E-02 0.39510E-02
EQ 3 VAR 1 0.00000 0.16050E-04 0.26463E-05 0.00000-0.21964E-04 0.00000-0.15863E-08
EQ 3 VAR 3 0.96563E 00 0.30816E 00-0.16803E-02-0.25961E 00-0.12789E-01 0.00000 0.11040E-03
EQ 3 VAR 4 0.30816E 00 0.96563E 00-0.41388E-04-0.20406E-02 0.30974E-08 0.00000 0.86745E-03
EQ= 3 A,L1,L2,L3,RES,SPLIT= -0.26165E 00-0.12811E-01 0.00000 0.97785E-03-0.25002E 00-0.20716E-03
EQ 4 VAR 1 0.00000 0.16050E-04 0.26463E-05 0.00000-0.38187E-02 0.00000 0.00000
EQ 4 VAR 3 0.00000 0.30816E 00-0.16803E-02 0.00000 0.00000 0.00000 0.16345E-03
EQ 4 VAR 4 0.10000E 01 0.96563E 00-0.41388E-04-0.66221E-02 0.48782E-07 0.00000 0.13337E-03
EQ= 4 A,L1,L2,L3,RES,SPLIT= -0.66221E-02-0.38186E-02 0.00000 0.29682E-03-0.35361E-02-0.43586E-03

```

LZ	Z	U-VEL	V-VEL	W-VEL	DENSITY	ENTHALPY	PBOT	PTOP	DP
1	0.00000000	0.29271E-07	0.00000	0.99995E 00	0.10000E 01	0.10385E 01	0.10007E 01	0.10007E 01	0.10000E 01
2	0.10526316E 00	0.25935E-07	0.00000	0.10001E 01	0.99966E 00	0.10385E 01	0.99998E 00	0.99998E 00	0.99965E 00
3	0.21052632E 00	0.22598E-07	0.00000	0.10001E 01	0.99930E 00	0.10385E 01	0.99927E 00	0.99927E 00	0.99929E 00
4	0.31578947E 00	0.22126E-07	0.00000	0.10001E 01	0.99893E 00	0.10385E 01	0.99890E 00	0.99890E 00	0.99892E 00
5	0.42105263E 00	0.22074E-07	0.00000	0.10001E 01	0.99857E 00	0.10385E 01	0.99853E 00	0.99853E 00	0.99855E 00
6	0.52631579E 00	0.22068E-07	0.00000	0.10001E 01	0.99820E 00	0.10385E 01	0.99816E 00	0.99816E 00	0.99819E 00
7	0.63157895E 00	0.22065E-07	0.00000	0.10001E 01	0.99783E 00	0.10385E 01	0.99779E 00	0.99779E 00	0.99782E 00
8	0.73684211E 00	0.22064E-07	0.00000	0.10001E 01	0.99746E 00	0.10385E 01	0.99743E 00	0.99743E 00	0.99745E 00
9	0.84210526E 00	0.22062E-07	0.00000	0.10001E 01	0.99709E 00	0.10385E 01	0.99706E 00	0.99706E 00	0.99708E 00
10	0.94736842E 00	0.22060E-07	0.00000	0.10001E 01	0.99672E 00	0.10385E 01	0.99669E 00	0.99669E 00	0.99671E 00
11	0.10526316E 01	0.22058E-07	0.00000	0.10001E 01	0.99636E 00	0.10385E 01	0.99632E 00	0.99632E 00	0.99634E 00
12	0.11578947E 01	0.22056E-07	0.00000	0.10001E 01	0.99599E 00	0.10385E 01	0.99595E 00	0.99595E 00	0.99598E 00
13	0.12631579E 01	0.22054E-07	0.00000	0.10001E 01	0.99562E 00	0.10385E 01	0.99558E 00	0.99558E 00	0.99561E 00
14	0.13684211E 01	0.22052E-07	0.00000	0.10001E 01	0.99525E 00	0.10385E 01	0.99521E 00	0.99521E 00	0.99524E 00
15	0.14736842E 01	0.22050E-07	0.00000	0.10001E 01	0.99488E 00	0.10385E 01	0.99485E 00	0.99485E 00	0.99487E 00
16	0.15789474E 01	0.22048E-07	0.00000	0.10001E 01	0.99451E 00	0.10385E 01	0.99448E 00	0.99448E 00	0.99450E 00
17	0.16842105E 01	0.22046E-07	0.00000	0.10001E 01	0.99414E 00	0.10385E 01	0.99411E 00	0.99411E 00	0.99413E 00
18	0.17894737E 01	0.22012E-07	0.00000	0.10001E 01	0.99378E 00	0.10385E 01	0.99374E 00	0.99374E 00	0.99376E 00
19	0.18947368E 01	0.21864E-07	0.00000	0.10002E 01	0.99341E 00	0.10385E 01	0.99337E 00	0.99337E 00	0.99340E 00
20	0.20000000E 01	0.21716E-07	0.00000	0.10002E 01	0.99301E 00	0.10385E 01	0.99300E 00	0.99300E 00	0.99300E 00

O START -- TOTAL MASS = 0.1985675364E 01 TOTAL ENERGY = 0.1561919368E 01
 CURRENT -- TOTAL MASS = 0.1925792633E 01 TOTAL ENERGY = 0.1562046685E 01
 PERCENT DIFFERENCE -- IN MASS = 0.00591 IN ENERGY = 0.00815

O** TIME STEP NO. 3 CPTIME= 0.00 MIN. TPHYS= 0.19063E-01 DT= 0.78125E-02 VISC STAB= 0.190E-06 IDTADJ= 1
 ** STEST= 0.8751E-02 AT LX= 19 LY= 1 LZ= 20 RATIO= 8.751 MAX. CHANGE -- (IEQ)=
 ** (1)= -0.1734E-03 (3)= -0.8751E-02 (4)= 0.1399E-03 (5)=
 O** REAVG= 0.114E 01 RESMAX= 0.238E 01 LX= 11 LY= 1 LZ= 19
 IEQ= 1 RESAVG= 0.508E-01 RESEQ= -0.353E 00 LX= 19LY= 1 LZ= 2 IEQ= 3 RESAVG= 0.114E 01 RESEQ= 0.238E 01 LX= 11 LY= 1 LZ= 19
 IEQ= 4 RESAVG= 0.211E 00 RESEQ= 0.491E 00 LX= 11LY= 1 LZ= 8 IEQ= 5
 CONV - ANP(L,M,H),RMS CONV . CONV+DIFF, AMP(L,M,H),RMS DIFF
 MAX -0.10000E 26 -0.10000E 26 -0.10000E 26 -0.10000E 26 -0.10000E 26 -0.10000E 26 -0.10000E 26 -0.10000E 26
 MIN 0.10000E 26 0.10000E 26 0.10000E 26 0.10000E 26 0.10000E 26 0.10000E 26 0.10000E 26 0.10000E 26
 DTISAV, JCBN= 0.12800E 03 0.14858E-03

AN	VAR(N)	DVAR(N+1)	A/DTMDVAR	L1MDVAR	L2MDVAR	L3MDVAR	DVAR(M)	A/DTMDVARM	L1M(DV-DVM)
EQ 1 VAR 1	0.96559E 00	0.18696E-04	0.24903E-05	0.30779E-03	0.15818E-03	0.00000	0.15764E-03		
EQ 1 VAR 3	0.00000	0.30648E 00	0.21801E-02	0.00000	0.93197E-01	0.00000	-0.72624E-06		
EQ 1 VAR 4	0.18696E-04	0.96559E 00	0.55478E-04	0.13276E-06	0.88454E-01	0.00000	-0.29576E-08		
EQ= 1 A,L1,L2,L3,RES,SPLIT=-0.30793E-03	0.45850E-02	0.00000	0.15691E-03	0.43471E-02	0.93970E-02				
EQ 3 VAR 1	0.00000	0.18696E-04	0.24903E-05	0.00000	0.20160E-02	0.00000	-0.65133E-08		
EQ 3 VAR 3	0.96559E 00	0.30648E 00	0.21801E-02	0.26945E 00	0.11496E-01	0.00000	0.25752E-03		
EQ 3 VAR 4	0.30648E 00	0.96559E 00	0.55478E-04	0.21763E-02	0.61880E-07	0.00000	0.41900E-03		
EQ= 3 A,L1,L2,L3,RES,SPLIT=-0.27163E 00	0.94796E-02	0.00000	0.67651E-03	0.26300E 00	0.17521E-03				
EQ 4 VAR 1	0.00000	0.18696E-04	0.24903E-05	0.00000	0.90953E-03	0.00000	0.00000		
EQ 4 VAR 3	0.00000	0.30648E 00	0.21801E-02	0.00000	0.00000	0.00000	0.36994E-03		
EQ 4 VAR 4	0.10000E 01	0.96559E 00	0.55478E-04	0.71012E-02	0.52699E-06	0.00000	0.68938E-04		
EQ= 4 A,L1,L2,L3,RES,SPLIT=-0.71012E-02	0.90901E-03	0.00000	0.43888E-03	0.70663E-02	0.43523E-03				

LZ	Z	U-VEL	V-VEL	W-VEL	DENSITY	ENTHALPY	PBOT	PTOP	DP
1	0.00000000	0.53564E-07	0.00000	0.99996E 00	0.10000E 01	0.10385E 01	0.10008E 01	0.10008E 01	0.10000E 01
2	0.10526316E 00	0.43330E-07	0.00000	0.10002E 01	0.99968E 00	0.10385E 01	0.10001E 01	0.10001E 01	0.99966E 00
3	0.21052632E 00	0.33097E-07	0.00000	0.10002E 01	0.99933E 00	0.10385E 01	0.99926E 00	0.99926E 00	0.99931E 00
4	0.31578947E 00	0.31073E-07	0.00000	0.10002E 01	0.99896E 00	0.10385E 01	0.99839E 00	0.99839E 00	0.99894E 00
5	0.42105263E 00	0.30766E-07	0.00000	0.10002E 01	0.99859E 00	0.10385E 01	0.99852E 00	0.99852E 00	0.99857E 00
6	0.52631579E 00	0.30720E-07	0.00000	0.10002E 01	0.99822E 00	0.10385E 01	0.99816E 00	0.99816E 00	0.99821E 00
7	0.63157895E 00	0.30709E-07	0.00000	0.10002E 01	0.99786E 00	0.10385E 01	0.99779E 00	0.99779E 00	0.99784E 00
8	0.73684211E 00	0.30703E-07	0.00000	0.10002E 01	0.99749E 00	0.10385E 01	0.99742E 00	0.99742E 00	0.99747E 00
9	0.84210526E 00	0.30696E-07	0.00000	0.10002E 01	0.99712E 00	0.10385E 01	0.99705E 00	0.99705E 00	0.99710E 00
10	0.94736842E 00	0.30690E-07	0.00000	0.10002E 01	0.99675E 00	0.10385E 01	0.99668E 00	0.99668E 00	0.99673E 00
11	0.10526316E 01	0.30684E-07	0.00000	0.10002E 01	0.99638E 00	0.10385E 01	0.99631E 00	0.99631E 00	0.99636E 00
12	0.11578947E 01	0.30678E-07	0.00000	0.10002E 01	0.99601E 00	0.10385E 01	0.99594E 00	0.99594E 00	0.99600E 00
13	0.12631579E 01	0.30672E-07	0.00000	0.10002E 01	0.99565E 00	0.10385E 01	0.99558E 00	0.99558E 00	0.99563E 00
14	0.13684211E 01	0.30666E-07	0.00000	0.10002E 01	0.99528E 00	0.10385E 01	0.99521E 00	0.99521E 00	0.99526E 00
15	0.14736842E 01	0.30659E-07	0.00000	0.10002E 01	0.99491E 00	0.10385E 01	0.99484E 00	0.99484E 00	0.99489E 00
16	0.15789474E 01	0.30653E-07	0.00000	0.10002E 01	0.99454E 00	0.10385E 01	0.99447E 00	0.99447E 00	0.99452E 00
17	0.16842105E 01	0.30644E-07	0.00000	0.10002E 01	0.99417E 00	0.10385E 01	0.99410E 00	0.99410E 00	0.99415E 00
18	0.17894737E 01	0.30540E-07	0.00000	0.10002E 01	0.99380E 00	0.10385E 01	0.99373E 00	0.99373E 00	0.99378E 00
19	0.18947368E 01	0.30240E-07	0.00000	0.10003E 01	0.99343E 00	0.10385E 01	0.99337E 00	0.99337E 00	0.99341E 00
20	0.20000000E 01	0.29940E-07	0.00000	0.10003E 01	0.99306E 00	0.10385E 01	0.99300E 00	0.99300E 00	0.99300E 00

OCP TIME PER STEP = 0.000
 OCP TIMES - TOTAL, ADI, MATRIX = 0.000 0.000 0.000

```

RESTART DUMP STARTED AT TIME STEP      3      UNIT NO. = 20  RESTART NO. = 1

```

```

ORESTART DUMP COMPLETED AT TIME STEP    3          UNIT NO. = 10  RESTART NO. = 1

```

```

1***** FINAL FLOW FIELD *****
RESULTS AT TSTEP NO.      3      TIME =0.190625E-01

```

***** U-VL

[illegible][illegible]

0***** W-VL

[illegible]

[illegible]

***** DENS		*****																			
0LZ=		1		2		3		4		5		6		7		8		9		10	
Z=		0.0000000		0.105263E		000.210526E		000.315789E		000.421053E		000.526316E		000.631579E		000.736842E		000.842105E		000.947368E	
20	0.96373E	00	0.96298E	00	0.96222E	00	0.96186E	00	0.96151E	00	0.96115E	00	0.96080E	00	0.96044E	00	0.96009E	00	0.95973E	00	0.95937E
19	0.96418E	00	0.96329E	00	0.96260E	00	0.96225E	00	0.96189E	00	0.96153E	00	0.96118E	00	0.96082E	00	0.96047E	00	0.96011E	00	0.96011E
18	0.96655E	00	0.96599E	00	0.96553E	00	0.96517E	00	0.96482E	00	0.96446E	00	0.96411E	00	0.96375E	00	0.96339E	00	0.96304E	00	0.96304E
17	0.96899E	00	0.96861E	00	0.96823E	00	0.96788E	00	0.96752E	00	0.96717E	00	0.96681E	00	0.96645E	00	0.96610E	00	0.96574E	00	0.96574E
16	0.97129E	00	0.97096E	00	0.97060E	00	0.97025E	00	0.96989E	00	0.96953E	00	0.96918E	00	0.96882E	00	0.96846E	00	0.96810E	00	0.96810E
15	0.97429E	00	0.97404E	00	0.97374E	00	0.97338E	00	0.97303E	00	0.97267E	00	0.97231E	00	0.97195E	00	0.97159E	00	0.97123E	00	0.97123E
14	0.98110E	00	0.98081E	00	0.98048E	00	0.98013E	00	0.97977E	00	0.97941E	00	0.97904E	00	0.97868E	00	0.97832E	00	0.97796E	00	0.97796E
13	0.99791E	00	0.99751E	00	0.99712E	00	0.99675E	00	0.99638E	00	0.99601E	00	0.99565E	00	0.99528E	00	0.99491E	00	0.99454E	00	0.99454E
12	0.10000E	01	0.99968E	00	0.99933E	00	0.99896E	00	0.99859E	00	0.99822E	00	0.99786E	00	0.99749E	00	0.99712E	00	0.99675E	00	0.99675E
11	0.10000E	01	0.99968E	00	0.99933E	00	0.99896E	00	0.99859E	00	0.99822E	00	0.99786E	00	0.99749E	00	0.99712E	00	0.99675E	00	0.99675E
10	0.10000E	01	0.99968E	00	0.99933E	00	0.99896E	00	0.99859E	00	0.99822E	00	0.99786E	00	0.99749E	00	0.99712E	00	0.99675E	00	0.99675E
9	0.10000E	01	0.99968E	00	0.99933E	00	0.99896E	00	0.99859E	00	0.99822E	00	0.99786E	00	0.99749E	00	0.99712E	00	0.99675E	00	0.99675E
8	0.99711E	00	0.99751E	00	0.99712E	00	0.99675E	00	0.99638E	00	0.99601E	00	0.99565E	00	0.99528E	00	0.99491E	00	0.99454E	00	0.99454E
7	0.98110E	00	0.98081E	00	0.98048E	00	0.98013E	00	0.97977E	00	0.97941E	00	0.97904E	00	0.97868E	00	0.97832E	00	0.97796E	00	0.97796E
6	0.97429E	00	0.97404E	00	0.97374E	00	0.97338E	00	0.97303E	00	0.97267E	00	0.97231E	00	0.97195E	00	0.97159E	00	0.97123E	00	0.97123E
5	0.97129E	00	0.97096E	00	0.97060E	00	0.97025E	00	0.96989E	00	0.96953E	00	0.96918E	00	0.96882E	00	0.96846E	00	0.96810E	00	0.96810E
4	0.96899E	00	0.96861E	00																	

01Z=	11	12	13	14	15	16	17	18	19	20
Z=	0.105263E	010.115789E	010.126316E	010.136842E	010.147368E	010.157895E	010.168421E	010.178947E	010.189474E	010.200000E
20	0.95938E	00.95902E	00.95867E	00.95831E	00.95796E	00.95760E	00.95725E	00.95689E	00.95654E	00.95619E
19	0.95976E	00.95940E	00.95905E	00.95870E	00.95834E	00.95799E	00.95763E	00.95728E	00.95692E	00.95657E
18	0.96268E	00.96233E	00.96197E	00.96161E	00.96126E	00.96090E	00.96055E	00.96019E	00.95983E	00.95948E
17	0.96538E	00.96502E	00.96467E	00.96431E	00.96395E	00.96360E	00.96324E	00.96288E	00.96253E	00.96217E
16	0.96774E	00.96739E	00.96703E	00.96667E	00.96631E	00.96596E	00.96560E	00.96524E	00.96488E	00.96452E
15	0.97087E	00.97051E	00.97015E	00.96980E	00.96944E	00.96908E	00.96872E	00.96836E	00.96800E	00.96764E
14	0.97760E	00.97724E	00.97688E	00.97651E	00.97615E	00.97579E	00.97543E	00.97507E	00.97471E	00.97435E
13	0.99618E	00.996381E	00.996344E	00.996307E	00.996271E	00.996234E	00.996197E	00.996160E	00.996123E	00.996086E
12	0.99638E	00.99601E	00.99565E	00.99528E	00.99491E	00.99454E	00.99417E	00.99380E	00.99343E	00.99306E
11	0.99638E	00.99601E	00.99565E	00.99528E	00.99491E	00.99454E	00.99417E	00.99380E	00.99343E	00.99306E
10	0.99638E	00.99601E	00.99565E	00.99528E	00.99491E	00.99454E	00.99417E	00.99380E	00.99343E	00.99306E
9	0.99638E	00.99601E	00.99565E	00.99528E	00.99491E	00.99454E	00.99417E	00.99380E	00.99343E	00.99306E
8	0.99618E	00.996381E	00.996344E	00.996307E	00.996271E	00.996234E	00.996197E	00.996160E	00.996123E	00.996086E
7	0.97760E	00.97724E	00.97688E	00.97651E	00.97615E	00.97579E	00.97543E	00.97507E	00.97471E	00.97435E
6	0.97087E	00.97051E	00.97015E	00.96980E	00.96944E	00.96908E	00.96872E	00.96836E	00.96800E	00.96764E
5	0.96774E	00.96739E	00.96703E	00.96667E	00.96631E	00.96596E	00.96560E	00.96524E	00.96488E	00.96452E
4	0.96538E	00.96502E	00.96467E	00.96431E	00.96395E	00.96360E	00.96324E	00.96288E	00.96253E	00.96217E


```

1 0.10385E 01 0.10385E 01 0.10385E 01 0.10385E 01 0.10385E 01 0.10385E 01 0.10385E 01 0.10385E 01 0.10385E 01
OLZ= 11 12 13 14 15 16 17 18 19 20
Z= 0.105263E 010.115789E 010.126316E 010.136842E 010.147368E 010.157895E 010.168421E 010.178947E 010.189474E 010.200000E 01

20 0.10385E 01 0.10385E 01 0.10385E 01 0.10385E 01 0.10385E 01 0.10385E 01 0.10385E 01 0.10385E 01 0.10385E 01
19 0.10381E 01 0.10381E 01 0.10381E 01 0.10381E 01 0.10381E 01 0.10381E 01 0.10381E 01 0.10381E 01 0.10381E 01
18 0.10349E 01 0.10349E 01 0.10349E 01 0.10349E 01 0.10349E 01 0.10349E 01 0.10349E 01 0.10349E 01 0.10349E 01
17 0.10320E 01 0.10320E 01 0.10320E 01 0.10320E 01 0.10320E 01 0.10320E 01 0.10320E 01 0.10320E 01 0.10320E 01
16 0.10295E 01 0.10295E 01 0.10295E 01 0.10295E 01 0.10295E 01 0.10295E 01 0.10295E 01 0.10295E 01 0.10295E 01
15 0.10262E 01 0.10262E 01 0.10262E 01 0.10262E 01 0.10262E 01 0.10262E 01 0.10262E 01 0.10262E 01 0.10262E 01
14 0.10192E 01 0.10192E 01 0.10192E 01 0.10192E 01 0.10192E 01 0.10192E 01 0.10192E 01 0.10192E 01 0.10192E 01
13 0.10022E 01 0.10022E 01 0.10022E 01 0.10022E 01 0.10022E 01 0.10022E 01 0.10022E 01 0.10022E 01 0.10022E 01
12 0.99998E 00 0.99998E 00 0.99998E 00 0.99998E 00 0.99998E 00 0.99998E 00 0.99998E 00 0.99998E 00 0.99998E 00
11 0.99998E 00 0.99998E 00 0.99998E 00 0.99998E 00 0.99998E 00 0.99998E 00 0.99998E 00 0.99998E 00 0.99998E 00
10 0.99998E 00 0.99998E 00 0.99998E 00 0.99998E 00 0.99998E 00 0.99998E 00 0.99998E 00 0.99998E 00 0.99998E 00
9 0.99998E 00 0.99998E 00 0.99998E 00 0.99998E 00 0.99998E 00 0.99998E 00 0.99998E 00 0.99998E 00 0.99998E 00
8 0.10022E 01 0.10022E 01 0.10022E 01 0.10022E 01 0.10022E 01 0.10022E 01 0.10022E 01 0.10022E 01 0.10022E 01
7 0.10192E 01 0.10192E 01 0.10192E 01 0.10192E 01 0.10192E 01 0.10192E 01 0.10192E 01 0.10192E 01 0.10192E 01
6 0.10262E 01 0.10262E 01 0.10262E 01 0.10262E 01 0.10262E 01 0.10262E 01 0.10262E 01 0.10262E 01 0.10262E 01
5 0.10295E 01 0.10295E 01 0.10295E 01 0.10295E 01 0.10295E 01 0.10295E 01 0.10295E 01 0.10295E 01 0.10295E 01
4 0.10320E 01 0.10320E 01 0.10320E 01 0.10320E 01 0.10320E 01 0.10320E 01 0.10320E 01 0.10320E 01 0.10320E 01
3 0.10349E 01 0.10349E 01 0.10349E 01 0.10349E 01 0.10349E 01 0.10349E 01 0.10349E 01 0.10349E 01 0.10349E 01
2 0.10381E 01 0.10381E 01 0.10381E 01 0.10381E 01 0.10381E 01 0.10381E 01 0.10381E 01 0.10381E 01 0.10381E 01
1 0.10385E 01 0.10385E 01 0.10385E 01 0.10385E 01 0.10385E 01 0.10385E 01 0.10385E 01 0.10385E 01 0.10385E 01
RESULTS AT TSTEP NO. 3 TIME =0.196625E-01

```

0***** VISC

```

OLZ= 1 2 3 4 5 6 7 8 9 10
Z= 0.000000E 0.105263E 000.210526E 000.315789E 000.421053E 000.526316E 000.631579E 000.736842E 000.842105E 000.947368E 00

20 0.10431E 01 0.10431E 01 0.10431E 01 0.10431E 01 0.10431E 01 0.10431E 01 0.10431E 01 0.10431E 01 0.10431E 01
19 0.10325E 01 0.10813E 01 0.10812E 01 0.10812E 01 0.10812E 01 0.10812E 01 0.10812E 01 0.10812E 01 0.10812E 01
18 0.16935E 01 0.18087E 01 0.18097E 01 0.18095E 01 0.18091E 01 0.18086E 01 0.18081E 01 0.18076E 01 0.18071E 01
17 0.31123E 01 0.32409E 01 0.32433E 01 0.32427E 01 0.32413E 01 0.32399E 01 0.32384E 01 0.32370E 01 0.32356E 01
16 0.10248E 02 0.10417E 02 0.10421E 02 0.10418E 02 0.10413E 02 0.10407E 02 0.10401E 02 0.10395E 02 0.10389E 02
15 0.69477E 02 0.69373E 02 0.69348E 02 0.69318E 02 0.69280E 02 0.69242E 02 0.69204E 02 0.69166E 02 0.69127E 02
14 0.31576E 03 0.31416E 03 0.31392E 03 0.31376E 03 0.31362E 03 0.31348E 03 0.31334E 03 0.31320E 03 0.31306E 03
13 0.18182E 03 0.18165E 03 0.18158E 03 0.18151E 03 0.18143E 03 0.18135E 03 0.18129E 03 0.18121E 03 0.18114E 03
12 0.12361E 02 0.12564E 02 0.12558E 02 0.12558E 02 0.12558E 02 0.12558E 02 0.12577E 02 0.12572E 02 0.12568E 02
11 0.15651E 01 0.12303E 01 0.10422E 01 0.10192E 01 0.10169E 01 0.10168E 01 0.10168E 01 0.10168E 01 0.10168E 01
10 0.15651E 01 0.12303E 01 0.10422E 01 0.10192E 01 0.10169E 01 0.10168E 01 0.10168E 01 0.10168E 01 0.10168E 01
9 0.12361E 02 0.12564E 02 0.12558E 02 0.12558E 02 0.12558E 02 0.12558E 02 0.12577E 02 0.12572E 02 0.12568E 02
8 0.18182E 03 0.18165E 03 0.18158E 03 0.18151E 03 0.18143E 03 0.18135E 03 0.18129E 03 0.18121E 03 0.18114E 03
7 0.31576E 03 0.31416E 03 0.31392E 03 0.31376E 03 0.31362E 03 0.31348E 03 0.31334E 03 0.31320E 03 0.31306E 03
6 0.69477E 02 0.69373E 02 0.69348E 02 0.69318E 02 0.69280E 02 0.69242E 02 0.69204E 02 0.69166E 02 0.69127E 02
5 0.10248E 02 0.10417E 02 0.10421E 02 0.10418E 02 0.10413E 02 0.10407E 02 0.10401E 02 0.10395E 02 0.10389E 02
4 0.31123E 01 0.32409E 01 0.32433E 01 0.32427E 01 0.32413E 01 0.32399E 01 0.32384E 01 0.32370E 01 0.32356E 01
3 0.16935E 01 0.18087E 01 0.18097E 01 0.18095E 01 0.18091E 01 0.18086E 01 0.18081E 01 0.18076E 01 0.18071E 01
2 0.10825E 01 0.10813E 01 0.10812E 01 0.10812E 01 0.10812E 01 0.10812E 01 0.10811E 01 0.10811E 01 0.10811E 01
1 0.10431E 01 0.10431E 01 0.10431E 01 0.10431E 01 0.10431E 01 0.10431E 01 0.10431E 01 0.10431E 01 0.10431E 01

```

```

OLZ= 11 12 13 14 15 16 17 18 19 20
Z= 0.105263E 010.115789E 010.126316E 010.136842E 010.147368E 010.157895E 010.168421E 010.178947E 010.189474E 010.200000E 01

20 0.10431E 01 0.10431E 01 0.10431E 01 0.10431E 01 0.10431E 01 0.10431E 01 0.10431E 01 0.10431E 01 0.10431E 01
19 0.10810E 01 0.10810E 01 0.10810E 01 0.10810E 01 0.10810E 01 0.10810E 01 0.10810E 01 0.10810E 01 0.10810E 01
18 0.18061E 01 0.18057E 01 0.18052E 01 0.18047E 01 0.18042E 01 0.18037E 01 0.18032E 01 0.18027E 01 0.18023E 01
17 0.32327E 01 0.32313E 01 0.32299E 01 0.32285E 01 0.32271E 01 0.32256E 01 0.32242E 01 0.32228E 01 0.32214E 01
16 0.10377E 02 0.10371E 02 0.10365E 02 0.10359E 02 0.10353E 02 0.10347E 02 0.10341E 02 0.10336E 02 0.10329E 02
15 0.69051E 02 0.69013E 02 0.68975E 02 0.68937E 02 0.68899E 02 0.68860E 02 0.68822E 02 0.68784E 02 0.68746E 02
14 0.31277E 03 0.31263E 03 0.31249E 03 0.31235E 03 0.31221E 03 0.31207E 03 0.31193E 03 0.31179E 03 0.31167E 03
13 0.18099E 03 0.18092E 03 0.18084E 03 0.18077E 03 0.18069E 03 0.18062E 03 0.18055E 03 0.18047E 03 0.18040E 03
12 0.12559E 02 0.12555E 02 0.12551E 02 0.12546E 02 0.12542E 02 0.12538E 02 0.12534E 02 0.12529E 02 0.12521E 02
11 0.10168E 01 0.10168E 01 0.10168E 01 0.10168E 01 0.10168E 01 0.10168E 01 0.10168E 01 0.10168E 01 0.10168E 01
10 0.10168E 01 0.10168E 01 0.10168E 01 0.10168E 01 0.10168E 01 0.10168E 01 0.10168E 01 0.10168E 01 0.10168E 01
9 0.12559E 02 0.12555E 02 0.12551E 02 0.12546E 02 0.12542E 02 0.12538E 02 0.12534E 02 0.12529E 02 0.12521E 02
8 0.18099E 03 0.18092E 03 0.18084E 03 0.18077E 03 0.18069E 03 0.18062E 03 0.18055E 03 0.18047E 03 0.18040E 03
7 0.31277E 03 0.31263E 03 0.31249E 03 0.31235E 03 0.31221E 03 0.31207E 03 0.31193E 03 0.31179E 03 0.31167E 03
6 0.69051E 02 0.69013E 02 0.68975E 02 0.68937E 02 0.68899E 02 0.68860E 02 0.68822E 02 0.68784E 02 0.68746E 02
5 0.32327E 01 0.32313E 01 0.32299E 01 0.32285E 01 0.32271E 01 0.32256E 01 0.32242E 01 0.32228E 01 0.32214E 01
4 0.18061E 01 0.18057E 01 0.18052E 01 0.18047E 01 0.18042E 01 0.18037E 01 0.18032E 01 0.18027E 01 0.18023E 01
3 0.10810E 01 0.10810E 01 0.10810E 01 0.10810E 01 0.10810E 01 0.10810E 01 0.10810E 01 0.10810E 01 0.10810E 01
2 0.10431E 01 0.10431E 01 0.10431E 01 0.10431E 01 0.10431E 01 0.10431E 01 0.10431E 01 0.10431E 01 0.10431E 01
1 0.10431E 01 0.10431E 01 0.10431E 01 0.10431E 01 0.10431E 01 0.10431E 01 0.10431E 01 0.10431E 01 0.10431E 01
RESULTS AT TSTEP NO. 3 TIME =0.196625E-01

```

0***** MIXL

012 Z=	1	2	3	4	5	6	7	8	9	10
	0.00000000	0.105263E	000.210526E	000.315789E	000.421053E	000.526316E	000.631579E	000.736842E	000.842105E	000.947368E
20	0.00000	0.000000	0.000000	0.000000	0.00000	0.000000	0.000000	0.000000	0.000000	0.000000
19	0.18276E-04	0.18126E-04	0.18117E-04	0.18113E-04	0.18110E-04	0.18107E-04	0.18103E-04	0.18100E-04	0.18097E-04	0.18094E-04
18	0.12487E-03	0.12487E-03	0.12489E-03	0.12489E-03	0.12487E-03	0.12485E-03	0.12483E-03	0.12482E-03	0.12480E-03	0.12478E-03
17	0.41989E-03	0.42558E-03	0.42568E-03	0.42566E-03	0.42560E-03	0.42554E-03	0.42548E-03	0.42541E-03	0.42535E-03	0.42529E-03
16	0.14378E-02	0.14443E-02	0.14444E-02	0.14443E-02	0.14441E-02	0.14439E-02	0.14437E-02	0.14435E-02	0.14434E-02	0.14432E-02
15	0.49169E-02	0.49160E-02	0.49157E-02	0.49153E-02	0.49149E-02	0.49144E-02	0.49139E-02	0.49135E-02	0.49130E-02	0.49125E-02
14	0.16865E-01	0.16834E-01	0.16834E-01	0.16833E-01	0.16833E-01	0.16822E-01	0.16822E-01	0.16816E-01	0.16816E-01	0.16810E-01
13	0.14829E-01	0.14836E-01	0.14837E-01	0.14837E-01	0.14836E-01	0.14836E-01	0.14836E-01	0.14835E-01	0.14835E-01	0.14835E-01
12	0.15467E-01	0.15477E-01	0.15478E-01	0.15478E-01	0.15478E-01	0.15478E-01	0.15478E-01	0.15478E-01	0.15478E-01	0.15478E-01
11	0.15467E-01	0.15477E-01	0.15478E-01	0.15478E-01	0.15478E-01	0.15478E-01	0.15478E-01	0.15478E-01	0.15478E-01	0.15478E-01
10	0.15467E-01	0.15477E-01	0.15478E-01	0.15478E-01	0.15478E-01	0.15478E-01	0.15478E-01	0.15478E-01	0.15478E-01	0.15478E-01
9	0.15467E-01	0.15477E-01	0.15478E-01	0.15478E-01	0.15478E-01	0.15478E-01	0.15478E-01	0.15478E-01	0.15478E-01	0.15478E-01
8	0.14829E-01	0.14836E-01	0.14837E-01	0.14837E-01	0.14836E-01	0.14836E-01	0.14836E-01	0.14835E-01	0.14835E-01	0.14835E-01
7	0.11665E-01	0.11665E-01	0.11665E-01	0.11663E-01	0.11663E-01	0.11682E-01	0.11682E-01	0.11681E-01	0.11681E-01	0.11680E-01
6	0.49169E-02	0.49160E-02	0.49157E-02	0.49153E-02	0.49149E-02	0.49144E-02	0.49139E-02	0.49135E-02	0.49130E-02	0.49125E-02
5	0.14378E-02	0.14443E-02	0.14444E-02	0.14443E-02	0.14441E-02	0.14439E-02	0.14437E-02	0.14435E-02	0.14434E-02	0.14432E-02
4	0.41989E-03	0.42558E-03	0.42568E-03	0.42566E-03	0.42560E-03	0.42554E-03	0.42548E-03	0.42541E-03	0.42535E-03	0.42529E-03
3	0.12408E-03	0.12487E-03	0.12489E-03	0.12489E-03	0.12487E-03	0.12485E-03	0.12483E-03	0.12482E-03	0.12480E-03	0.12478E-03
2	0.18276E-04	0.18126E-04	0.18117E-04	0.18113E-04	0.18110E-04	0.18107E-04	0.18103E-04	0.18100E-04	0.18097E-04	0.18094E-04
1	0.00000	0.000000	0.000000	0.000000	0.00000	0.000000	0.000000	0.000000	0.000000	0.000000

```
01Z=      11      12      13      14      15      16      17      18      19      20
Z= 0.105263E 010.115789E 010.126316E 010.136842E 010.147368E 010.157895E 010.168421E 010.178947E 010.189474E 010.200000E 01
```

[illegible]

```

1      0.000000      0.000000      0.000000      0
RESULTS AT TSTEP NO.      3      TIME =0.190625E-01

```

***** MACH *****

0LZ=	1	2	3	4	5	6	7	8	9	10
Z=	0.0000000	0.105263E	0.00.210526E	0.00.315789E	0.00.421053E	0.00.526316E	0.00.631579E	0.00.736842E	0.00.842105E	0.00.947368E

[illegible]

```

01Z=      11      12      13      14      15      16      17      18      19      20
Z= 0.105263E 010.115789E 010.126316E 010.136842E 010.147368E 010.157895E 010.168421E 010.178947E 010.189474E 010.200000E 01

```

20	0.00000	0.00000	0.00000	0.00000	0.00000	0.00000	0.00000	0.00000	0.00000	0.00000	0.00000
19	0.45114E-01	0.45110E-01	0.45107E-01	0.45103E-01	0.45099E-01	0.45096E-01	0.45092E-01	0.45088E-01	0.45085E-01	0.45081E-01	0.45077E-01

```

18 0.13123E 00 0.13123E 00 0.13123E 00 0.13123E 00 0.13123E 00 0.13123E 00 0.13123E 00 0.13123E 00 0.13122E 00
17 0.17692E 00 0.17692E 00 0.17692E 00 0.17692E 00 0.17692E 00 0.17692E 00 0.17692E 00 0.17692E 00 0.17692E 00 0.17692E 00
16 0.20879E 00 0.20879E 00 0.20879E 00 0.20879E 00 0.20879E 00 0.20879E 00 0.20879E 00 0.20879E 00 0.20879E 00 0.20879E 00
15 0.24479E 00 0.24479E 00 0.24479E 00 0.24479E 00 0.24479E 00 0.24479E 00 0.24479E 00 0.24479E 00 0.24479E 00 0.24479E 00
14 0.30810E 00 0.30810E 00 0.30810E 00 0.30810E 00 0.30810E 00 0.30810E 00 0.30810E 00 0.30810E 00 0.30810E 00 0.30810E 00
13 0.42537E 00 0.42537E 00 0.42537E 00 0.42537E 00 0.42537E 00 0.42537E 00 0.42537E 00 0.42537E 00 0.42537E 00 0.42537E 00
12 0.43891E 00 0.43891E 00 0.43891E 00 0.43891E 00 0.43891E 00 0.43891E 00 0.43891E 00 0.43891E 00 0.43891E 00 0.43891E 00
11 0.43892E 00 0.43892E 00 0.43892E 00 0.43892E 00 0.43892E 00 0.43892E 00 0.43892E 00 0.43892E 00 0.43892E 00 0.43892E 00
10 0.43892E 00 0.43892E 00 0.43892E 00 0.43892E 00 0.43892E 00 0.43892E 00 0.43892E 00 0.43892E 00 0.43892E 00 0.43892E 00
9 0.43891E 00 0.43891E 00 0.43891E 00 0.43891E 00 0.43891E 00 0.43891E 00 0.43891E 00 0.43891E 00 0.43891E 00 0.43891E 00
8 0.42537E 00 0.42537E 00 0.42537E 00 0.42537E 00 0.42537E 00 0.42537E 00 0.42537E 00 0.42537E 00 0.42537E 00 0.42537E 00
7 0.30810E 00 0.30810E 00 0.30810E 00 0.30810E 00 0.30810E 00 0.30810E 00 0.30810E 00 0.30810E 00 0.30810E 00 0.30810E 00
6 0.24479E 00 0.24479E 00 0.24479E 00 0.24479E 00 0.24479E 00 0.24479E 00 0.24479E 00 0.24479E 00 0.24479E 00 0.24479E 00
5 0.20879E 00 0.20879E 00 0.20879E 00 0.20879E 00 0.20879E 00 0.20879E 00 0.20879E 00 0.20879E 00 0.20879E 00 0.20879E 00
4 0.17692E 00 0.17692E 00 0.17692E 00 0.17692E 00 0.17692E 00 0.17692E 00 0.17692E 00 0.17692E 00 0.17692E 00 0.17692E 00
3 0.13123E 00 0.13123E 00 0.13123E 00 0.13123E 00 0.13123E 00 0.13123E 00 0.13123E 00 0.13123E 00 0.13123E 00 0.13122E 00
2 0.45114E-01 0.45114E-01 0.45107E-01 0.45103E-01 0.45099E-01 0.45096E-01 0.45092E-01 0.45088E-01 0.45085E-01 0.45081E-01
1 0.00000 0.00000 0.00000 0.00000 0.00000 0.00000 0.00000 0.00000 0.00000 0.00000 0.00000

```

RESULTS AT TSTEP NO. 3 TIME = 0.190625E-01

***** TIME PLOTS *****

***** DIR1 PLOTS *****

***** DIR3 PLOTS *****

```

CHCHW400 TERMINATED: STOP
RELEASE FT
ERASE R9
0512 CANCELLED: R9 UNKNOWN.
ERASE R14
0512 CANCELLED: R14 UNKNOWN.
ERASE MINT
ERASE PROCN
ERASE M
0512 CANCELLED: M UNKNOWN.
ERASE SC01
ERASE SC10
ERASE SC20
LOGOFF
R007 LOGOFF AT 15:31 ON 11/10/82 - CPU TIME= 0.68 MINUTES.

```

1. Report No. NASA CR-3723		2. Government Accession No.		3. Recipient's Catalog No.	
4. Title and Subtitle NUMERICAL SOLUTIONS OF NAVIER-STOKES EQUATIONS FOR COMPRESSIBLE TURBULENT TWO/THREE DIMENSIONAL FLOWS IN THE TERMINAL SHOCK REGION OF AN INLET/DIFFUSER				5. Report Date August 1983	
				6. Performing Organization Code	
7. Author(s) N.-S. Liu, S. J. Shamroth, and H. McDonald				8. Performing Organization Report No. None	
				10. Work Unit No.	
9. Performing Organization Name and Address Scientific Research Associates, Inc. P. O. Box 498 Glastonbury, Connecticut 06033				11. Contract or Grant No. NAS3-22747	
				13. Type of Report and Period Covered Contractor Report	
12. Sponsoring Agency Name and Address National Aeronautics and Space Administration Washington, D.C. 20546				14. Sponsoring Agency Code 505-31-02B (E-1653)	
15. Supplementary Notes Final report. Project Manager, Thomas J. Benson, Aerodynamics and Engine Systems Division, NASA Lewis Research Center, Cleveland, Ohio 44135.					
16. Abstract The multi-dimensional ensemble-averaged compressible time-dependent Navier-Stokes equations in conjunction with mixing length turbulence model and shock capturing technique have been used to study the terminal shock type of flows in various flight regimes occurring in a diffuser/inlet model. The numerical scheme for solving the governing equations is based on a linearized block implicit approach and the following high Reynolds number calculations have been carried out: (1) 2-D, steady, subsonic; (2) 2-D, steady, transonic with normal shock; (3) 2-D, steady, supersonic with terminal shock; (4) 2-D, transient process of shock development and (5) 3-D, steady, transonic with normal shock. The numerical results obtained for the 2-D and 3-D transonic shocked flows have been compared with corresponding experimental data; the calculated wall static pressure distributions agree well with the measured data.					
17. Key Words (Suggested by Author(s)) Numerical solutions; Navier-Stokes equations; Compressible turbulent 2-D and 3-D flows; Terminal shocks; Inlets and diffusers				18. Distribution Statement Unclassified - unlimited STAR Category 34	
19. Security Classif. (of this report) Unclassified		20. Security Classif. (of this page) Unclassified		21. No. of pages 105	
				22. Price* A06	